

Riassunto

Gli studi teorici sulla dinamica degli ammassi globulari condotti negli ultimi vent'anni hanno messo in evidenza come la popolazione di stelle binarie sia strettamente legata all'evoluzione stessa dell'ammasso e alla creazione di oggetti esotici, come le stelle binarie x, le blue stragglers, le millisecond pulsars.

Alcuni modelli -ad es. Heggie & Aarseth 1992- prevedono che sia sufficiente una piccola percentuale di sistemi binari, il 3%, per cambiare drasticamente l'evoluzione dinamica di un ammasso globulare; questi sistemi, rilasciando la loro energia gravitazionale attraverso incontri con altre stelle, singole o binarie, sono considerati delle efficienti fonti di calore in grado di bloccare il collasso della regione centrale degli ammassi globulari.

L'esistenza di sistemi binari, e in particolare di sistemi binari primordiali, é stata evidenziata con varie tecniche osservative (Hut et al. 1992 e riferimenti bibliografici all'interno), tuttavia, al momento, non é chiaro quale sia il valore di parametri come la frequenza numerica di tali oggetti e la distribuzione dei periodi delle loro orbite.

L'obiettivo di questa tesi é quello di stabilire la frequenza di sistemi binari all'interno di un ammasso globulare (M4) studiando la variazione di velocità delle stelle in epoche differenti, e determinare quindi la loro distribuzione radiale e la distribuzione dei periodi.

L'oggetto preso in considerazione in questo lavoro é l'ammasso globulare galattico M4 (NGC 6121). Le ragioni di questa scelta derivano dal fatto che non mostra evidenza di collasso delle regioni centrali (Trager et al. 1995) nonostante la sua età stimata sia superiore al tempo di rilassamento di un fattore di circa 400; inoltre possiede una regione centrale estesa e relativamente poco densa, caratteristica che dovrebbe agevolare la ricerca di sistemi binari laddove si suppone che questi siano in proporzione maggiore; infine, essendo uno degli ammassi più vicini, permette lo studio di oggetti deboli, fin sotto il turn-off.

Effettuando una vasta campagna osservativa multi epoca effettuata con lo spet-

trografo ad alta risoluzione FLAMES +GIRAFFE situato al Very Large Telescope in Cile, abbiamo ottenuto 5973 spettri individuali per 2469 stelle dalla punta del braccio gigante rosso fino ad una magnitudine sotto il turn-off. Queste stelle sono state osservate in tre diverse epoche: la prima é stata ottenuta nel 2003; la seconda nel 2006 con lo scopo di identificare le binarie larghe, aventi periodi dell'ordine di anni, dal centro dell'ammasso fino al suo esterno; la terza e ultima epoca é stata ottenuta 5 settimane dopo la seconda al fine di studiare le binarie strette, quelle con periodi di poche settimane, situate al centro dell'ammasso.

Riassumendo, abbiamo ottenuto due epoche per 2469 stelle e tre epoche per 484 stelle.

La riduzione dati é stata effettuata usando la pipeline sviluppata a Ginevra e all'osservatorio di Parigi (Blecha et al. 2000): la versione 1.13 del GIRAFFE BaseLine Data Reduction Software (girBLDRS). La velocità radiale media ottenuta per il campione di stelle osservato é di $70.29 \pm 0.07 (\pm 0.3) (\pm 0.1) \text{ km s}^{-1}$, dove gli errori sistematici in parentesi includono effetti come il redshift gravitazionale, i moti convettivi, e l'incertezza sul punto zero delle velocità radiali. Il primo termine é l'errore interno stimato sulle nostre misure.

Il valore della velocità trovato per le stelle di M4 é in buon accordo con gli studi precedenti. Nessun errore sistematico é stato riscontrato nel calcolo della velocità media in funzione della magnitudine o del colore delle stelle.

Dallo studio sulla variazione delle velocità radiali per le stelle aventi osservazioni multiple abbiamo ricavato 57 candidati sistemi binari. La variazione di velocità oltre la quale abbiamo considerato le stelle candidate binarie é di $\sim 0.3 \text{ km s}^{-1}$ per le stelle brillanti (magnitudine $V \leq 15$), e $\sim 0.5 \text{ km s}^{-1}$ per le stelle deboli (magnitudine $V > 15 \text{ mag}$).

Utilizzando questo criterio sono state individuate 4 candidate binarie su 97 stelle nel centro dell'ammasso, e 53 candidate binarie su 2372 stelle nelle regioni esterne.

Abbiamo in seguito mostrato che, aumentando il numero di osservazioni da due a tre epoche per tutte le stelle osservate, il numero di candidate aumenta del 40%. Tendendo conto di questo effetto di incompletezza, abbiamo trovato che il limite inferiore di frazione di binarie in M4 é $f = 3.0 \pm 0.3\%$; in particolare la frazione di binarie al centro dell'ammasso é $f = 5.1 \pm 2.3\%$, valore che decresce a $f = 3.0 \pm 0.4\%$ andando verso le regioni esterne.

Come previsto dalla teoria, la frazione di binarie trovata é più alta nelle regioni centrali dell'ammasso.

Nella seconda parte della tesi, abbiamo considerato la discrepanza tra il numero di sistemi binari che é possibile identificare in una campagna osservativa e quello che effettivamente caratterizza un determinato ammasso globulare.

Un'osservazione, infatti, può essere fortemente affetta da una serie di fattori, come eventuali configurazioni sfavorevoli dei parametri orbitali di un sistema, o limitazioni intrinseche alla tecnica osservativa, che pongono dei limiti superiori alla completezza dei risultati. Ci si aspetta quindi che il numero di binarie trovato nella prima parte del lavoro, rappresenti una stima inferiore rispetto al valore reale.

Per interpretare correttamente e correggere i risultati ottenuti, abbiamo generato, tramite simulazioni Monte Carlo, un vasto numero di velocità radiali associate a stelle con parametri tipici dell'ammasso M4 per poter valutare da queste una frazione teorica di binarie. Gli effetti della dinamica dell'ammasso vengono inseriti confrontando il risultato delle nostre simulazioni con il modello di evolutivo di M4 creato da Heggie & Giersz (2008). In questo modo, siamo in grado di calcolare la frazione di sistemi binari persi nella nostra campagna osservativa e la correzione sulla frequenza ricavata dai dati osservativi.

Simulando le nostre osservazioni e considerando gli effetti dell'evoluzione dinamica abbiamo trovato che la frazione totale di binarie in M4 è circa 14%.

Nelle simulazioni di Heggie & Giersz il valore della frazione di binarie è circa $1/3$ di quello originale, a causa della distruzione delle binarie larghe: pertanto sulla base del risultato trovato in questa tesi, possiamo affermare che la frazione di binarie primordiali in M4 è circa 40%.

Abstract

In recent years it has been widely recognized that the binary star population in a star cluster is related intimately to both the cluster dynamical evolution and the formation of various exotic objects in the clusters.

A primordial binary frequency as small as 3% can change the dynamical evolution of the entire globular cluster (Heggie & Aarseth 1992), as binary stars are an efficient heating source that can halt the core collapse, releasing their gravitational binding energy through close stellar encounters.

In addition, encounters between binaries and other stars or binaries can not only profoundly affect the dynamical evolution of the clusters: they can disrupt the widely separated binaries and catalyze the formation of exotic objects such as blue stragglers, X-ray binaries and millisecond pulsars.

The existence of the binary systems, and in particular primordial binaries in the globular clusters, has been demonstrated by a number of observational techniques (see Hut et. al 1992, and references therein), but the binary frequencies, and in particular the period distributions, are still very uncertain.

With this work, by studying the radial velocity variations of the stars in different epochs, we want to establish the true frequency of binaries in the galactic globular cluster (GGC) M4 (NGC 6121), to determine the radial distribution within the cluster, and to constrain the period distribution of the binaries, three quantities which are intimately linked to the internal dynamics of the globular clusters.

The reasons to select M4 as our target are the following: first of all, it shows no evidence for any central brightness cusp (Trager et al. 1995) indicative of core collapse, despite the fact that the cluster's age exceeds its central relaxation time (Harris 1996) by a factor of approximately 400. Additional reasons which make M4 our first priority target are that it has an extended (relatively uncrowded) core, making feasible the search for binaries with a multifiber facility as FLAMES@VLT, where the portion of binaries should be highest. Moreover,

M4 is the cluster closest to the Sun, which enables us to study the binaries below the turn-off, and these are pristine tracers, as binaries containing giants might be destroyed by internal mass transfer.

By conducting a large multi-epoch high resolution spectroscopic investigation search for binary candidates in M4 using the multifiber facility FLAMES+GIRAFFE at VLT, we have obtained 5973 individual spectra of 2469 from the Red Giant Tip to one magnitude below the Turn-Off. We observed these stars in three different epochs: the first epoch was taken in 2003, the second was collected in 2006 in order to study the soft binaries from the center of the cluster to its outskirts, the third was collected 5 weeks after the second in order to identify the hard binaries in the core of the cluster with a periods of up to few weeks. At the end, we obtained two epochs for 2469 stars, and three epochs for 484 stars.

The data reduction was performed using the pipeline developed at Geneva and Paris Observatories (Blecha et al. 2000): the GIRAFFE BaseLine Data Reduction Software (girBLDRS), version 1.13. With it we removed the instrumental signature from the observed data, subtracting the bias and dividing by the normalized flat-field.

Radial velocities were obtained with the classical cross-correlation technique, using a solar type spectrum as the template.

The average radial velocity of the observed stars is 70.29 ± 0.07 . This value is in a very good agreement with the previous studies. No systematic shift in average velocity is observed as a function of the stellar magnitude and color.

The search for variations in radial velocities among the stars with multi-epoch observations yielded 57 binary star candidates. The candidates in the bright sample ($V \leq 15$) have 3σ velocity variations larger than $\sim 0.3 \text{ km s}^{-1}$, while the fainter candidates ($V > 15 \text{ mag}$) have 3σ velocity variations larger than $\sim 0.5 \text{ km s}^{-1}$. There are four binary star candidates out of 97 observed targets inside the core radius, and 53 candidates out of 2372 observed stars outside the core radius.

We have shown that increasing the stellar coverage from two epochs to three epochs, the number of binary candidates increases by 40%. Accounting for this incompleteness affecting stars with only two epochs, we have found that the lower limit for the binary fraction is $f = 3.0 \pm 0.3\%$; the binary fraction in the cluster core is $f = 5.1 \pm 2.3\%$, which decreases to $f = 3.0 \pm 0.4\%$ outside the core. Similarly, we found $f = 4.5 \pm 0.4\%$ and $f = 1.8 \pm 0.6\%$ for the binary fraction inside and outside the half mass radius. As expected from energy equipartition, the binary fraction is higher in the central parts of the cluster.

In the second part of this thesis we investigate the completeness of our study by comparing the observations with a model. Indeed, the number of binary

systems that is possible to find in a radial velocity survey is strongly limited by several parameters: the survey can typically detect a subset, often a small subset, of all binaries, because not all stars in the cluster can be surveyed. Furthermore, unfavorable orbital configurations would cause a fraction of binary systems to be missing from our detection sample.

Thus, to properly interpret the measurements in our survey, we use a Monte Carlo simulation method to generate a large number of simulated radial velocity data sets and infer from them the expected binary stars. We also compare the results of our simulations with the evolutionary modeling of Heggie & Giersz (2008) in order to take into account the dynamic of the cluster. With this model we want to determine the frequency of binary systems in M4 in the simulation and then compare with the frequency found with the observational data. In this way we are able to calculate from the simulated data the fraction of binary systems missed in our survey in order to correct the observed binary frequencies.

We found that with our survey and considering the dynamical effects, the discovery efficiency is about 20%. This yields a binary frequency of 14%.

In the Heggie & Giersz (2008) simulations the current binary fraction is about 1/3 of the original (because of the destruction of soft binaries). Therefore, on the basis on the results that we found in this thesis, the primordial binary fraction in M4 could have been about 40%. Value very close to what would be expected for young populations (Kroupa 2008).

Comparing the distribution of the semi-major axis and the periods of the simulated binaries in the two models, as expected, we notice that the wide, long-period binaries have been eliminated by dynamical destruction.

Contents

Riassunto	iii
Abstract	vii
1 Introduction	1
1.1 Evolution of clusters	1
1.1.1 The negative heat capacity	1
1.2 The importance of binary stars in globular clusters	2
1.3 Techniques to find binary systems	4
1.3.1 Binaries in the Color-Magnitude Diagram	4
1.3.2 Eclipsing binaries	5
1.3.3 Radial velocity variables	6
1.3.4 Comparison between binary search techniques	8
1.4 Other types of binaries	9
1.4.1 Cataclysmic variables	9
1.4.2 Low-mass X-ray binaries	10
1.4.3 Millisecond pulsars	10
1.5 The Galactic Globular Cluster M4 (NGC6121)	11
1.5.1 Why we choose M4	11
2 Observations and FLAMES	15
2.1 Description of the observations	15
2.2 FLAMES	19
2.2.1 The field corrector	22
2.2.2 UVES	23
2.2.3 GIRAFFE	23
2.2.4 The fiber Positioner	25

3	Data reduction	27
3.1	The pipeline	29
4	The radial velocity of M4	37
4.1	Radial Velocities	37
4.1.1	The zero point velocity shift between the epochs	40
4.1.2	M4 radial velocity	42
5	The binary candidates	47
5.1	The radial velocity variations	47
5.2	The binary fraction	49
6	Monte Carlo simulations	55
6.1	The model	56
6.2	The results	57
6.2.1	The dependence of the eccentricities	58
6.2.2	Comparison with the observations	62
7	Comparison with the dynamical models	67
7.1	The dynamical model	68
7.2	The dynamical interaction of binary systems	68
7.3	Comparison with the previous results	69
7.3.1	Periods and semi-axis distribution	70
7.3.2	Comparison with the observations.	73
7.3.3	The discovery efficiency	73
7.4	The previous studies on the frequency of binaries	74
8	Conclusions	77
8.1	Results of the observations	77
8.2	Results of the simulations	78
A	The binary candidates	81
B	The catalogue	89
	Bibliography	123

List of Figures

2.1	Small dots show the color-magnitude diagram for all the stars in our astro-photometric catalog. The stars highlighted with thick dots (in red in the electronic version) are the stars for which we have collected spectra.	17
2.2	Spatial distribution of the target stars with respect to the center reported in Tab. 1. The coordinates are given in arcminutes. Observations from different epochs are shown with different symbols (and colors). The core radius is 0.83, corresponding to 0.53pc assuming a distance of 1.7 kpc for M4. The white stripes are due to gaps between the CCDs of the WFI at 2.2m camera where our astrometry comes from.	18
2.3	Estimated <i>signal – to – noise</i> ratio for each of our spectra (see text). Different symbols indicate stars observed with different exposure times.	22
2.4	The spectrograph GIRAFFE.	24
3.1	In this figure five spectra of the simultaneous calibration flat-field in MEDUSA mode are shown for the high resolution (HR9). The upper graphs show the localization lane over the full CCD field (dispersion direction is strongly compressed) while the three bottom panels show the spectra cross-sections recentered in the localization lane of each spectral bin. Each dot corresponds to a single pixel. The full lane is fitted exponential model of the PSF_{\perp} (Eq. 1).	31
3.2	Localization of the orders.	32

3.3	Plot of the differences between the estimated and the observed positions of the five lamps that are in the frame. This graphics give a goodness of the wavelength calibration: indeed it is possible to notice that this differences are around zero, that means that the calibration are carried out properly.	34
3.4	Schematic layout of the MEDUSA spectral format. Blue solid lines: object fibres. Red dotted lines: calibration fibres. The directions of the increasing fibre number in the slit (FPS) and of increasing wavelength are indicated.	35
3.5	Extracted spectra for three stars with different magnitudes: in the upper panel for a bright star with V magnitude 12, in the middle panel for an intermediate star with V magnitude 14, and in the bottom panel for a faint star with V magnitude 16.	36
4.1	Correlation between the template and the stellar spectra.	38
4.2	Fit of the cross-correlation peak km s^{-1}	39
4.3	Radial velocities as a function of color (upper panel) and magnitude (bottom panel) obtained for our individual spectra. Different colors refer to different epochs. The horizontal line indicates the mean radial velocity (value at the top) of all the stars.	40
4.4	The average radial velocity differences for the simultaneous calibration fibers between the reference plate and all the other plates (Px) plotted as a function of the Modified Julian day. There is a systematic offset in the radial velocity zero point between the two epochs.	41
4.5	Histogram of differences of multiple radial velocity measurements used to evaluate the reliability of our calibrations. In this case no corrections have been applied to our measurements. The upper panel shows the bright stars ($V < 15$) the bottom panel shows the faint stars ($V > 15$). The solids lines are the mean, and the dotted lines are the median. The thick black line mark the position of a null difference.	43
4.6	Histogram of differences of multiple radial velocity measurements used to evaluate the reliability of our calibrations. In this case the shift found in the way described in the text has been applied. In the upper panel we show the results for the bright stars ($V < 15$), the bottom panel for the faint stars ($V > 15$). The solid lines are the mean, and the dotted lines are the median. The thick black line mark the position of a null difference.	44

4.7	<i>Left:</i> Color magnitude diagram of the stars in our photometric catalog. Thick dots indicate the target stars for which we have spectra. <i>Right:</i> For five different magnitude intervals, the histogram of the radial velocity distribution. Note that, in order to increase the statistics, the brightest bin cover a wider range in magnitude.	45
5.1	The weighted rms as a function of the magnitude is shown for all the M4 stars that have been observed in at least two epochs. A large rms is likely to be due to an intrinsic variation of the radial velocity. The solid line connecting $\langle \sigma_{\overline{V_r}} \rangle$ values computed in each magnitude bin is an indication of the precision of the radial velocity measurement for non-variable stars. The dotted lines indicate the 3, 4, and 5 $\langle \sigma_{\overline{V_r}} \rangle$ level. The candidate binaries are indicated with red dots.	49
5.2	Location of the binary candidates large red dots in the CMD. The green triangle indicates a binary candidate found also in the photometric sample (Milone et al. 2008).	52
5.3	Radial distribution of the binary system candidates. The inner circle represents the cluster core. The outer circle indicates the total area of the cluster covered by observations. The dotted circle contains the binaries inside the half mass radius.	53
6.1	Number of simulated binaries found at different values of eccentricity	58
6.2	Histogram of semi axis at different values of eccentricity. The red line is the histogram for all the simulated populations, the black is the histogram for the binaries found in magnitude range of the observations.	59
6.3	Histogram of the logarithm of periods at different values of eccentricity. The red line is the histogram for all the simulated populations, the black is the histogram for the binaries found in magnitude range of the observations.	60
6.4	In this figure we show the scattered plot of radial velocity variation σ_{vr} against the V magnitude for the simulated population whit eccentricity 0: the dotted lines indicate the 3, 4, and 5 $\langle \sigma_{\overline{V_r}} \rangle$ level, the triangles represent the binary candidates with $\sigma_{vr} > 3\sigma$, where sigma is the standard deviation from the observational errors.	61

- 6.5 The same of the previous Figure for the results with a thermal distribution of eccentricities: the dotted lines indicate the 3, 4, and $5 < \sigma_{\sqrt{V_r}} >$ level, the triangles represent the binary candidates with $\sigma_{vr} > 3\sigma$, where sigma is the standard deviation from the observational errors. 62
- 6.6 Cumulative distributions for the observed (dash line), the simulated with e=0 (dot line) and the simulated with thermal distribution of the eccentricities (solid line) of the binary candidates (respectively blue, red and black line in the electronic version . . . 65
- 6.7 This plot represent the Discovery efficiency D_b as a function of the periods (in years) for both the simulations with circular orbits e=0 (black dots) and for thermal distributions $f(e)=2e$ (red triangles). Each point in the plot represents the mean of 500 simulation tries. 66
- 7.1 Comparison of the semi-major axis found in the different simulations that we are dealing with. In the upper panel the result for the Heggie & Giersz, in the middle the result for our Monte Carlo simulation assuming thermal distributions of the eccentricity, and in the bottom panel the result for our Monte Carlo simulation with eccentricity equal to zero. The semi-major axis are in the solar units. 69
- 7.2 Comparison of the periods found in the different simulations that we are dealing with. In the upper panel the result for the Heggie & Giersz, in the middle the result for our Monte Carlo simulation assuming thermal distributions of the eccentricity, and in the bottom panel the result for our Monte Carlo simulation with eccentricity equal to zero. The periods are in years. 70
- 7.3 In this figure we show the plot of radial velocity variation σ_{vr} against the V magnitude for the simulated population of HG: the big dots represent the binary candidates with $\sigma_{vr} > 3\sigma$, where sigma is the standard deviation assuming the observational errors. 71
- 7.4 Cumulative distributions for the observed (dash line), the simulated with e=0 (dot line), the simulated with thermal distribution of the eccentricities (solid line) of the binary candidates and the HG simulations (dash-dot line). 72

- 7.5 The discovery efficiency as a function of the period for the three simulations: the stars represent our Monte Carlo simulation with eccentricity equal to zero, the dots represent our Monte Carlo simulation considering the thermal distribution of the eccentricities, and the triangles represent the HG simulations. 75

1

Introduction

In the first chapter I will explain the importance of studies of the binary systems in globular cluster. Then I will describe the techniques that until now were used to look for binaries and the principal searches carried out in the past years. At the end I will talk about M4 and the reasons which led us to choose M4 as the primary target for this project.

1.1 Evolution of clusters

Globular clusters are on stable equilibrium on a dynamical time scale, characterized by the time needed for a star to cross the half-mass radius, of order of 10^6 yr. However, on a “thermal” time scale, in which individual stars can exchange significant amount of energy, no cluster can achieve stability. At the half mass radius, this two body relaxation time scale lies in the range $10^8 - 10^{10}$ yr, while in a dense core it can have much smaller values. At first, evaporation of the stars causes the core to shrink. A sufficiently high central density causes an increasingly rapid shrinking of the core.

The process of core collapse occurs on a time scale which is only a few times larger than the half mass relaxation time. During and after the collapse, infinite central density can be avoided only when some energy source turns on.

The binaries can increase in binding energy and they can also stop the most dramatic phenomenon in the evolution of a globular cluster.

1.1.1 The negative heat capacity

Let us consider a binary star in a cluster encountering a single star, where the relative speed between the binary and the single star is smaller than the orbital speed in the binary system. When the three stars get close enough to interact,

systems will start to transfer some energy to the single star. At the end of the encounter, one of the three stars will have relative velocity higher than the initial single star had. Since the binary gave up some energy to a star, during the process it became more bound and thus have a larger orbital speed.

This kind of binary is an "hard" system. Hard binaries are defined as having a binding energy $\gg 1kT$, where $(\frac{3}{2})kT$ is the mean stellar kinetic energy. In the equal mass case, a hard binary has an orbital velocity clearly exceeding the velocity dispersion of the system. The other type of binaries are called "soft" and defined as having energy of $\sim 1kT$. The hard binaries tend to become harder as a result of dynamical interaction, instead the other tend to be quickly destroyed by such encounters.

Therefore, in general, the hard primordial binaries will act as an energy source that can support a core of a cluster against collapse through dynamical scattering interactions.

It is possible to make an order of magnitude estimate of the importance of binaries in a cluster.

Let us consider a cluster with N objects, of which f_b are hard binaries. We define the total energy of the cluster E_{ext} and the total binary binding energy E_{int} . The binding energy of a binary with the hardness η is

$$E_b = \eta kT \sim \frac{\eta E_{ext}}{N},$$

and the total internal energy is

$$E_{int} \sim f_b \eta E_{ext}.$$

Since a binary releases energy of order of E_b through the interactions, binaries are important when $f_b \eta \geq 1$.

For instance, for a system with $\eta = 10$ (reasonable value), a binary fraction of $\sim 10\%$ can be enough to unbind a cluster.

1.2 The importance of binary stars in globular clusters

The binary fraction is an important parameter of any stellar population. For dense stellar systems, like the globular clusters, it is also an essential ingredient for realistic models of their dynamical evolution.

The first search for the spectroscopic binary systems in Globular Cluster carried out by Gun & Griffin (1979), led to surprising conclusion that the binaries were much rarer in globular cluster than in the field. This result became difficult to understand in the light of numerical simulations (e.g. Cohn 1980) which demonstrated that, in absence of the additional heat source such as provided

by a population of primordial binaries, most globular clusters should by now have settled into a state of core collapse. In the past years it has been realized that a primordial binary frequency as small as 3% can fundamentally change the dynamical evolution of entire globular cluster (Heggie & Aarseth 1992). Therefore, the frequency of binary systems is one of the key parameters for dynamical models of star clusters (see review by Hut et al. 1992, and references therein).

The second reason is that primordial binaries play a key role in cluster dynamics (see the previous section). In fact, interactions between binary stars play the same role as nuclear reactions in stars. The core collapse is the most dramatic phenomenon in the evolution of globular clusters. It corresponds to the pre-main sequence stage of stellar evolution, when the energy losses from the photosphere are not yet balanced by nuclear energy generation in the center. In contrast, during the post collapse evolution of a star cluster some form of central energy source turns on, which make up for the energy lost through conduction and evaporation of stars from the central regions. In other words, the role of the binaries is to prevent collapse of the central core, just as nuclear energy sustains a star in near-equilibrium.

At one time it was thought that binaries would first form in high densities reached at the end of core collapse, heralding a succession of core oscillations as the cluster steadily loose stars across the galactic tidal boundary. The discovery of primordial binaries dramatically changed this picture. Idealized theoretical modeling showed that primordial binaries would segregate to the core, soon dominating the dynamical interactions there. Hardening of binaries in the core would halt core collapse at much lower central densities, leading to a long near-equilibrium phase while stars escape over the tidal boundary (Meylan & Heggie 1997). Therefore the binaries fraction seems to be a key parameter for determining the dynamical evolution of a globular cluster.

Until now observational limitations prevented any test of this picture, and yet it raises a paradox: why are any post-collapse clusters observed at all, if binaries prevent deep core collapse? For example, M4, our target, shows no evidence for any central brightness cusp (Trager et al. 1995), despite the fact that its age exceeds its central relaxation time (Harris 1996) by a factor ~ 400 . Is the lack of evidence of core collapse due to the presence of a large fraction of binaries? And let us compare M4 with NGC6397. NGC6397 has a mass, relaxation time and orbit similar to those of M4. Therefore it should be at a similar stage of its evolution, and yet it has a completely different structure with a collapsed core. Is this due to a lack of primordial binaries?

The last reason is that the encounters between binaries and other stars or binaries can not only profoundly affect the dynamical evolution of the clusters:

they can disrupt the widely separated binaries and catalyze the formation of exotic objects such as blue stragglers, X-ray binaries and millisecond pulsars. In fact, exchange interactions between hard primordial binaries and neutron stars inevitably produce large numbers of X-ray binaries and recycled pulsar in globular clusters (Hut, Murphy & Verbunt 1991, Rasio, Pfahl & Rappaport 2000). Resonant interactions of primordial binaries result in dramatically increased collision rate from main sequence stars in globular clusters and even open clusters. Direct observational evidence for stellar collisions and mergers of main sequence stars in globular clusters comes from the detection of large numbers of bright blue stragglers concentrated in dense cluster cores.

1.3 Techniques to find binary systems

There are three basic search techniques for binary systems in a star cluster: (i) photometric study of the so-called secondary sequence in the color-magnitude diagram created by the superposition of two main sequence stars (e.g. Bellazzini et al. 2002, Sollima et al. 2007, Milone et al. 2008). (ii) the study of the light curves of eclipsing binaries (e.g. Yan & Mateo 1994, Albrow et al. 2001, Kaluzny et al. 2008); and (iii) the search for spectroscopic radial velocity variations of the stars at different epochs (e.g. Côté & Fischer 1996, Pryor et al. 1988, Côté et al. 1996). In the next few paragraphs I will briefly describe these techniques and the search carried out until now.

1.3.1 Binaries in the Color-Magnitude Diagram

Over the past few years, technological knowledge advances have allowed deep stars counts to be obtained with high photometry accuracy, allowing the full two dimensional distribution of the CMD to be exploited. Variations in metallicity, age dispersion, and unresolved binaries all contribute to the shape of the main sequence. Since a binary system combines the light from two stars, the object will appear on the CMD in a different location from the primary alone. For instance, if both main-sequence members of a binary system have the same mass and therefore the same color and luminosity, the CMD for a cluster with a population of binary is simple: the binaries give rise to a sequence with identical color but brightened by $2.5 \log 2 = 0.75 \text{mag}$ because of the factor of 2 larger luminosity. On the other hand, if one member of the binary system has a much smaller luminosity than the primary, the CMD appears to be only a slightly wider than for single stars alone. In Table 1 I summarize a list of all the published photometric binary star investigations: the first column gives the name of the globular cluster, the second the binary fraction found and in the

TABLE 1.1— Literature photometric binary fraction.

Globular Cluster ID	f	reference
NGC288	0.15 ± 0.015	Bellazzini et al. (2002)
	> 0.06	Sollima et al. (2007)
NGC2808	0.02 ± 0.04	Alcaino et al. (1998)
NGC4590	> 0.09	Sollima et al. (2007)
NGC5053	> 0.08	Sollima et al. (2007)
NGC5466	> 0.08	Sollima et al. (2007)
NGC5897	> 0.07	Sollima et al. (2007)
NGC6101	> 0.09	Sollima et al. (2007)
NGC6362	> 0.06	Sollima et al. (2007)
NGC6397	< 0.06	Cool & Bolton (2002)
NGC6723	> 0.10	Sollima et al. (2007)
NGC6981	> 0.10	Sollima et al. (2007)
M15	~ 0.07	Gebhardt et al. (1994)
M55	> 0.06	Sollima et al. (2007)
M92	0.00	Anderson (1997)
ARP 2	> 0.08	Sollima et al. (2007)
Terzan 7	> 0.21	Sollima et al. (2007)
Palmoar 13	0.30 ± 0.04	Clark et al. (2004)
47 Tucanae	0.14 ± 0.04	Albrow et al. (2001)
	> 0.05	de Marchi & Paresce (1995)
	~ 0.02	Anderson (1997)
ω Cen	< 0.05	Elson et al. (1995)
M4	0.10	Milone et al (2008)

last the literature reference.

1.3.2 Eclipsing binaries

Eclipsing binary stars appear as a single point of light to an observer, but based on their brightness variation and spectroscopic observations we can say for certain that the single point of light is actually two stars in close orbit around one another. When the orbital plane of a binary is nearly parallel to an observer's line of sight (i.e. with an inclination of $i \simeq 90^\circ$), the binary components will be seen periodically eclipsing one another. If such system is fortuitously so aligned with respect to Earth, it is termed as eclipsing binary (EB). The observed fraction is biased downwards by the fact that many EBs have very long orbital

TABLE 1.2— Some example of literature eclipsing binary fraction.

Globular Cluster	f_b	reference
M71	10-72%	Yan & Mateo (1994)
M5	22-39%	Yan & Reid (1996)
47Tuc	13%	Albrow et al. (2001)
M4	~ 0.05	Ferdam et al. (2004)

periods and shallow eclipses, making them difficult to identify. The most direct way to detect EBs is by compiling a series of multi-epoch photometric observations of stars, thus monitoring how their brightness changes as a function of time. These time series are called light curves.

EBs are generally divided in three classes according to the shape of their light curve: Algol-type, β Lyrae-type, and W Ursae Majoris-type variables. Algol-type variables (EA) are EBs whose brightness remains almost constant between eclipses. In this type of EB, the eclipse duration is a small fraction of the binary's orbital period, indicating that the binary components are detached from one another. In contrast, β Lyrae-type variables vary their brightness continuously between eclipses, indicating that their components are sufficiently close to bring about significant tidal distortions. Finally, W Ursae Majoris-type are similar to β Lyrae variables in that their brightness varies continuously, however these variables are nearly identical, indicating that the components have similar temperatures.

In Table 2 are presented some of the representative searches for eclipsing binaries.

1.3.3 Radial velocity variables

Spectroscopic binaries are pairs of stars which are too close to each other to be seen from the earth as resolved into two stars. The only way to identify the multiplicity of these systems is by the radial velocity variations of these stars in different epochs. Until now there have been few searches for binary stars in globular clusters through spectroscopic observations of radial velocity variations. In particular, most of the previous work has been limited either to bright red giant branch stars (e.g. M22 observations by Côté et al. 1996), or, due to the relatively low multiplex capabilities of instruments, to a relatively small number of stars per cluster (e.g. Yan & Cohen 1996; Côté & Fischer 1996). A list of all the published spectroscopic binary star investigations is shown in Table 1.3: the first column gives the name of the globular cluster, the second

column the number of stars considered, the third one the number of binary candidates found, and the last one the literature reference.

Here I will described in more details the searches mentioned in the table 1.3.

Gunn & Griffin were the first to study the binary stars by the radial velocities variations. They obtain a total of 85 velocity measurements for 33 giants stars with V magnitude between 12 and 14. They did not discover any velocity variations for these stars, therefore they argued that the binaries with separation between 0.3–10 AU (i.e. periods 0.1–30 yr) were much rarer in globular cluster than in the field population I.

An other important study to search binaries during the early 1980s was that of Mayor et al. (1984). They observed 169 giant stars in 47 Tucanae, and measured their velocities with an accuracy of 0.6 km s^{-1} . Of these, 64 cluster members had two observations separated by more than 200 days. As in M3 sample, they didn't discover any binary systems.

In the mid-1980s, spectroscopic binaries were discovered in a number of globular cluster by the CORAVEL group and by a group using a Dominion Astrophysical Observatory radial velocity spectrometer on the Canada-France-Hawaii Telescope (Pryor et al. 1989). The data consisted of 1253 velocities for 393 giants in the globular cluster 47 Tucanae, M2, M3, M71, M13 and M12. They found six binary candidates.

In 1988, combining Gunn & Griffin's data in M3 with new MMT observations, Pryor et al produced a larger dataset containing 111 giant stars, each with three multiple measurements over a timespan of more than ten years and with a typical accuracy of 0.9 km s^{-1} . They found one binary candidate, which later was confirmed as a system with a period of 7.3 yr.

In 1994 Côté et al. published a similar survey in the globular cluster NGC 3201. A total of 786 velocities were obtained for 276 giant stars with V magnitude of 11-16.5 over a total timespan of 6 yr. They found 2 good binary candidates, plus 13 possible candidates, and the derived binary frequency was 5% – 18%. The most complete spectroscopic binary-search in M4 is by Côté & Fischer (1996), who analyzed 33 turn-off dwarf stars. Their observations were tuned to search for ultra-hard binaries on the main sequence of the cluster. From the observed variability of two stars, they conclude that the best-fit binary fraction in this cluster is $15 \pm 15\%$.

In this work we analyze several thousand stars in order to estimate of the binary fraction in M4 on a firmer ground. We did not observe any stars in common with their.

In another work Côté et al. (1996) discussed the results on the search for spectroscopic binaries in M22. Based on the radial velocity measurements of 92 red giant stars ($10.8 < V < 14$) which span for more than two decades the

binary fraction found is $f_b = 1 - 3\%$. It is of interest to notice that in this paper the authors wanted to understand if it is possible to find some evidence for the disruption of the soft binaries in the radial velocity surveys alone. By the comparison of the results found in all the other spectroscopic surveys done until that moment, they concluded that the radial velocity survey alone point to a frequency-period distribution in which binaries with periods in excess of “hard-soft transition” have been disrupted by stellar encounter.

In 1996 Yan & Cohen carried out a radial velocity survey to search binaries in a low density globular cluster NGC 5053. They observed 77 giant and subgiant stars in the V magnitude range of 14.5 and 18.6, of which 66 had on average of 3 or 4 measurements with a total of 236 velocities. In this sample they found 6 binary candidates.

In the same year Barden et al. carried out a study of 121 red giant stars ($12.5 < V < 17.2$) of the globular cluster M71 in 4 different epochs obtaining a total of 794 radial velocity measurements. They discovered a total of 12 binary candidates.

In 2002 Odenkirchen et. al. studied 18 giant stars in Pal 5, and discovered only one binary candidate.

Moni Bidin et al. 2006 observed a sample of 51 hot horizontal branch stars in five consecutive nights. They did not find any binary system among these stars.

1.3.4 Comparison between binary search techniques

All three methods have some advantages and some limitations. For instance, the photometric study has the advantage of needing only one observational campaign, but it cannot constrain the orbital parameters. On the other hand, the search for eclipsing binaries is sensitive only to systems with periods less than 10 days (Mateo 1993), and moreover it has some limitations given by the inclination of the systems, and it requires multi-epoch observations. The latter limitation is common to the spectroscopic search for velocity variations. However, this method has important advantages over the last two, because it allows to determine orbital period and the eccentricity in an unbiased way. Observational constraints of the period distribution for binary systems are interesting, not only because dynamical processes preferentially eliminate the wider systems (Heggie 1975, Hut 1983), but also because when the period is known it is possible to discriminate between tidal capture and primordial binaries and give some constraints on the system’s mass.

TABLE 1.3— Previous spectroscopic binary star investigations.

Globular Cluster ID	number target	number binary	reference
M3	33	0	Gunn & Griffin (1979)
47 Tuc	64	0	Mayor et al. (1984)
M3	111	1	Pryor et al. (1988)
47 Tuc,M2,M3,M12,M13,M71	393	6	Pryor et al. (1989)
NGC 3201	276	2	Côté et al. (1994)
NGC 5053	66	6	Yan & Choen (1996)
M71	121	12	Barden et al. (1996)
M22	109	1	Côté et al. (1996)
M4	33	2	Côté et al. (1996)
Pal 5	18	1	Odenkirchen et. al. (2002)
NGC 6752	51	0	Moni Bidin et al. (2006)
M4	2469	57	Sommariva et al. (2008)

1.4 Other types of binaries

1.4.1 Cataclysmic variables

Cataclysmic variables (CVs) are white dwarfs accreting matter from a companion that is usually a dwarf star or another white dwarf. They have been detected in globular clusters through identification of the white dwarf itself or through evidence of the accretion process (Margon et al. 1981, Paresce & de Marchi 1994, Bond et al. 2005). White dwarfs managed to avoid detection until observations with the Hubble Space Telescope revealed photometric sequences in several globular clusters. Spectral identification of white dwarfs in globular clusters has begun both from the ground with the VLT (Moehler et al. 2000, Moehler et al. 2004) and in space with the Hubble Space Telescope (Shara et al. 1996, Anderson et al. 2003). With spectral identification, it will be possible to identify those white dwarfs in hard binaries through Doppler shifts in the $H\beta$ line. This approach has promise for detecting a large number of the expected double white dwarf binaries in globular clusters. Photometry has also begun to reveal orbital periods of CVs in globular clusters. A more productive approach has been to look for direct evidence of the accretion around the white dwarf (Ferraro et al. 2001, Dieball et al. 2005). This can be in the form of excess UV emission and strong $H\alpha$ emission from the accretion disk. The accretion disk can also be discerned by very soft X-ray emissions.

1.4.2 Low-mass X-ray binaries

X-ray binaries belong to the systems in which a compact object and a stellar companion orbit each other at a distance small enough to enable a mass transfer from the companion star onto the compact object.

Those X-ray binaries containing a neutron star or a black hole can be divided into two classes based on the mass of the companion star: the high mass X-ray binaries (HMXBs) having a stellar companion usually more massive than $10M_{\odot}$, and the low mass X-ray binaries (LMXBs) having a stellar companion with a mass around $1M_{\odot}$ or less. In HMXBs the mass transfer is caused by the stellar wind of the companion star, while in the LMXBs Roche lobe overflow is responsible for the mass transfer through the inner Lagrange point L_1 .

Because both binary components orbit each other, and because of the conservation of the angular momentum, the transferred mass is not able to fall straight to the compact object and therefore forms a disk in which matter spirals inwards (called accretion disk) transporting its angular momentum outward by friction and viscosity. Due to the large amounts of gravitational energy (up to several $10^{38} \text{ ergs}^{-1}$) that are released by this accretion, matter is heated up to $\sim 10^7$ Kelvin which is enough for thermal X-ray emission; in fact X-ray binaries are the brightest X-ray sources in the sky.

1.4.3 Millisecond pulsars

Pulsars are highly magnetized, rotating neutron stars which emit a narrow radio beam along the magnetic dipole axis. As the magnetic axis is inclined to the rotation axis, the pulsar acts like a cosmic light-hose emitting a radio pulse that can be detected once per rotation period when the beam is directed towards earth. There is a type of pulsars, the so-called millisecond pulsars, that are very fast rotating, have very small periods (of the order of milliseconds), and appear much older than ordinary pulsars. A model for their evolution history suggests that the millisecond periods are obtained when mass and thereby angular momentum is transferred from an evolving binary companion while it overflows its Roche lobe. In this model, millisecond pulsars are recycled from a dead binary pulsar via an X-ray binary phase.

This model implies a number of observational consequences: for instance, for surviving binary systems, X-ray binary pulsars represent the progenitor systems for millisecond pulsars, the final spin period of recycled pulsars depends on the mass of the binary companion. A more massive companion evolves faster, limiting the duration of the accretion process, and the majority of millisecond pulsars have low-mass white-dwarf companions as the remnant of the binary star. These systems evolve from low-mass X-ray binary systems (LMXBs); e)

high-mass X-ray binary systems (HMXBs) represent the progenitors for double neutron star systems (DNSs). DNSs are rare since these systems need to survive a second supernova explosion. The resulting millisecond pulsar is only mildly recycled with a period of tens of millisecond. The properties of millisecond pulsars and X-ray binaries are consistent with the described picture. For instance, it is striking that $\sim 80\%$ of all millisecond pulsars are in a binary orbit while this is true for only less than 1% of the non-recycled population. For millisecond pulsars with a low-mass white dwarf companion the orbit is nearly circular. In case of double neutron star systems, the orbit is affected by the unpredictable nature of the kick imparted onto the newly born neutron star in the asymmetric supernova explosion of the companion. If the system survives, the result is typically an eccentric orbit with an orbital period of a few hours. Lyne et al. in 1988 discovered a millisecond pulsar (PSR162026) in M4. It was the fifth millisecond pulsar to be found, and the second in a globular cluster.

1.5 The Galactic Globular Cluster M4 (NGC6121)

Messier 4 (M4, NGC 6121) is one of the nearest globular clusters in the sky at an estimated distance of about 1.7 kpc (Peterson et al 2005). Situated prominently about 1.3 degrees west of Antares, in constellation Scorpius, and being as bright as mag 5.6 visually, it can be detected by the naked eye under very dark skies, and is prominent with the small optical aid.

Globular cluster M4 was discovered by De Chseaux in 1745-46 and listed by him as No. 19, and included in Lacaille's catalog as Lacaille I.9. Charles Messier cataloged it on May 8, 1764 and was the first to resolve it into a "cluster of very small [faint] stars;" this is the only globular cluster he could resolve with his moderate instruments, and thus the first globular cluster ever to be resolved. Only about 20 years later, William Herschel was able to resolve all Messier globulars with his large telescopes.

M4 is a globular cluster of moderately low concentration. It also harbors an hierarchical triple pulsar system (Rasio et al. 1995), the first triple star ever detected in a globular cluster. These facts combine to make M4 a promising target for an extensive investigation of its population and dynamical properties. As I already said above, M4 falls near the Sc0-Oph clouds, and so is rather heavily reddened.

Table 1.4 shown the fundamental parameters of M4.

1.5.1 Why we choose M4

We choose M4 as a first target for this kind of project for several reasons. First of all it shows no evidence for any central brightness cusp (Trager et al.

TABLE 1.4— The fundamental parameters of M4.

Parameter	<i>Value</i>	<i>Ref.</i>
$(\alpha, \delta)_{J2000.0}$	$(16^h 23^m 35.5^s, -26^\circ 31' 31'')$	1
$(\ell, b)_{J2000.0}$	$(350^\circ.97, 15^\circ.97)$	1
distance	1.7 kpc	2
core radius r_c	0.53pc	3
half mass radius r_h	2.3pc	3
tidal radius	21pc	3
[Fe/H]	-1.07	4
Present-day Total Mass	63,000 M_\odot	5
Age	12Gyr	6
Radial velocity	70.29 kms ⁻¹	7

¹ Djorgovski & Meylan (1993)

² Peterson et al. (1995)

³ Trager et al. (1993)

⁴ Marino et al. (2008)

⁵ Richer et al. (2004)

⁶ Hansen et al. (2004)

⁷ This work

1995) indicative of core collapse, despite the fact that the cluster age exceeds its central relaxation time (Harris 1996) by a factor of approximately 400. On this basis, M4 should now be in the post-collapse phase of its evolution. As I already suggest above, probably this behavior is due to the presence of binaries in the core of M4.

Additional reasons which make M4 our first priority target are that it has an extended (relatively uncrowded) core, making feasible the search for binaries with a multifiber facility as FLAMES@VLT, where the portion of binaries should be highest.

Moreover, M4 is the cluster closest to the Sun, which enables us to study the binaries below the turn-off, and these are pristine tracers, as binaries containing

giants might be destroyed by internal mass transfer (a prediction that we want to check by observing a few hundred giants).

And more, M4 was chosen as a target by an international collaboration, MODEST (Modeling of Dense Stellar System), within which experts on stellar dynamics, stellar evolution, and observers have joined their efforts for a comprehensive study of the origin and evolution of star clusters.

The aim of this investigation is to test the theoretical picture for the first time against observations. This is a fundamental test of our current understanding of the problem, and vital input for future theoretical research. In fact, the advent of dedicated machines like the GRAPEs (Hut & Makino 1999), already allows realistic N-body modelling of (open) star clusters with up to 5×10^4 particles (Portegies Zwart et al. 2004). In a few years from now, with GRAPE-DR, realistic N-body modeling of GC with up to 5×10^5 particles (like the estimated original number of stars in M4 and NGC6397, which makes these two clusters the ideal test beds) will be feasible. At that point, observational inputs, and the comparison of the model with the observed parameters will become of fundamental importance for our understanding of the evolution of the GC, similarly to what happens when we compare stellar evolution models with observed color-magnitude diagrams and luminosity functions.

In order to make realistic models, a number of observational data are needed. Most of them are already available for M4, including mass functions at different radial distances, the proper motion and the radial velocity information. This work provides significant improvement to the latter. Only the fundamental information on its binary population is missing. The ultimate goal of the present study is to establish the frequency of binary systems in M4, and to determine their radial distribution within the cluster. These two quantities are intimately linked to the internal dynamics of the cluster.

Comparing the current binary frequency in the cluster with the results of dynamical modeling, it is then possible to infer important constraints on the primordial binary population.

Heggie & Giersz (2008) recently constructed a dynamical evolutionary model for M4. It is based on a Monte Carlo simulation including an appropriate stellar initial mass function, a primordial binary population, galactic tidal effects, synthetic stellar and binary evolution, relaxation, and three- and four-body interactions. The most surprising discovery from this model was that M4 was found to be a post-collapse cluster sustained by binary burning. The model provides also detailed predictions for the period and spatial distribution of binary systems.

2

Observations and FLAMES

2.1 Description of the observations

In July 2003, we collected a single spectrum for 2684 stars in the Galactic Globular Cluster M4 (NGC6121). The main purpose of this original project (ESO-program 71.D-0205) was the study of the internal velocity dispersion field of M4. In the following, we will refer to these observations as the first epoch (epoch I). For 2469 stars observed in the first epoch we obtained a second spectrum between July and September 2006 (epoch II) under ESO-program 77.D-0182 with the aim of measuring radial velocity variations for those stars in order to identify binary candidates.

In addition to these, for a subsample of 364 stars, mainly in the core of the cluster, we collected a third epoch (epoch III), separated by ~ 5 weeks from epoch II, with the intent of detecting short-period binaries.

All data were obtained with the high resolution spectrograph *FLAMES* + *GIRAFFE* at the VLT (Pasquini et al. 2000). FLAMES is the Fibre Large Array Multi Element Spectrograph mounted at the Nasmyth A platform of the 8.2m Kueyen (UT2) telescope, which is part of the Very Large Telescope (VLT) of the European Southern Observatory (ESO) situated on Cerro Paranal. With FLAMES in MEDUSA mode it is possible to observe up to 132 targets at the same time over a field of view of 25 arcmin diameter.

The fibers are accurately placed with the aid of magnetic buttons on a metallic plate (two plates are available at any time: one in place, and the other preparing the buttons for the next pointing). In the next section we will describe in details the instrumentation. During epoch I twenty five plates were collected, during epoch II in addition to the same number of plates, three plates with stars placed mainly in the core were taken. These three plates have been

repeated during epoch III.

The GIRAFFE spectrograph operates at resolutions $R=6,000-48,000$ across the entire visible range, 360–940 nm. It is equipped with two gratings, high (HR) and low (LR) resolution and with a single $2K \times 4K$ EEV CCD (15 μm pixels).

In total 5973 spectra were collected in three different epochs from the red giant tip to below the Turn–Off (TO). Our sample covers most of the cluster extension, from the inner core out to the cluster outskirts. For 2469 stars we have spectra in two epochs; for a subsample of 484 stars, we have three epochs. For 34 stars we obtained also a fourth epoch. This is due to the fact that together with the 364 stars in the core for which we obtained the third epoch (three repeated plates), we observed an additional 120 stars randomly selected among the targets of epoch II. These repeated stars will provide important cross-checks of the registration of different plates to a common radial velocity system.

Epochs I and II have the purpose of detecting mainly soft-binary candidates with periods up to few years from the cluster center to its outskirts. Epoch III was taken a few weeks after epoch II with the purpose of identifying hard binaries with periods up to a few weeks inside the cluster core, where binaries are expected to be more numerous because of mass-segregation.

All stars, at all epochs, were selected from our astrometric and photometric catalog (Anderson et al. 2006) with the following criterion: each star at any given magnitude V had no neighbors brighter than a magnitude $V + 2.5$ within an angular distance of 1.2 arcsec (for comparison, the radius of the fibre correspond to only 0.6 arcsec). The catalogue is based on Wide Field Imager (WFI) data from the ESO/MPIA 2.2m telescope, and has astrometric internal precision of $\sim 7\text{mas}$. More recently the photometry has been revised by Momany (private communication). Therefore we decided to use that photometry in the following. The target stars are shown as thick (red) points color-magnitude diagram presented in Fig.1.

All stars were observed with HR9 setup (514.3-535.6nm) centered at 525.8nm. This instrumental configuration offers high resolution ($R = 25,800$) and the best radial velocity accuracy (Royer et al. 2002). This setup covers 200 Å, and a CCD pixel corresponds to 0.05 Å. It provides the best compromise in terms of signal-to-noise ratio (SNR) achievable for red giant stars and the number of spectral lines necessary for accurate Doppler measurements.

The stars were grouped in three different subsample centered at $V = 16.5$, 17, and 17.5, and their spectra were collected with an exposure time of 1200s, 1500s, and 1800s, respectively, in order to guarantee that each spectrum has a minimum $\text{SNR}=10$. On the basis of previous experience with previous M4 ob-

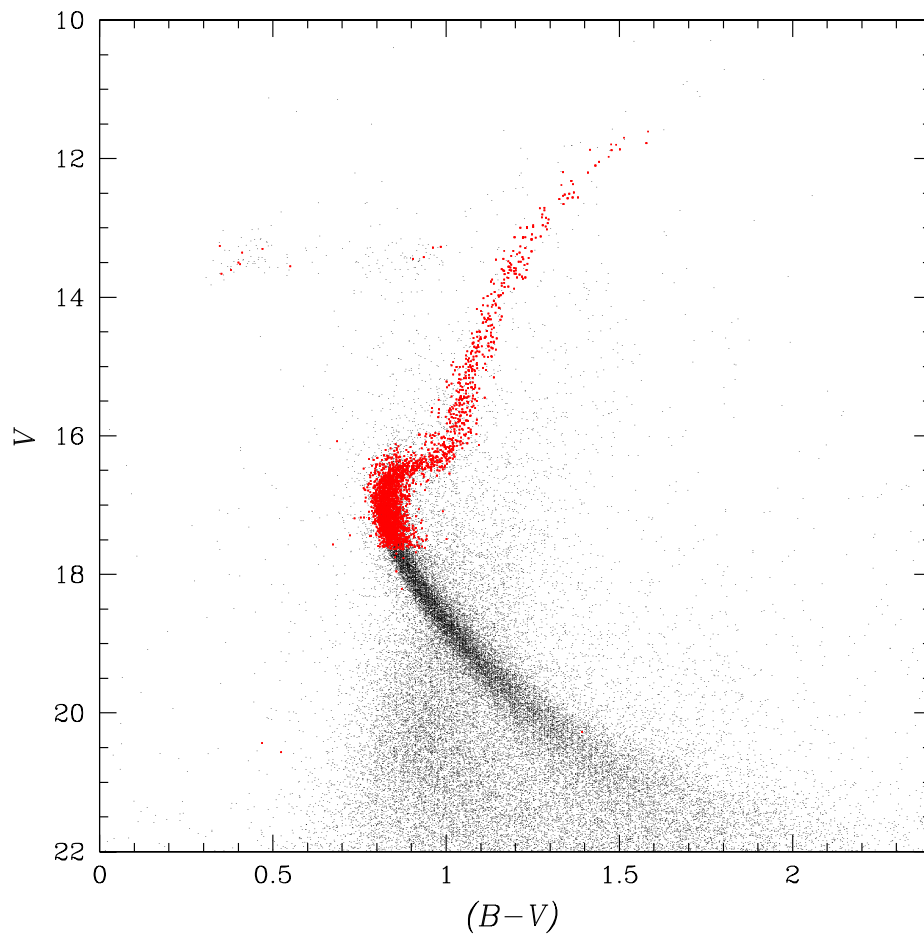


FIGURE 2.1— Small dots show the color-magnitude diagram for all the stars in our astrophotometric catalog. The stars highlighted with thick dots (in red in the electronic version) are the stars for which we have collected spectra.

servations and the GIRAFFE pipeline, this is the minimum signal to noise ratio that we need to reach the required radial velocity precision of a few hundreds m/s.

Figure 2 shows the positions of the target stars with respect to the cluster center. In our observational strategy we covered all the isolated bright stars in the FLAMES field of view. Table 1 contains the list of all the plates used for the present work. The first column lists the plate ID (which, according to

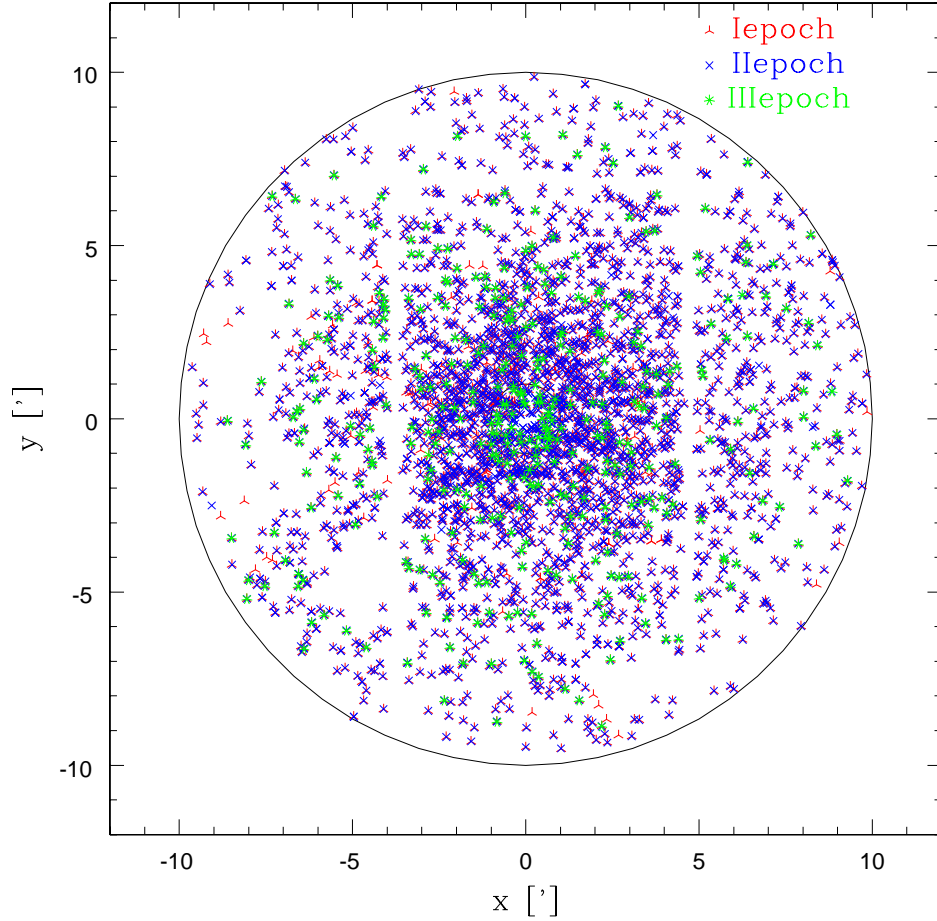


FIGURE 2.2— Spatial distribution of the target stars with respect to the center reported in Tab. 1. The coordinates are given in arcminutes. Observations from different epochs are shown with different symbols (and colors). The core radius is 0.83, corresponding to 0.53pc assuming a distance of 1.7 kpc for M4. The white stripes are due to gaps between the CCDs of the WFI at 2.2m camera where our astrometry comes from.

ESO file naming convention, contains also the time and date of the exposure start), the second column contains the exposure times, and the third one gives the value of the air mass during the observation. The last column reports the seeing as measured by DIMM, the ESO seeing monitor in Paranal.

Figure 3 displays the value of the signal to noise ratio for all our spectra as a function of the visual magnitude. To estimate the SNR we selected three

regions of the spectrum dominated by the continuum, and took the average of the three vales of SNR determined with the IRAF¹ `splot` task. Inspection of the spectra confirms these values to be consistent with the Poisson noise associated with object+sky signal. In the figure the asterisks indicate the stars observed with 1200s exposures, the squares the stars observed with 1500s exposures, and the three point stars the stars observed with 1800s exposure.

2.2 FLAMES

FLAMES (Fiber Large Array Multi-Element Spectrograph) is the multi-object, intermediate and high resolution spectrograph of the VLT. Mounted at UT2, FLAMES can access targets over a field of view 25 arcmin in diameter. FLAMES feeds two different spectrograph covering the whole visual spectral range: GIRAFFE, a medium-high spectrograph, and UVES (Ultra-violet Visual Echelle Spectrograph), a high resolution spectrograph, located at the Nasmyth B platform. It consists of five principal component:

- The Nasmyth corrector which provides at high quality image over a field of view of 25 arcmin.
- a fiber link to the red arm of the high-resolution UVES spectrograph.
- a medium-high resolution optical spectrograph, GIRAFFE, fed by three types of fiber systems
- a Fiber Positioner (also know as OzPoz)
- a fiber system which connects two of the plate of GIRAFFE and to red arm of UVES

Obviously such a complex system needs a rather sophisticated central control, capable of interacting with the VLT and of coordinates the simultaneous observations. This is FLAMES Observing Software (OS).

FLAMES is the ideal instrument for this kind of study thanks to the large field of view, the high multiplex capability, the precision in radial velocities and the faint magnitudes that it can reach.

For this project the ability to register the radial velocities of stars into a common reference system is a crucial issue. Any unexpected systematic error between epochs would introduce serious limits to the accuracy of the radial velocity

¹IRAF (Image Reduction and Analysis Facility) is distributed by the National Optical Astronomy Observatories, which are operated by the Association of Universities for Research in Astronomy, Inc., under cooperative agreement with the National Science Foundation.

Plate ID [archive name]	Exp. [s]	airmass sec(z)	Seeing ["]
epoch I			
GIRAF.2003-06-01T01:55:28	1200	1.213	0.8
GIRAF.2003-06-29T02:49:33	1200	1.002	0.6
GIRAF.2003-07-02T05:11:52	1200	1.256	1.3
GIRAF.2003-07-09T04:27:48	1200	1.200	0.7
GIRAF.2003-07-09T04:59:48	1200	1.318	0.6
GIRAF.2003-07-09T05:41:10	1200	1.548	0.7
GIRAF.2003-07-09T06:22:54	1200	1.935	0.6
GIRAF.2003-07-20T04:56:23	1200	1.538	0.6
GIRAF.2003-07-08T03:32:29	1500	1.066	0.7
GIRAF.2003-07-08T04:09:32	1500	1.139	0.7
GIRAF.2003-07-08T04:51:48	1500	1.269	0.6
GIRAF.2003-07-08T05:31:32	1500	1.461	0.7
GIRAF.2003-07-08T06:13:11	1500	1.785	0.7
GIRAF.2003-07-21T04:07:03	1500	1.295	0.5
GIRAF.2003-07-22T03:49:21	1500	1.242	0.5
GIRAF.2003-07-22T04:24:29	1500	1.394	0.5
GIRAF.2003-07-07T04:25:37	1800	1.170	1.3
GIRAF.2003-07-20T01:42:22	1800	1.006	0.9
GIRAF.2003-07-20T03:33:25	1800	1.167	0.9
GIRAF.2003-07-20T04:16:24	1800	1.318	0.7
GIRAF.2003-07-21T01:54:33	1800	1.015	0.7
GIRAF.2003-07-21T02:40:59	1800	1.066	0.8
GIRAF.2003-07-21T03:25:57	1800	1.158	0.4
GIRAF.2003-07-21T04:50:01	1800	1.522	0.6
GIRAF.2003-07-22T02:02:22	1800	1.024	0.5

TABLE 2.1— Summary of the observations. Repeated plates between epoch II and epoch III are marked with an *.

Plate ID [archive name]	Exp. [s]	airmass sec(z)	Seeing ["]
epoch II			
* GIRAF.2006-07-31T01:34:42	1200	1.032	0.8
GIRAF.2006-09-04T23:24:34	1200	1.045	0.8
GIRAF.2006-09-04T23:59:28	1200	1.101	0.9
GIRAF.2006-09-05T01:24:01	1200	1.380	1.0
GIRAF.2006-09-05T00:50:39	1200	1.238	0.9
GIRAF.2006-09-06T00:53:35	1200	1.264	0.8
GIRAF.2006-09-06T02:10:30	1200	1.728	0.8
* GIRAF.2006-07-31T02:09:45	1500	1.080	0.8
GIRAF.2006-08-01T23:28:08	1500	1.025	0.9
GIRAF.2006-08-02T01:12:13	1500	1.019	0.8
GIRAF.2006-08-02T01:52:06	1500	1.064	0.7
GIRAF.2006-08-02T02:27:43	1500	1.132	0.7
GIRAF.2006-08-02T03:03:13	1500	1.234	0.8
GIRAF.2006-09-04T01:04:04	1500	1.274	0.8
GIRAF.2006-09-04T00:20:55	1500	1.139	0.8
GIRAF.2006-09-05T02:01:48	1500	1.620	0.9
* GIRAF.2006-07-31T02:48:50	1800	1.166	0.8
GIRAF.2006-07-31T03:38:40	1800	1.346	0.7
GIRAF.2006-08-10T00:25:57	1800	1.009	1.4
GIRAF.2006-09-03T23:40:14	1800	1.061	1.6
GIRAF.2006-09-06T00:11:51	1800	1.137	0.6
GIRAF.2006-09-06T01:28:52	1800	1.427	1.0
GIRAF.2006-09-07T01:08:31	1800	1.343	1.0
GIRAF.2006-09-14T23:55:17	1800	1.187	1.1
GIRAF.2006-09-15T23:54:20	1800	1.196	1.2
GIRAF.2006-09-16T23:56:54	1800	1.216	0.9
GIRAF.2006-09-17T00:37:45	1800	1.384	1.0
GIRAF.2006-09-18T00:02:53	1800	1.251	0.8
epoch III			
* GIRAF.2006-09-05T23:39:26	1200	1.394	1.3
* GIRAF.2006-09-05T02:37:05	1500	1.072	1.1
* GIRAF.2006-09-06T23:45:30	1800	1.190	1.0

TABLE 2.1— continue.

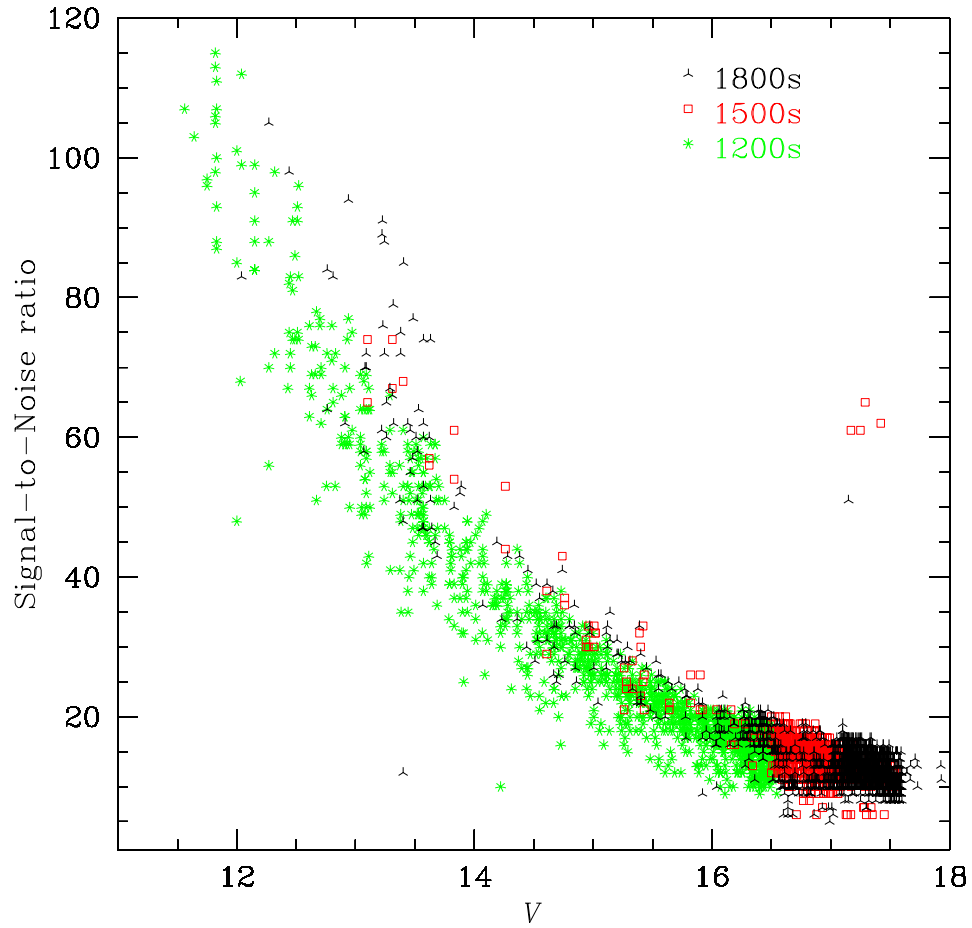


FIGURE 2.3— Estimated *signal-to-noise* ratio for each of our spectra (see text). Different symbols indicate stars observed with different exposure times.

variations that we could see. For this reason during our observations we implemented simultaneous calibrations using the Th-Ar lamp.

In the next subsections I will briefly describe the main component of FLAMES.

2.2.1 The field corrector

The first optical component is the Nasmyth corrector.

The Nasmyth corrector is a system of lenses that allows the exploitation of the full 25 arcmin diameter field of view of the Nasmyth focus of the VLT. The

diameter of the lenses is approximately 90 cm. The selected lens material is equivalent to BK7 with a single layer MgF2 coating guaranteeing a very good transmission over the whole 370-1400 nm range.

The corrector has three main purpose: to improve the field aberrations, to reduce the field curvature and to provide a concentric exit pupil to the field curvature. The corrector configuration providing an image quality better than 0.15 arcsec over the whole field of view.

The corrector is mounted on a mechanical structure which serves two purposes: 1) to attach the corrector to the Nasmyth adapter and 2) to support the positioner plate during observations.

2.2.2 UVES

UVES is the high resolution spectrograph of the VLT, located at the B Nasmyth platform of Kueyen.

UVES has been designed to work in long slit mode, but thanks to a rather small modification, it was possible to add a fibre mode on its red arm. The fibres are injected just before the slit through a projector, which changes the F/3 fibre exit to the F/10 UVES aperture.

Each positioner plate has 8 fibres connected to the Red Arm of UVES. With an aperture on the sky of 1.0 arcsec, the fibres projects on 5 UVES pixels resulting in a resolving power $R=47000$. Only three standard UVES setups are offered, with central wavelengths of 520 nm, 580 nm, and 860 nm. All 16 fibres coming from the two positioner plates are mounted on two parallel slits.

In addition to the 8 fibres per plate, an extra fibre is available for simultaneous calibration. This fibre is used to obtain very accurate radial velocities with UVES with the method pioneered by the Geneva group. However, due to the large UVES interorder separation, only 7 fibres can be devoted to astronomical objects when the simultaneous calibration fibre is used. For faint objects, one or more fibres can be devoted to record the sky contribution.

One attractive aspect is that UVES can be simultaneously used with GIRAFFE within FLAMES. The exposure times for the two spectrographs need not be the same.

2.2.3 GIRAFFE

GIRAFFE (the name comes from the first design, where the spectrograph was supposed to stay vertical on the platform) is a medium-high resolution ($R=7500-30000$) spectrograph for the entire visible range 370-900 nm.

GIRAFFE is equipped with two gratings, high and low resolution, which uses filters to select the required spectral range. GIRAFFE has a single 2Kx4K EEV

CCD (15 m pixels) and allows the observation of up to 130 targets over a 25 arcmin diameter of field of view (0.136degree). Figure 4 shows a picture of GIRAFFE.

Three observing modes are available:

- MEDUSA: up of 130 separated objects (including sky fibres) can be observed simultaneously in this mode, with 5 additional fibres each for simultaneous calibration (SIMCAL fibres).

One MREDUSA fibre has a diameter of 1.2 arcsec;

- 2 IFU (Integral Field Units) slit: each IFU consists of an array of 20 microlenses. 15 such IFUs form an IFU slit, with a total of 300 objects fibres plus 15 dedicated sky fibres plus 5 SIMCAL. One IFU cover 3×2 arcsec;

- in ARGUS mode a single integral field unit containing 300 fibers covering a rectangular area of 11.5×7.3 arcsec or 6.6×4.2 arcsec. as for the IFU mode, 15 sky fibers are available distributed anywhere around the Argus field. The two gratings are mounted back to back on a turn-table. Filters are used to select the required spectral range. Each object can be only observed in a single echelle order at once.

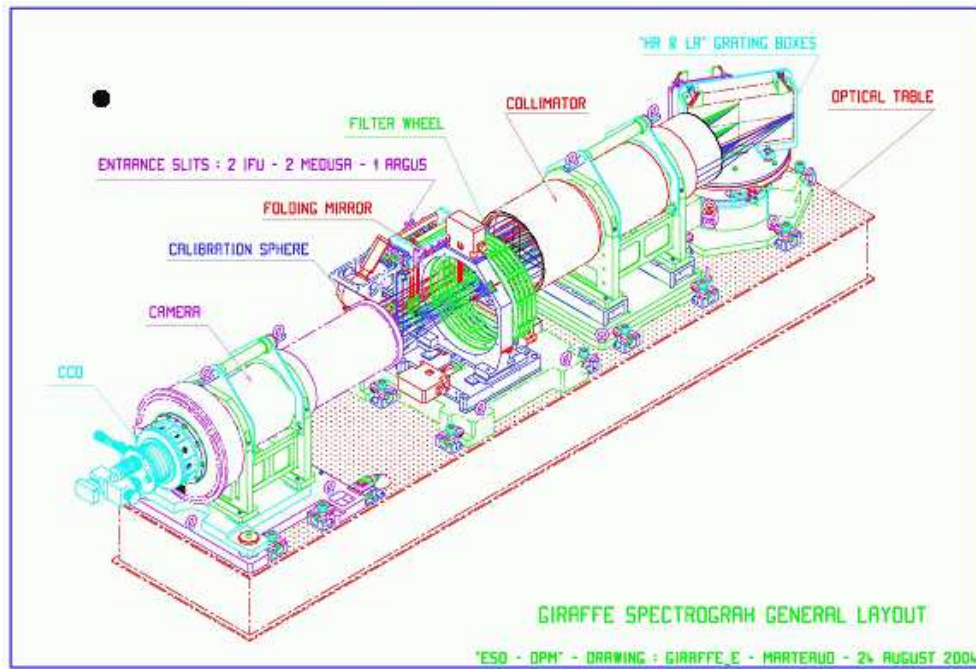


FIGURE 2.4— The spectrograph GIRAFFE.

2.2.4 The fiber Positioner

The Fibre Positioner, OzPoz, is the core component of the FLAMES facility. It is a rather large and complex system whose main function is to position fibers, held by magnetic buttons, onto the focal plates with high accuracy in order to collect light from individual target object. It host two plates: while one plate is observing the other positions the fibres for the subsequent observations, therefore limiting the dead time between one observation and the next to less than 15 minutes, including the telescope preset and the acquisition of the next field. Plate One is hosting 132 GIRAFFE MEDUSA buttons, 30 GIRAFFE IFU buttons (15 objects plus 15 sky), and 8 UVES buttons. With Plate One it is possible to use UVES and GIRAFFE simultaneously. Plate Two is hosting the same buttons as above plus a central GIRAFFE IFU “Argus” facility and 15 Argus-sky buttons.

3

Data reduction

The data reduction was performed using the pipeline developed at Geneva and Paris Observatories (Blecha et al. 2000): the GIRAFFE BaseLine Data Reduction Software (girBLDRS), version 1.13. With it was possible to remove the instrumental signature from the observed data, subtracting the bias and dividing by the normalized flat-field. Flat-field observations were also used to trace the position of all the fibres, and to derive the parameters for the optimal extraction of science exposures. Finally, the wavelength calibration was determined using the day-time Th-Ar lamp exposures.

The standard set of calibrations consist of a set of five bias, a set of three fiber flats per configuration and one Th-Ar arc-lamp exposure. The specific aspect of the GIRAFFE Data Reduction Software are:

- Pre-processing: this module executes the basic reduction on the raw frames: bias and dark subtraction, detection and elimination of the cosmic ray hits, removal of scattered light;
- Localization: the localization process is carried out using the flat-field calibration frames. First a localization mask is derived from scratch using threshold detection. Prior to the thresholding, the frame is approximately normalized on both axes in order to get rid of intensity variation from spectrum to spectrum as well as to remove the global shape of the flat-field spectrum. Using this mask, the PSF perpendicular to the dispersion is fitted in each spectrum inside the localization mask. Each spectrum is divided in 64 slices of 64 bins. The spectra limits are determined for each

spectral bin of each spectrum, then the central position of each spectrum is fitted by 1D chebychev polynomial, and a global 2D fit is made for the width of the spectra. Within each slice, all spectra bins are superimposed using the localization mask as a reference center so as to produce a single 1D compressed profile for a given slice. The points are fitted by an exponential profile to PSF, using a non-linear fit (Levenberger-Marquat):

$$PSF_{\perp}(Y)_{X,n} = A_{X,n} \exp\left(-\left|\frac{Y - Y_{X,n}}{W'_{X,n}}\right|^{W''_{X,n}}\right) + B_{X,n}$$

where n is the number of the spectrum, an (X,Y) the pixel position (X is the dispersion direction). The fitted parameters $A_{X,n}$, $B_{X,n}$, $W'_{X,n}$, $W''_{X,n}$, $Y_{X,n}$ are respectively the amplitude, the background, the two width parameters and the localization of the center in the direction perpendicular to the dispersion of the spectrum n for the bin X . the results are show in Fig. XX. The local PSF is therefore described by its center $Y_{X,n}$, the two shape parameters $W'_{X,n}$ and $W''_{X,n}$, the amplitude and the background. For scientific frames, the localization is adjusted using the simultaneous calibration spectra. The $PSF_{\perp}(Y)_{X,n}$ is fitted of the emission lines of the five Th-Ar spectra. The five Tr-Ar spectra, present in each scientific frame, allow the adjustment of the wavelength solution. This function insure that any variation of the slit, due to different motion, can be recovered in order to provide the best estimation of wavelength solution. Wavelength solution is used to rebin the spectra in physical units along the dispersion axis. Operations are very similar to the full calibration described above except that the slices here correspond to the pixel ranges where reliable lines are found, and that profiles perpendicular to the dispersion are beforehand normalized by the expected profile in the dispersion direction in order to remove the flux variation along the emission line profile. The localization mask is updated using the shifts derived from these fits.

- Extraction: this function applies to any processed science or calibration frames. The extraction of the spectra is carried out inside the localization lines.

The extraction proceeds as follows:

by default, the pixel are weighted proportionally of their estimated variances; for each spectral bin an analytical model is fitted on the multiple spectra profile (including all spectra in spectral bin); the intensities, the standard deviations σ and the local backgrounds of the extracted spec-

tra are set to the amplitudes, errors and background terms of the fitted model.

The standard error σ of the flux at each pixel of the extracted spectra is estimated and saved. This provide an independent estimate of the overall error for each spectral element to be compared to the expected shot-noise limit.¹

3.1 The pipeline

The most outstanding feature of this software is the accuracy in the radial velocity measurements. In order to assure that, in each scientific frames five simultaneous calibration spectra are present to guarantee the accuracy in the wavelength solution.

In order to achieve this scientific goals it is fundamental to register all the radial velocity measurements into a common reference system free –as much as possible– of any systematic error down to $\sim 1 \text{ km s}^{-1}$.

Drifts inside the instrument could introduce *fiber-to-fiber*, *plate-to-plate*, and *epoch-to-epoch* systematic errors in the radial velocity measurements. These drifts are due to different conditions of the instrument (for example a variation of the temperature between the night-time calibrations and during the night-time science exposures, or small mechanical shifts caused by earthquakes that occur rather frequently in northern Chile). Such differences would result not only in a different global shift of the velocities derived in the two cases, but also in a fiber-to-fiber difference as result of a different rotation of the slit geometry.

In the chapter xxx we will deal with the plate-to-plate and epoch-to epoch systematic errors that can be treated as global shifts. Most of the fiber-to-fiber correction is achieved by adjusting the slit geometry using the day-time Th-Ar exposure closest in time to science observations. This is done with the `wcalslit` pipeline task. The remaining fibre-to-fibre drifts are corrected using the five simultaneous Th-Ar fibres that are present in all our scientific frames. I first describe `wcalslit` and its application, because it has to be done prior to final fibre extraction and wavelength calibration.

The pipeline uses the physical description of the slit geometry and therefore iteratively, using the first guess of the wavelength solution, matches the measured to expected positions of the emission Th-Ar lamp lines. However, if there are any drifts in the instrument, the slit geometry needs to be adjusted. The

¹Shot noise is a type of electronic noise that occurs when the finite number of particles that carry energy, such as electrons in an electronic circuit or photons in an optical device, is small enough to give rise to detectable statistical fluctuations in a measurement.

procedure on how to correct the slit geometry and therefore improve the wavelength calibration using only the day-time Th-Ar calibration frames is given at the url <http://girbldrs.sourceforge.net/> by the authors of the pipeline. The `wcalslit` task determines the positions of all the 135 fibres in the Th-Ar day-time lamp frame and compares them with the expected positions in the `girSlitGeoMedusa1(2)H9.tfits` file which is one of the necessary calibration files of the pipeline. If differences are found, `wcalslit` updates the table. This task has to be run separately for Medusa1 and Medusa2, i.e. the two plates that are available for FLAMES-Medusa observations.

After adjusting the slit geometry calibration files in this way, we proceeded with the data reduction, by re-extracting the calibration frame using the following steps:

- `biasMast`: in this first step the biases are averaged through cosmic removal averaging. Then two polynomial models are built using the averaged bias in order to reduce pixel-to-pixel noise in the averaged frame and subtract this model from the scientific frames.
- `locMast`: this part produces the localization necessary for the extraction, the model of the transverse PSF required by the `OPTIMAL` extraction, and the spectroscopic extracted flat-field. The 2k x 4k data are displayed here compressed vertically, to enhance the curvature of the fibre signal. The pipeline uses the continuous signal per fibre to find its location. In a second step, the signal is traced, a Gaussian with variable width and height is fitted and the signal is extracted. The final pipeline version will use an algorithm to determine the PSF more precisely, and to use optimal extraction. In Figure 1 five spectra of the simultaneous calibration flat-field in MEDUSA mode are shown for the high resolution (HR9). The upper graphs show the localization lane over the full CCD field (dispersion direction is strongly compressed) while the three bottom panels show the spectra cross-sections recentered in the localization lane of each spectral bin. Each dot corresponds to a single pixel. The full lane is fitted exponential model of the PSF_{\perp} (Eq. 1).
- `wcalMast`: this is the full processing step for the ThAr calibration frames in order to get master wavelength solution from the Th-Ar exposures. It does extraction, wavelength-calibration and rebinnig. In order to check if the wavelength calibration obtained running this task is good, the pipeline produce same control graphics, show in the Figure 2 and 3. In the first, is shown for three different spectra the localization of the lines for the calibration lamp. Figure 3 shows the residual between the estimated and

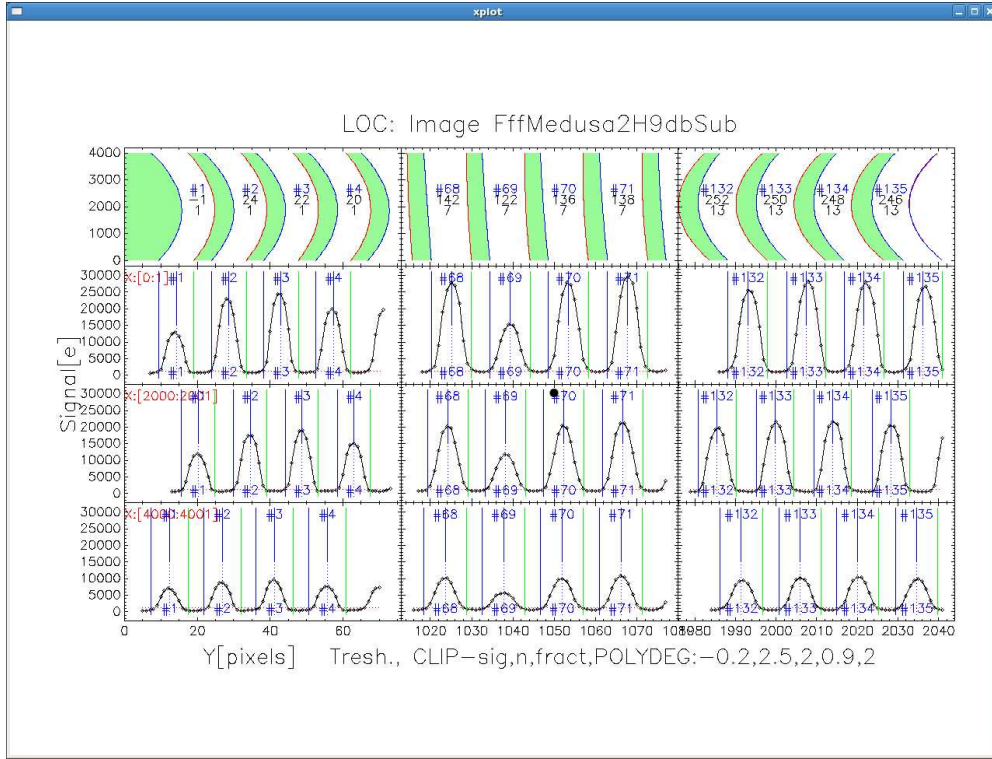


FIGURE 3.1— In this figure five spectra of the simultaneous calibration flat-field in MEDUSA mode are shown for the high resolution (HR9). The upper graphs show the localization lane over the full CCD field (dispersion direction is strongly compressed) while the three bottom panels show the spectra cross-sections recentered in the localization lane of each spectral bin. Each dot corresponds to a single pixel. The full lane is fitted exponential model of the PSF_{\perp} (Eq. 1).

the observed positions of the five lamps that are in the frame. In this plot it worth noticing that all the residuals are around zero, that means that the calibration done was good.

- **extract:** this task does the full processing of the scientific frames. After the subtraction of the averaged bias, it adjusts the localization using the lamp of calibration spectra, it does the optimal extraction and flat-fielding on extracted spectra, rebinning on the linear scale and adjusting the wavelength-calibration trough Cross-Correlation of 5 simultaneous wavelength-calibration spectra. Figure4 shows the reduced science frame. Each column represents a science spectrum, with the wavelength increasing upwards.

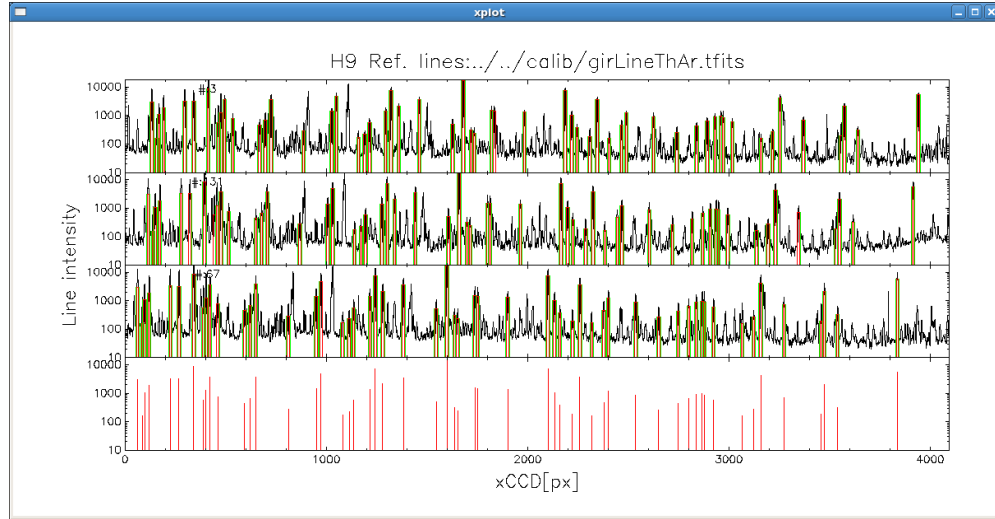


FIGURE 3.2— Localization of the orders.

As already mentioned, FLAMES offers the possibility to observe *simultaneously* with the on-sky exposure also the Th-Ar calibration lamp source through five MEDUSA fibres, which are distributed uniformly over the detector: fibres 1, 32, 63, 94, and 125. These five simultaneous fibres are essential to achieve the optimal wavelength calibration.

Therefore, in order to verify and eliminate any residual wavelength drifts across the 130 fibres, we acquired simultaneous calibration spectra in each of our observations. The unfortunate drawback in having the simultaneous Th-Ar lamps on during the 30min long exposures is some contamination of the stellar spectra in the fibres located directly next to the simultaneous fibres on the detector. In the subsequent analysis I discarded those spectra, because their velocity measurements had larger errors or in few a cases of faint stellar spectra could not be reliably determined.

The current version of girBDLRS corrects the variations of wavelength solution across the CCD in an automated way. After the fibre extraction, and wavelength calibration of all the fibres (including simultaneous calibration fibres) according to the solution obtained using the reference Th-Ar day-time calibration frame, it computes the shift between the expected and measured position of Th-Ar lines for each of the five simultaneous fibres. For each of the five simultaneous calibration fibres, the average shift is computed and then a linear regression is fitted to fibre position vs. average shift. Wavelength calibrations for all the fibres are then corrected by applying the computed linear

correction. In the second iteration the shifts between the expected and measured average positions of Th-Ar lines of the simultaneous calibration fibres are typically smaller than 0.001 nm (i.e. $\sim 0.6 \text{ km s}^{-1}$).

At the end of the data reduction, in total we had 56 frames, each with 80–130 spectra, including the sky and the simultaneous calibration fibers. At the end we obtained a total of 5973 stellar spectra. In Figure 4 we show examples of the spectra that we obtained after the reduction for bright, intermediate and faint stars ($V = 12, 14$, and 16 , respectively).

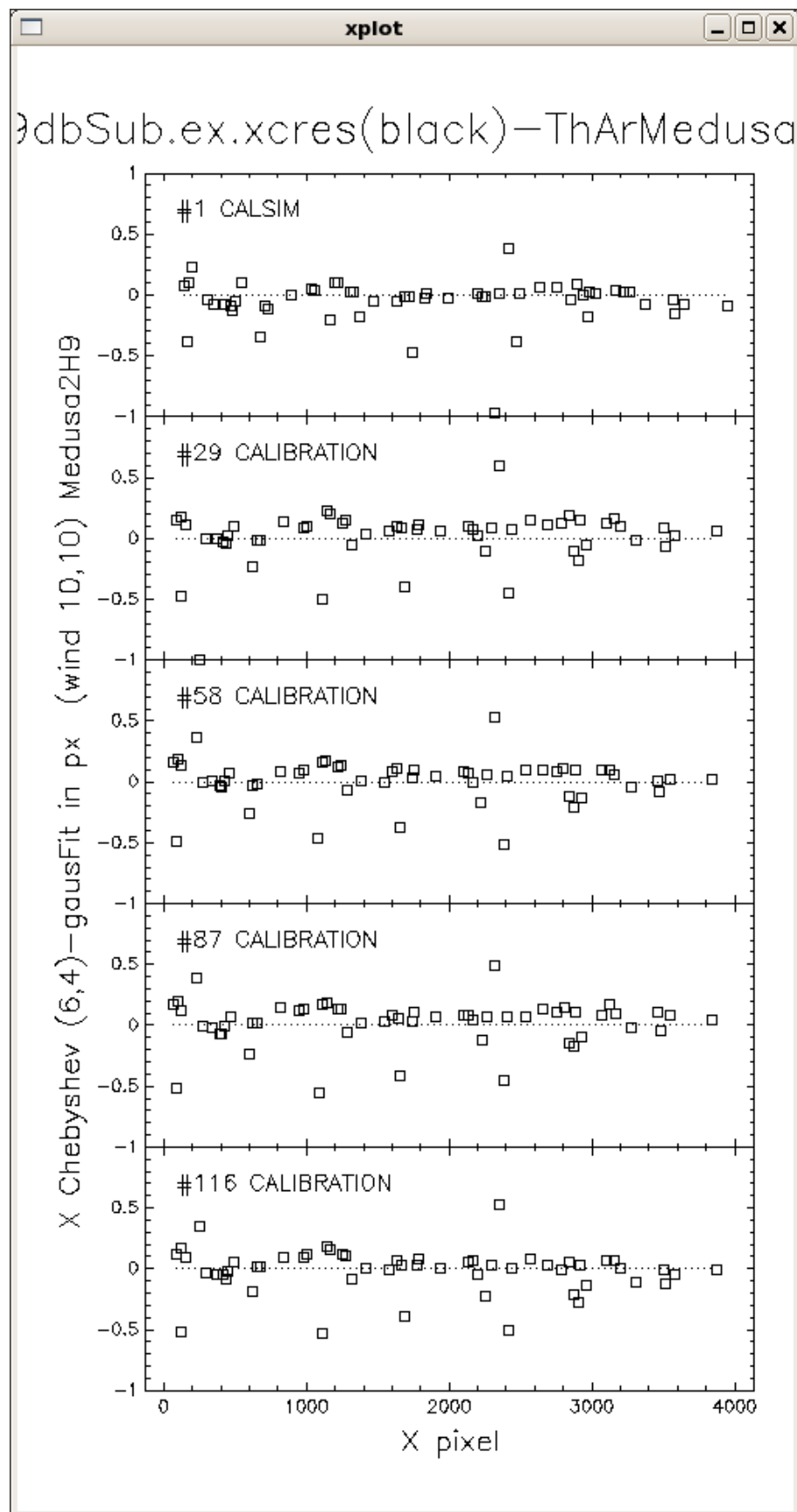


FIGURE 3.3— Plot of the differences between the estimated and the observed positions of the five lamps that are in the frame. This graphics give a goodness of the wavelength calibration: indeed it is possible to notice that this differences are around zero, that means that the calibration are carried out properly.

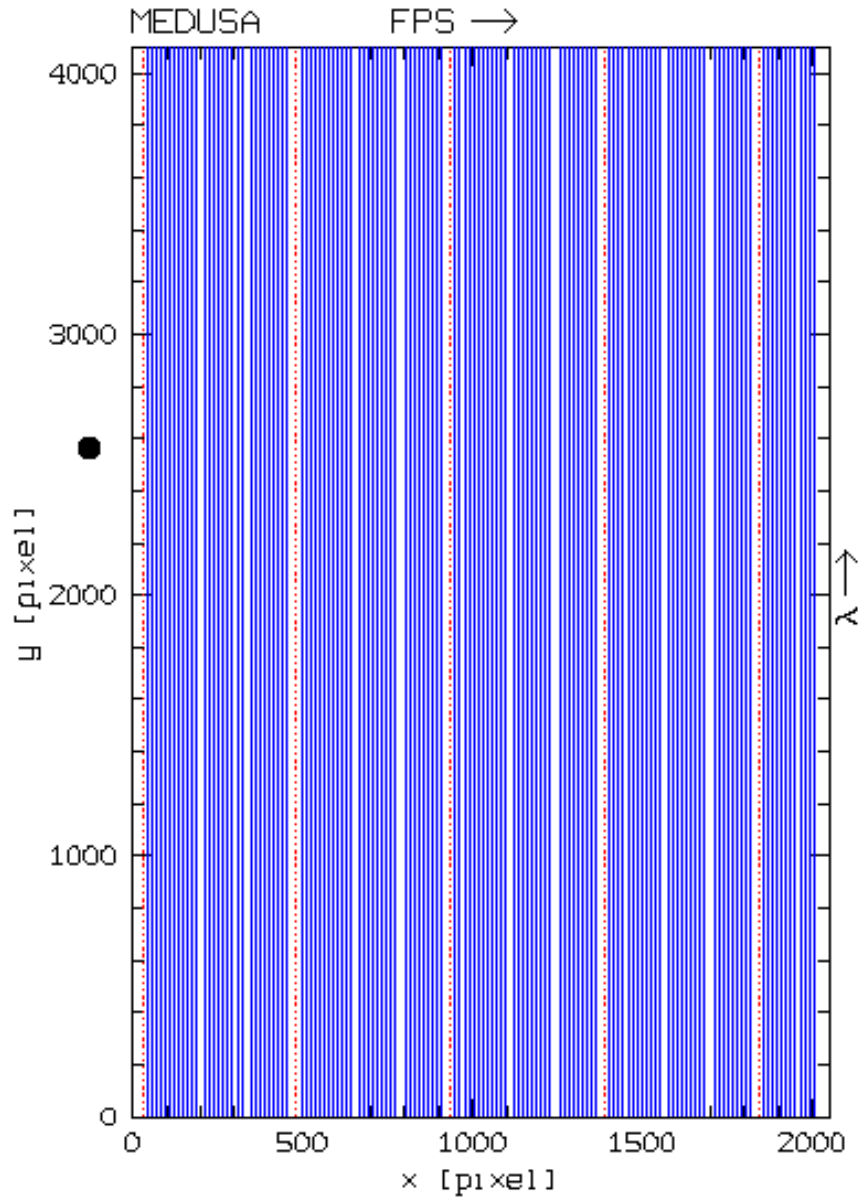


FIGURE 3.4— Schematic layout of the MEDUSA spectral format. Blue solid lines: object fibres. Red dotted lines: calibration fibres. The directions of the increasing fibre number in the slit (FPS) and of increasing wavelength are indicated.

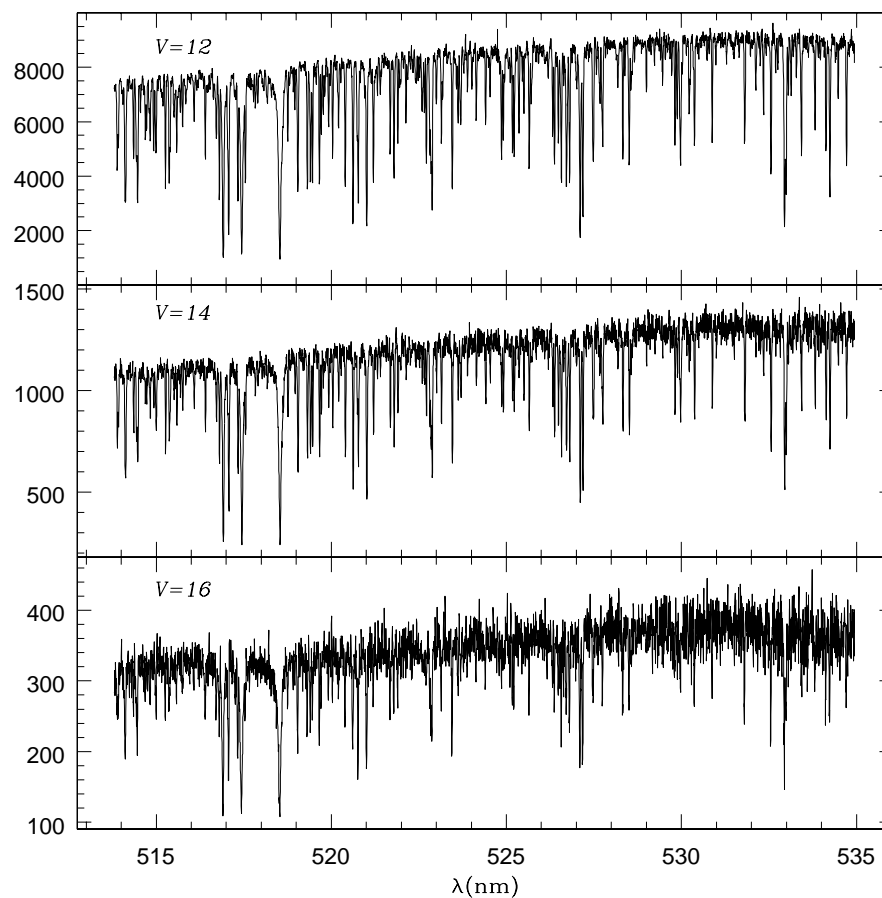


FIGURE 3.5— Extracted spectra for three stars with different magnitudes: in the upper panel for a bright star with V magnitude 12, in the middle panel for an intermediate star with V magnitude 14, and in the bottom panel for a faint star with V magnitude 16.

4

The radial velocity of M4

4.1 Radial Velocities

We used a cross-correlation technique (Griffin 1967; Tonry & Davis 1979) to measure the radial velocities of all the targets. The cross-correlation of the extracted and wavelength calibrated spectra is included in the girBLDRS pipeline, in the last step, after the correction of the wavelength calibration using the simultaneous calibration fibres.

In the cross-correlation technique the observed spectrum is matched (correlated) with the template. The observed and template spectra should be of a similar spectral type in order to minimize systematic errors due to template mismatch. The template spectrum is shifted in wavelength (velocity) space and the difference with respect to the observation computed until the best fit is found.

The particular implementation of the cross-correlation technique adopted in the girBLDRS is described by Baranne et al. (1996), and Dubath et al. (1990). It uses the numerical mask as the template for cross correlation, in our case based on the solar spectrum from the Solar Flux Atlas of Kurucz et al. (1984). For most solar spectral lines the mask provides the lower and upper limits of a wavelength window centered on the line. For any shift in wavelength between the observed spectrum and the numerical mask, the integral of the observed spectrum within the mask windows is calculated. The whole cross-correlation function is then constructed by evaluating the integrals for shifts ranging from a minimum to a maximum selected velocity. More specifically, the template is shifted to a minimum radial velocity and the integral of the observed spectrum passing through the numerical mask evaluated. Then the template is shifted by steps of 0.005 nm (2.8 km s^{-1}) up to the highest chosen radial velocity.

The cross-correlation function is computed at each step over the whole velocity domain. In this way, the cross-correlation function is an “average spectral line” over all the lines present in the template. It is fitted with a Gaussian, and its peak corresponds to the wavelength (velocity) shift of the object spectrum, and therefore it represents a direct measure of the radial velocity. The girBLDRS pipeline computes the radial velocity for all the stars, including the heliocentric correction.

Template (red) girG2H9+spectrum #7(blue) [px] 0[424:3817] JD:53984.493

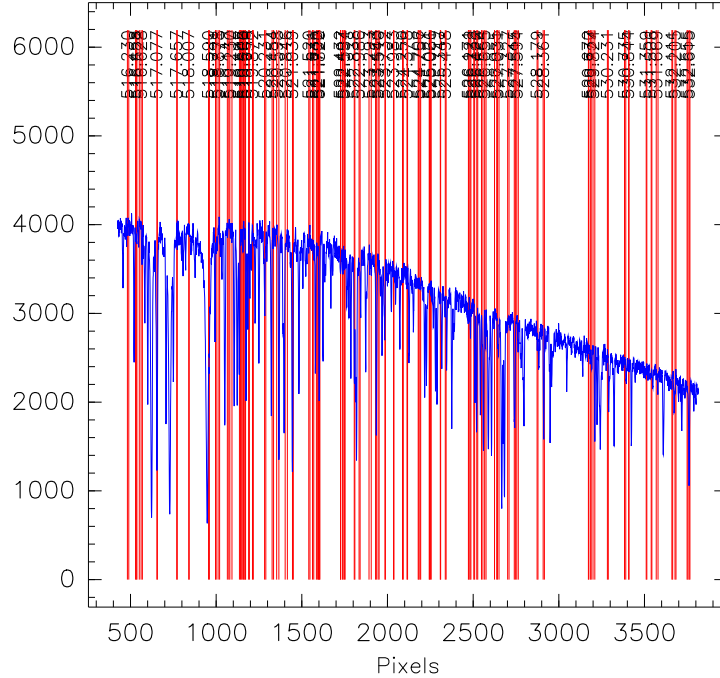


FIGURE 4.1— Correlation between the template and the stellar spectra.

The width of the cross-correlation function depends on the instrumental and object line broadening.

The larger the number of spectral lines in the considered wavelength interval, and the higher the resolution of the spectrum, the higher is the precision of the velocity determination. Therefore, in order to achieve the best possible precision, we have used the HR9 setup of the FLAMES+GIRAFFE spectrograph, because it covers a wavelength region very rich in iron lines, has one of the highest resolutions offered by the instrument, and the highest throughput

E 0 ID984 sp #7[424,3817] 524.4[nm] girG2H9 38075 JD:53984.493

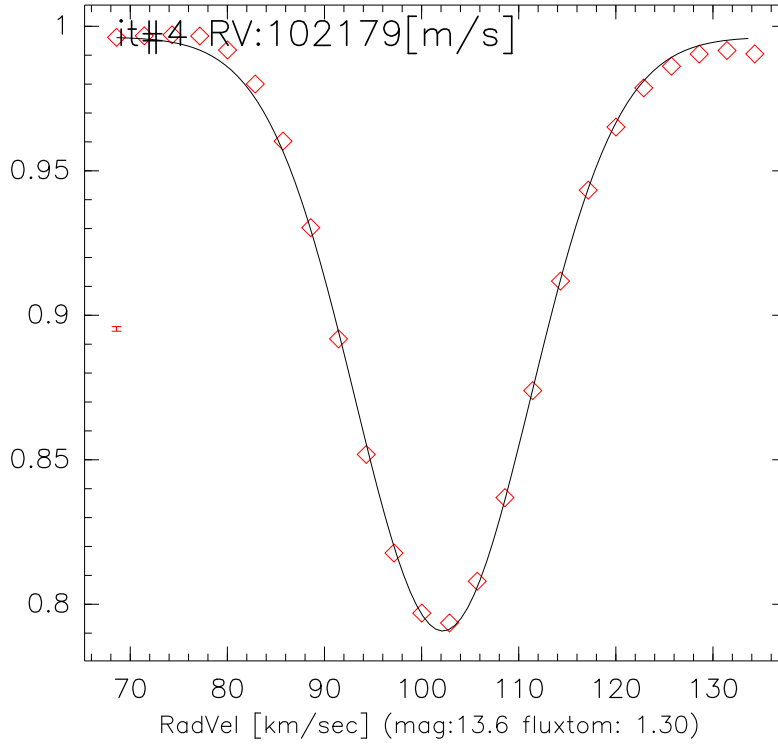


FIGURE 4.2— Fit of the cross-correlation peak in km s^{-1}

for the G and K-type stars. For the cross-correlation process we selected a solar template mask (G2), because it corresponds to the average spectral type of our targets, given that we observed red giant branch stars with magnitudes ranging from the tip of the RGB ($V = 11$) to one magnitude below the turn off ($V = 16.8$).

In order to check whether our radial velocities are affected by systematic errors due to template mismatch we made the following test. First of all, we plotted all radial velocities as a function of the color $B - V$ and of the V magnitude. Figure 1 shows that there is no evidence of any systematic dependence of the radial velocity either with the magnitude, or with the $B - V$ color.

We computed the radial velocities for several plates also using an F0 star template mask. In order to compare the two results, we calculated the radial velocity differences computed by using the two different templates: we found an average value of $65 \pm 11 \text{ m s}^{-1}$. we repeated the same test only with the few stars that we observed in the Horizontal Branch, and we found that the mean

radial velocity difference computed using the two different templates is about $80 \pm 34 \text{ m s}^{-1}$.

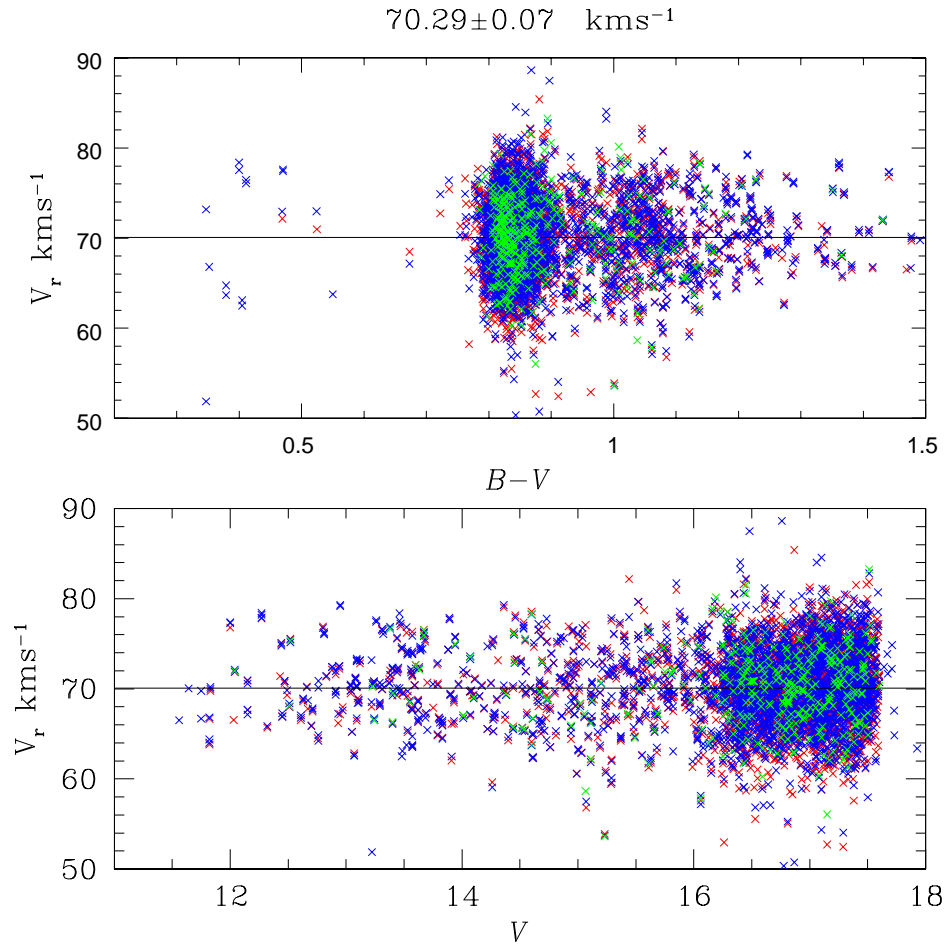


FIGURE 4.3— Radial velocities as a function of color (upper panel) and magnitude (bottom panel) obtained for our individual spectra. Different colors refer to different epochs. The horizontal line indicates the mean radial velocity (value at the top) of all the stars.

4.1.1 The zero point velocity shift between the epochs

In this section we describe how we minimized the plate-to-plate and epoch-to-epoch systematic errors (global shifts in the velocity reference frame).

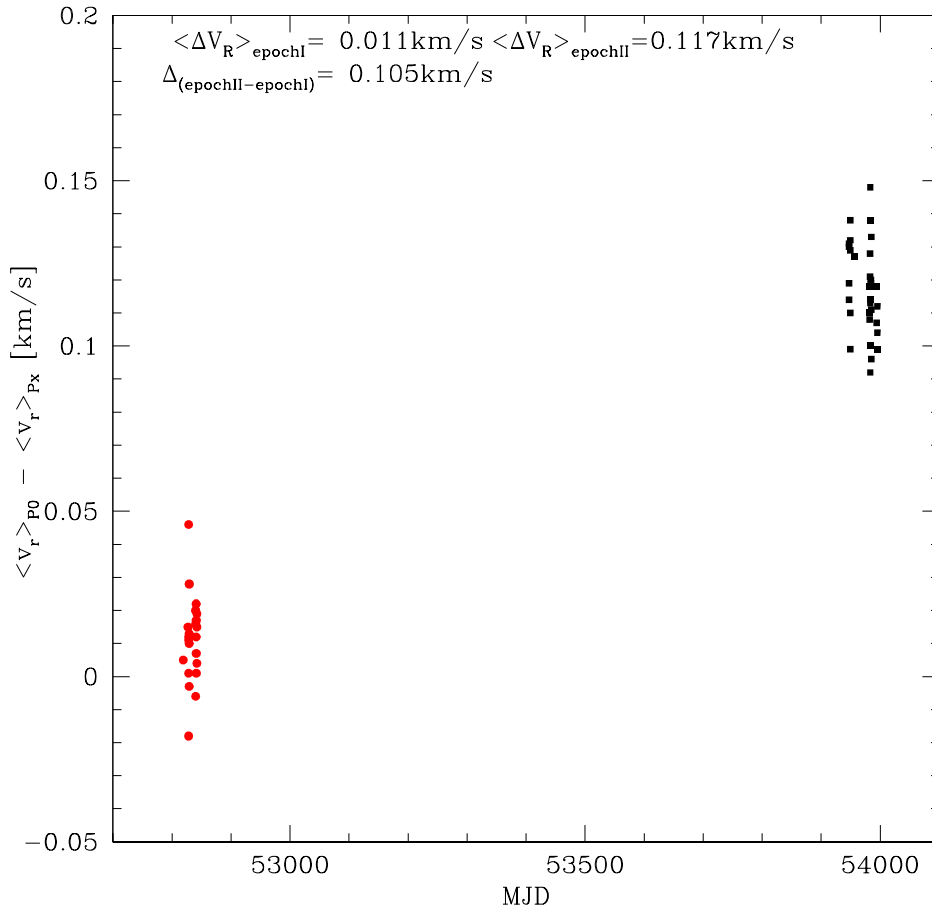


FIGURE 4.4— The average radial velocity differences for the simultaneous calibration fibers between the reference plate and all the other plates (Px) plotted as a function of the Modified Julian day. There is a systematic offset in the radial velocity zero point between the two epochs.

As described in the previous chapter, within each plate the velocities were computed on the common reference system, which –if there were no systematic errors– should be the same for all the plates, and should coincide with the Solar system barycentric rest-frame. In order to measure any possible deviations from this, we considered –in each plate– the five simultaneous calibration fibres (described in chapter 3). In all our plates, these fibres provide Th-Ar calibration-lamp spectra for which we can measure also wavelength shifts.

To test the presence and size of the average radial velocity differences between different plates we first defined a radial velocity system common to all the plates. This has been assumed to be the average of the five calibration fiber velocities *of the first plate, of the first night, and of the first epoch*. In the following we will refer to this plate as the *reference-plate*. We then calculated the difference of the velocities from the calibration fibres of other plates, with respect to that of the reference-plate.

The result is shown in Figure 2 where the amount of the global shift in km s^{-1} is plotted as a function of the Modified Julian day. It appears that within each epoch the velocities of plates are registered to a common reference system within $\sim 50 \text{ m s}^{-1}$. Going from epoch I to epoch II/epoch III the shifts are larger, being of the order of $\sim 100 \text{ m s}^{-1}$.

We then corrected our plate-to-plate, and epoch-to-epoch, global shifts simply applying to all plates their velocity difference with respect to the reference plate. This put all the velocities from different plates into a common radial velocity system within $\sim 100 \text{ m s}^{-1}$ (not necessarily coincident with the true Solar system barycenter).

Figures 3 and 4 show the results of application of the above procedure. The two figures shows the differences in radial velocity for stars with multiple spectra before (Figure 3) and after (Figure 4) the application of the correction. In the upper panel, there are the bright stars with ($V < 15$), in the bottom panel, the faint stars with ($V > 15$).

In these figures the thick black line mark the position of the zero, the solid lines represent the mean and the dotted lines the median. After the subtraction of the zero point shifts the mean and the median are close to zero, as expected.

4.1.2 M4 radial velocity

Some systematic trends in our radial velocities are expected. Effects such as gravitational redshift ($\sim 0.5 \text{ m s}^{-1}$ for red dwarf stars) and convective blue shifts (~ -0.2 – -0.3 Madsen et al. 2002) km s^{-1} for Red Giants) are not affecting differential measurements for the binary search, but they do affect the absolute value of the velocity in the Solar system barycenter rest-frame. We did not attempt any correction for them, since these two effects are pushing in opposite direction, we simply add an average contribution of 0.3 km s^{-1} to our uncertainties on the absolute radial velocities.

Moreover, because of the zero point global shifts mentioned in Section 4.1, we have an additional systematic error of $\sim 0.1 \text{ km s}^{-1}$. In conclusion, the resulting

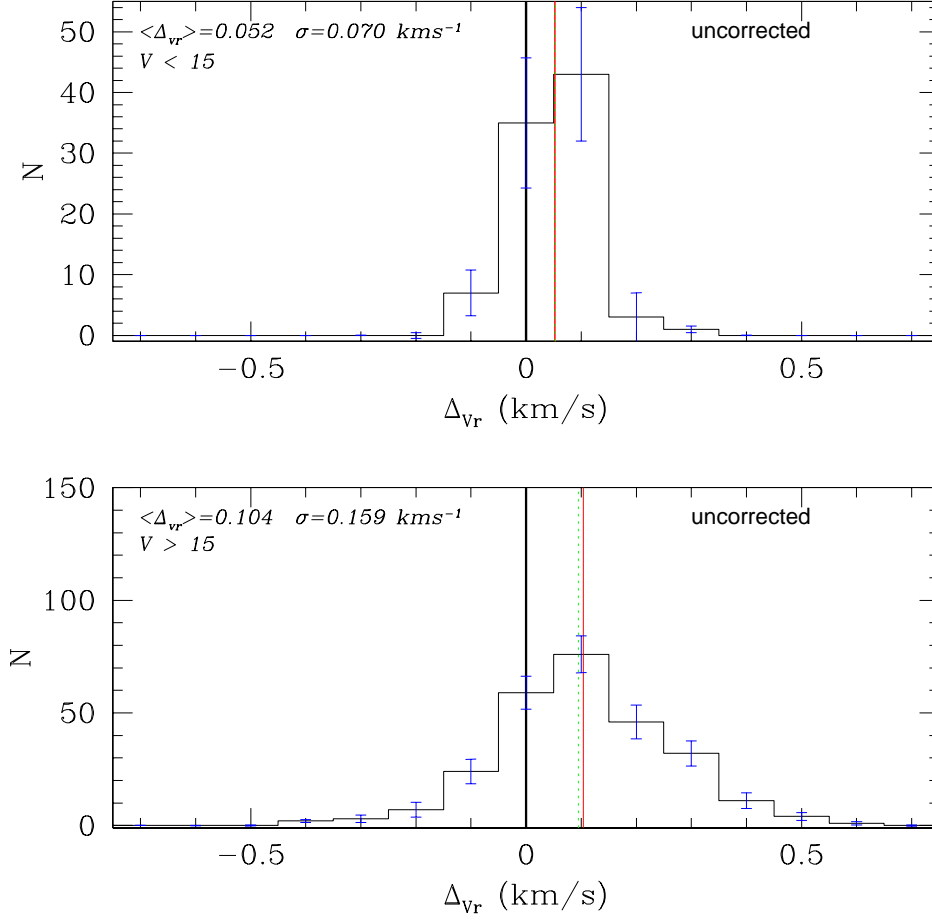


FIGURE 4.5— Histogram of differences of multiple radial velocity measurements used to evaluate the reliability of our calibrations. In this case no corrections have been applied to our measurements. The upper panel shows the bright stars ($V < 15$) the bottom panel shows the faint stars ($V > 15$). The solids lines are the mean, and the dotted lines are the median. The thick black line mark the position of a null difference.

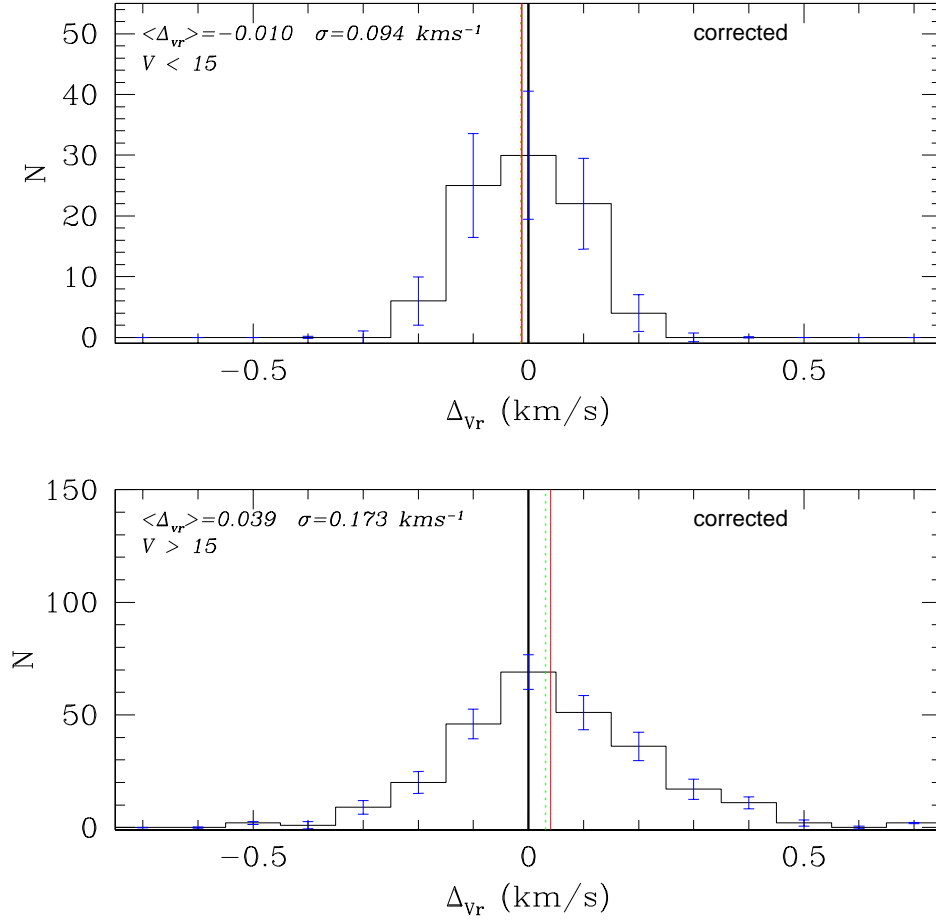


FIGURE 4.6— Histogram of differences of multiple radial velocity measurements used to evaluate the reliability of our calibrations. In this case the shift found in the way described in the text has been applied. In the upper panel we show the results for the bright stars ($V < 15$), the bottom panel for the faint stars ($V > 15$). The solid lines are the mean, and the dotted lines are the median. The thick black line mark the position of a null difference.

average velocity for M4 is:

$$\overline{V_r} = 70.29 \pm 0.07 (\pm 0.3) (\pm 0.1) \text{ km s}^{-1}$$

where the first source of of uncertainties is my estimated internal error.

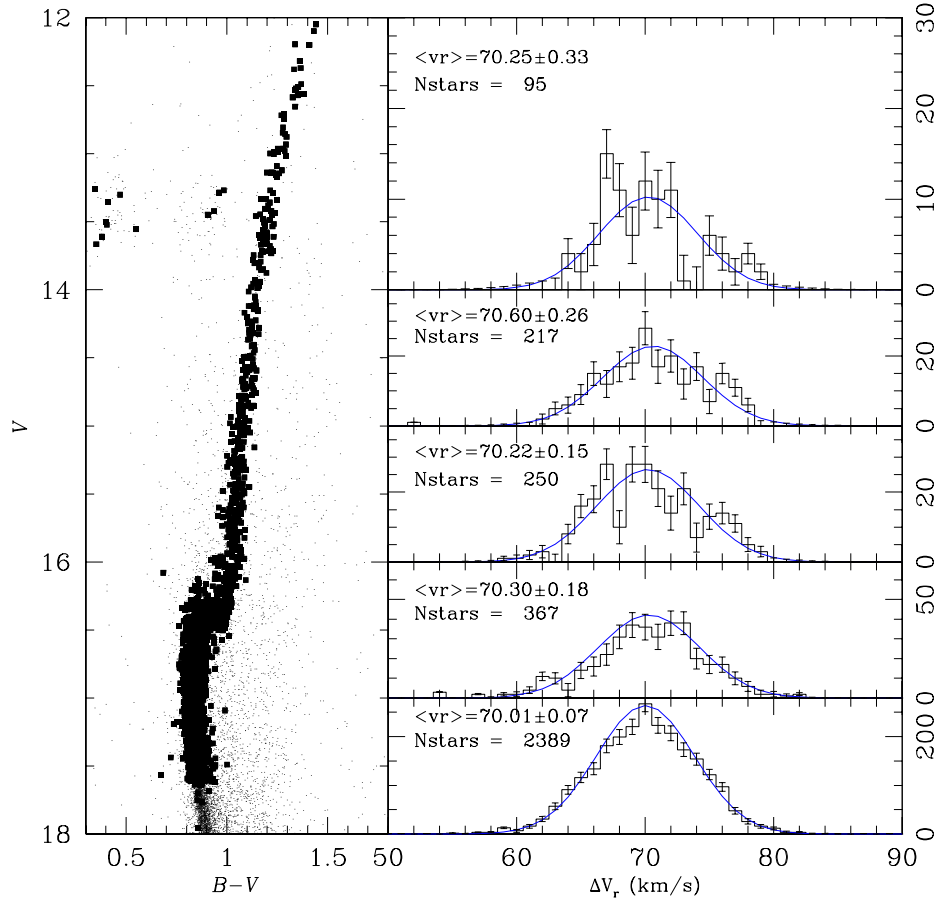


FIGURE 4.7— *Left:* Color magnitude diagram of the stars in our photometric catalog. Thick dots indicate the target stars for which we have spectra. *Right:* For five different magnitude intervals, the histogram of the radial velocity distribution. Note that, in order to increase the statistics, the brightest bin cover a wider range in magnitude.

The left side of Figure 5 shows the CMD for the target stars. We divided our sample of stars in five bins in V magnitude. The right panel of Figure 5

shows the histogram of the distribution in radial velocity V_r of the stars in each bin, and the least square best fit Gaussian. The labels in each panel give the values of the average radial velocity ($\overline{V_r}$) for that bin and its dispersion ($\sigma_{\overline{V_r}}$). The weighted mean of the five independent values is

$$\langle \overline{V_r} \rangle = 70.27 \pm 0.19 \text{ km s}^{-1}$$

in perfect agreement with the value obtained above.

The measured radial velocity is in good agreement with previous studies. In particular, Peterson et al. (1995) measured the average radial velocity of M4 to be $V_r = 70.9 \pm 0.6 \text{ km s}^{-1}$ from the radial velocities of 200 giant stars. Côté & Fisher (1996) analyzed 33 Turn-off dwarf stars and reported a value of $70.3 \pm 0.7 \text{ km s}^{-1}$.

5

The binary candidates

In the first section of this chapter I will describe the selection of the binary candidates from the measured radial velocity variations. Then I will present the binary fraction that I found.

5.1 The radial velocity variations

The approach, which is adequate for stars with two or more epochs, is based on the comparison of the observed weighted rms velocity for single stars with the average rms for each star at the same magnitude. Stars with rms several times larger than expected are likely to be binary candidates.

The weight $w_{i,j}$ for the i -star, observed in the j -plate used to compute the rms, is provided by the pipeline formal errors $\sigma_{i,j}$, according to the relation: $w_{i,j} = 1/\sigma_{i,j}^2$. We note that these errors underestimate the true errors, but they contain valuable information on the goodness of the Gaussian fit to the cross-correlation function, which is related to the goodness of the observed spectrum (see Sect.3). More explicitly, this strategy turns out to be the most robust against false detections caused by a bad spectrum (which received an almost null weight), i.e. spectra with particularly low SNR, or altered by cosmic ray events.

The weighted mean radial velocity for the i -star observed in n plates, labeled as j -plate, with j from 1 to n (with $n = 2, 3$, or 4 , depending on the available number of epochs) has been calculated as:

$$\overline{V_{r;i}} = \frac{\sum_{j=1}^n w_{i,j} V_{r;i,j}}{\sum_{j=1}^n w_{i,j}}.$$

Accordingly, we could define a *weighted radial velocity rms* as:

$$(\sigma_{\overline{V_{r;i}}})^2 = \frac{\sum_{j=1}^n w_{i,j} (V_{r;i,j} - \overline{V_{r;i}})^2}{\sum_{j=1}^n w_{i,j}}.$$

However, for small population sample –such as in this case– it is customary to use an unbiased estimator for the population variance. In normal unweighted samples, the (n) in the denominator (corresponding to the sample size) is changed to $(n - 1)$. While this is simple in unweighted samples, it becomes tedious for weighted samples. Thus, the unbiased estimator of the weighted population variance is given by:

$$(\sigma_{\overline{V_{r;i}}})^2 = \frac{\sum_{j=1}^n w_{i,j}}{(\sum_{j=1}^n w_{i,j})^2 - \sum_{j=1}^n w_{i,j}^2} \sum_{j=1}^n w_{i,j} (V_{r;i,j} - \overline{V_{r;i}})^2.$$

For each star with multiple observations i compute this quantity and plot it in Figure 1 as a function of its magnitude. The majority of the objects occupy a well defined locus on this observational plane.

We divided the stars in Figure 1 in 6 equally populated magnitude bins, with ~ 400 stars in each bin. For each one could compute the median and naively think that it would be representative of the average radial velocity error $< (\sigma_{\overline{V_r}}) >$ for that magnitude bin.

However, although the observed distributions are satisfactorily fitted with a Gaussian (with standard deviation σ), the median of the error distribution is not a good estimate of the sigma. The relation between the median and the σ can be easily computed, and we obtain the final $< (\sigma_{\overline{V_r}}) >$ as 0.675σ . Therefore, to avoid underestimating the errors, we applied this correction to the value of the median.

We note, that it also would be possible to estimate the σ from the root mean square value of the $< \sigma_{\overline{V_{r,i}}} >$ but this estimate is too sensitive to the outliers, most of which are binary candidates.

The operation was repeated twice to converge on the value of the median, and so of the σ ; in the second step, all stars deviating by more than $3.5 < \sigma_{\overline{V_r}} >$ from the first median estimate have been removed.

The $1- < \sigma_{\overline{V_r}} >$ value as a function of the magnitude is indicated with a solid thin-red-line in Figure 1. This is the simple connection of the $< \sigma_{\overline{V_r}} >$ values computed in each magnitude bin. The dotted lines indicate the 3, 4, and 5- $< \sigma_{\overline{V_r}} >$ level.

For the rest of the thesis I use σ to denote $< \sigma_{\overline{V_r}} >$. All the stars above the $3-\sigma$ level shall be considered as binary candidates in the following discussion. They are also indicated as red dots in Figure 2.

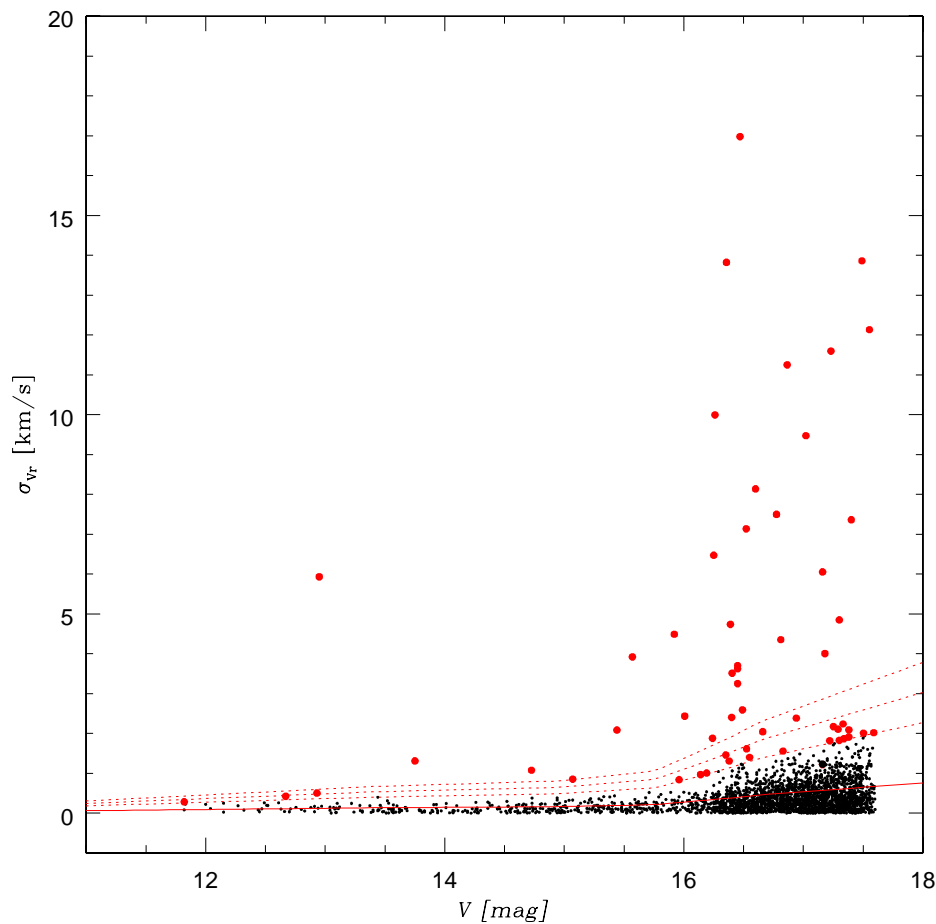


FIGURE 5.1— The weighted rms as a function of the magnitude is shown for all the M4 stars that have been observed in at least two epochs. A large rms is likely to be due to an intrinsic variation of the radial velocity. The solid line connecting $\langle \sigma_{\overline{V_r}} \rangle$ values computed in each magnitude bin is an indication of the precision of the radial velocity measurement for non-variable stars. The dotted lines indicate the 3, 4, and 5 $\langle \sigma_{\overline{V_r}} \rangle$ level. The candidate binaries are indicated with red dots.

5.2 The binary fraction

The present data allow to identify a the 3σ level binary candidates with velocity variation greater than $\sim 0.3 \text{ km s}^{-1}$ for the bright stars ($V \leq 15$), and velocity variations greater than $\sim 0.5 \text{ km s}^{-1}$ for the faint stars ($V > 15$). We found

57 binary candidates. Figure 2 shows the location of the binary candidates in the CMD. With the triangle is shown the binary candidate found also in the photometric binary sample of Milone et al. (2008).

In Appendix 1 we give the list of the binary system candidates coming from two epochs, three epochs, and in one case with four epoch spectra. For each star, the table gives the radial velocity as measured in the different epochs with the corresponding errors, the coordinates (RA and DEC) in degrees, the Modified Julian Date of the observations, the number of epochs that each star has been observed, the radial distance from the center in arcmin, and the B and V magnitudes from the calibrated photometric catalogue (Momany, private communication).

Figure 2 shows the radial distribution of the binary candidates. The total binary fraction that we found is $f = 2.3 \pm 0.3\%$. The quoted error is $1\text{-}\sigma$ error. This is significantly smaller than the binary fraction presented by Coté & Fischer (1996), but within the errors it is consistent, since Coté & Fischer quote $\pm 15\%$ error.

We split our sample in two subsamples on the basis of the magnitude of the star in order to calculate the percentage of the binary system candidates below and above the turn off. We found that the fraction of binaries among stars below the turn off is $f = 1.9 \pm 0.3\%$, while the fraction above the TO is $f = 2.7 \pm 0.4\%$. we detected a total of 4 candidates out of 97 observed targets inside the core radius, and 53 candidates out of 2372 observed stars outside the core radius. These numbers imply a lower limit for the binary fraction $f = 4.1 \pm 2.1\%$ inside the cluster core, and $f = 2.2 \pm 0.5\%$ outside the core. We also found that the fraction of binaries inside the half mass radius ($r_h = 2.3\text{pc}$) is $f = 3.0 \pm 0.4\%$, while outside $1r_h$ we have $f = 1.5 \pm 0.3\%$.

It is worth noticing that the sample that we found represents only spectroscopic binary candidates and not the total population of binary systems: based on Gaussian statistic it is probable that our sample includes some false detections, and is incomplete.

With at least one other epoch we could confirm the candidates found with this survey, and reach a significantly higher completeness in our estimate of the binary fraction. In order to quantify what we would gain from one additional epoch, and to have an empirical estimate of the completeness of our present search, we analyzed the binary fraction we obtained from the subsample of stars with three epochs. We calculated how many binary candidates have been detected using three epochs of the data and we compared this number with the candidates that would be detected using only two epochs. We found that using only two epochs we can identify 8 candidates out of the available 484

targets. We analyzed all the possible combinations between the epochs, and the results were the same, and therefore robust. Using all three epochs ifound 12 candidates out of the 484 targets. All the 8 candidates from the two epoch observations could be confirmed by adding the third epoch. A third epoch of observations is extremely important: this simple test shows that the binary fraction from two epochs suffers from an incompleteness of at least of 40%.

Accounting for this incompleteness, and considering the number of targets with two and three epochs observed inside and outside the core, we have that the fraction of binary candidates in the whole sample is $f = 3.0 \pm 0.3\%$, inside the core becomes $f = 5.1 \pm 2.3\%$, and $f = 3.0 \pm 0.4\%$ outside the core. In the same way, we find $f = 4.5 \pm 0.4\%$ and $f = 1.8 \pm 0.6\%$ for the fraction of binaries inside and outside the cluster half mass radius.

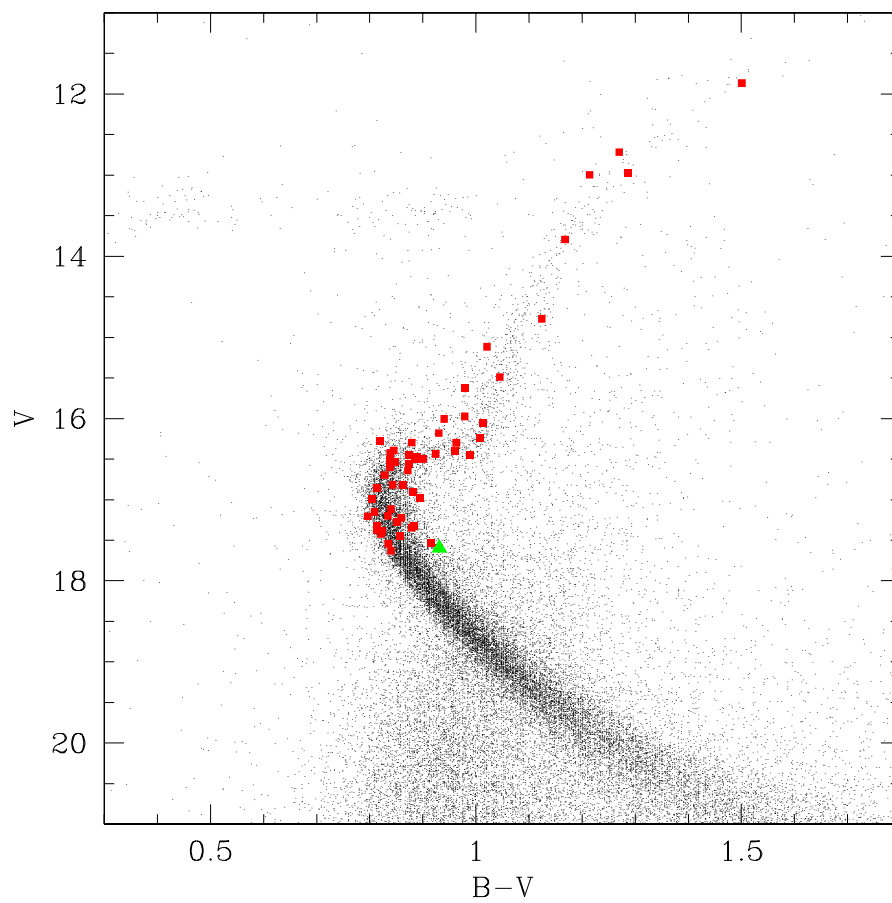


FIGURE 5.2— Location of the binary candidates large red dots in the CMD. The green triangle indicates a binary candidate found also in the photometric sample (Milone et al. 2008).

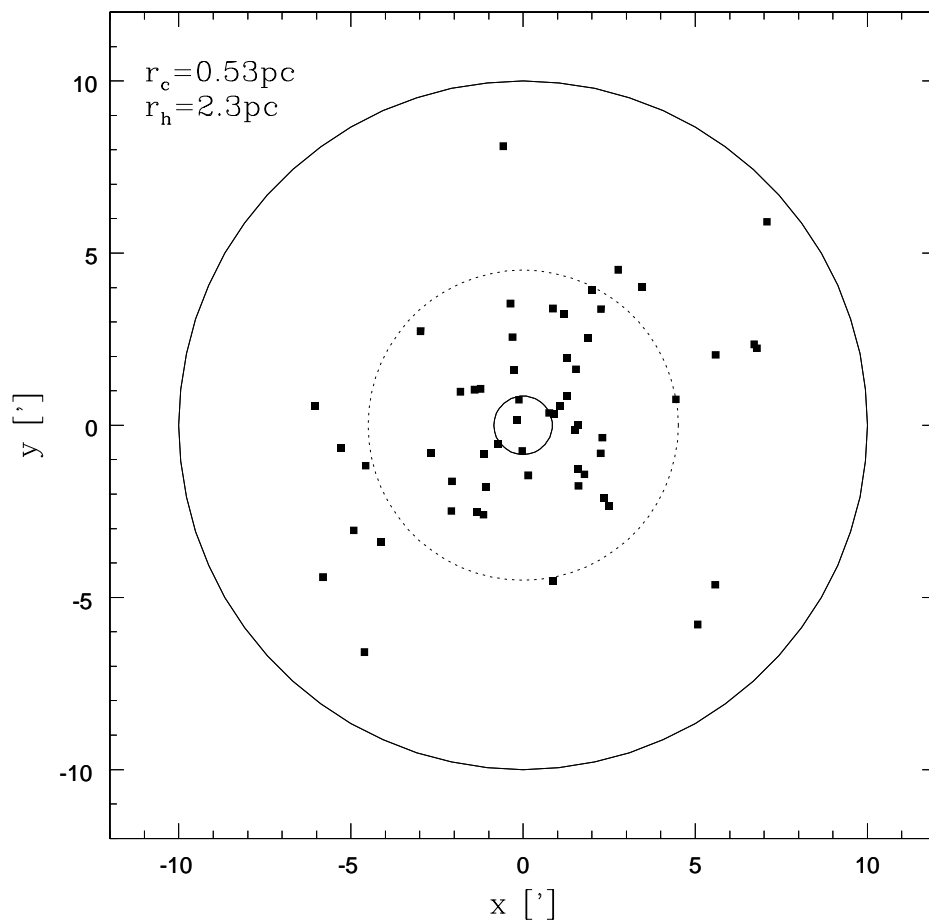


FIGURE 5.3— Radial distribution of the binary system candidates. The inner circle represents the cluster core. The outer circle indicates the total area of the cluster covered by observations. The dotted circle contains the binaries inside the half mass radius.

6

Monte Carlo simulations

Contrary to what was thought in early 80s, we now know that binaries do exist in globular clusters.

Since, as we already highlighted in the first chapter, the formation and the destruction of the binary systems play a fundamental role in the dynamical evolution of a stellar systems, especially during core collapse phase, the principal aim of all search of binary stars in globular clusters is the knowledge of their frequency.

Extracting a binary fraction from a catalogue of radial velocities is a difficult task, since the number of stars expected to show some radial velocity differences depends not only on the time, on the number and on the precision of the survey, but also on a wide set of unknown parameters including the orbital period, the total mass of the system, the eccentricity, the inclination and the longitude and time of periastron.

Unfavorable binary orbit configurations would cause the loss of a fraction of binary systems from our sample.

Thus to properly estimate the binary frequency of M4, we used Monte Carlo simulations to generate a large sample of simulated radial velocities in order to compare them with the measured radial velocities.

The aim of these simulations, is to understand the completeness of our study and make first comparison of the observations with a model.

From the simulation we will be able to estimate the fraction of binary systems missed in our survey, and to correct the observed binary frequencies.

The main motivation for this work is that we will be able to determine the true frequency of binary systems in M4 at the present day. Finally, by comparing this with the binary frequency found in dynamical simulations, we may be

able to determine the primordial binary frequency, which is an important input parameter in such simulations.

6.1 The model

In order to simulate a population of binaries to compare with the observations we make a Monte Carlo simulation based on the following set of assumptions:

- the period distribution was taken from Kroupa (2008).
He adopted distribution for P based on those found by Duquennoy & Mayor (1991) in their study of multiplicity among solar type stars in the solar Neighborhood.

$$f_p(\log P) = f_{tot} \left(\frac{1}{\sigma_{\log P} \sqrt{2\pi}} \right) e^{\left[-0.5 \frac{(\log P - \langle \log P \rangle)^2}{\sigma_{\log P}^2} \right]}$$

with $\langle \log P \rangle \sim 4.8$ and $\sigma_{\log P} \sim 2.3$,

and $\int_{all} \log P f_{\log P}(\log P) d\log P = f_{tot} \sim 0.5$. P is expressed in days.

The corresponding semi-axis (a) distribution of each group of binaries can be derived by considering the third Kepler's law:

$$a^3 = \left[\frac{G(m_1 + m_2) * P^2}{4\pi^2} \right]$$

where m_1 and m_2 are respectively the mass of the primary and secondary star. We didn't impose any limit on the values of m_1 and m_2 .

- The distribution of the total mass of a binary was taken according to the mass function of Kroupa, Gilmore and Tout (1991).

$$M(X) = 0.33 \left[\frac{1}{(1-X)^{0.75} + 0.04(1-X)^{0.25}} - \frac{1}{1.04}(1-X)^2 \right]$$

where X is a random variable with uniform distribution in the range $[0,1]$.

When $X=0$ $M=0$, and $M(X)$ becomes very large as $X \rightarrow 0$.

- The distribution of the mass ratio was considered uniform.
- Assumption concerning the distribution of the eccentricities can affect the results for the derived binary fraction (see fig. 1 of Hut et al. (1992)). We have carried out simulations for two different assumed distributions:

(i) with circular orbits, i.e. with $e = 0$; (ii) with a thermal distribution of eccentricities $f(e)=2e$ (expected if the distribution is a function of energy only, see Heggie 1975).

- We randomized the initial phase.
- We took the distribution $f(i) = \frac{(\sin i)}{2}$ for the inclination.

Assuming that, each binary was evolved forwards 12 Gyr using Hurley’s BSE (Binary Star Evolution) package (Hurley, Tout & Pols 2002). The BSE algorithm allows the entire evolution of even the most complicated binary systems to be modeled in a very rapid way. In order to conduct statistical model, i.e. population synthesis, this model can reproduce any type of binary stars that is observed in enough detail. This package is therefore ideal for synthesizing a large population of binary stars. Also the colors and the V magnitude were calculated using routines supplied by J. Hurley.

In this algorithm the re-circularization of eccentric orbits and synchronization of stellar rotation with the orbital motion owing to tidal interaction is modelled in detail. Angular momentum loss mechanisms, such as gravitational radiation and magnetic braking, are also modelled. Wind accretion, where the secondary may accrete some of the material lost from the primary in a wind, is allowed with the necessary adjustments made to the orbital parameters in the event of any mass variations. Mass transfer also occurs if either star fills its Roche lobe and may proceed on a nuclear, thermal or dynamical time-scale. In the latter regime, the radius of the primary increases in response to mass-loss at a faster rate than the Roche-lobe of the star. Stars with deep surface convection zones and degenerate stars are unstable to such dynamical time-scale mass loss unless the mass ratio of the system is less than some critical value. On the other hand, mass transfer on a nuclear or thermal time-scale is assumed to be a steady process.

To run our simulation we choose the approximate cadence of the observations that we collected for M4, to have a precise comparison of the results.

Assuming the initial conditions described above and using this package, we simulated the radial velocities and the relative errors σ_{vr} for a population of 10000 binaries which survived for 12 Gyr.

6.2 The results

In this section we present the results for the model described above.

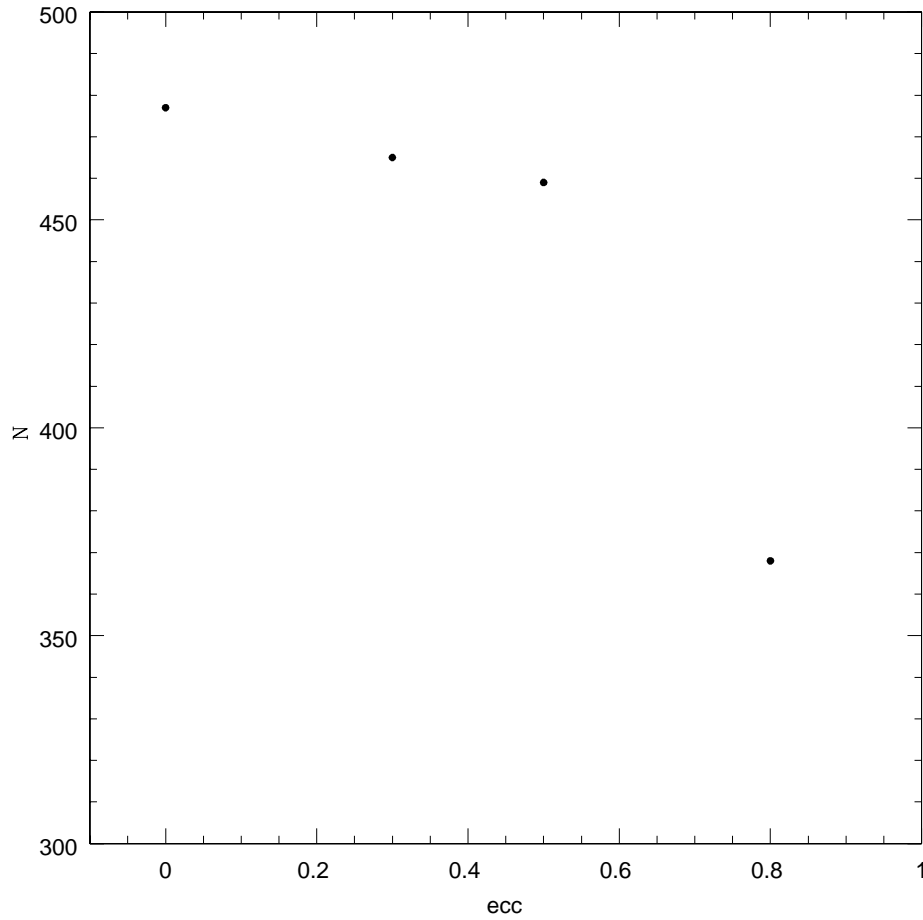


FIGURE 6.1— Number of simulated binaries found at different values of eccentricity.

6.2.1 The dependence of the eccentricities

As is written above, we ran the simulation with two different values of the eccentricity.

In order to check how the discovery of binary candidates in simulated data can depend on value of eccentricity, we ran the simulation a given precise value at this quantity. We decided to compare the results for $e=0, 0.3, 0.5$ and 0.8 .

In Figure 6.1 is shown the number of binaries expected to be discovered in a simulated sample as a function of the eccentricity. It is worth noticing that in this plot we are considering only the simulated population of binaries having

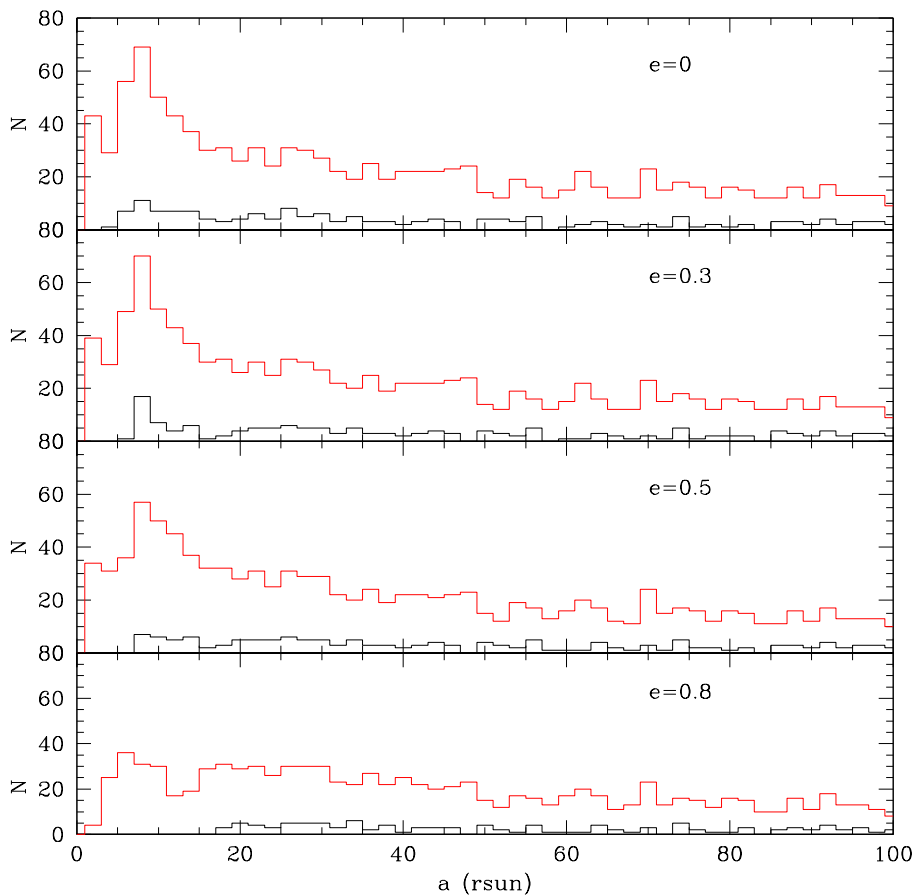


FIGURE 6.2— Histogram of semi axis at different values of eccentricity. The black line is the histogram for all the simulated populations, the red is the histogram for the binaries found in magnitude range of the observations.

the same magnitude range of the observations.

It is easy to notice that the number of binaries decreases going from eccentricity 0 to 0.8. This seems an indication that the binaries with elliptical orbits are generally harder to find than those with circular orbits, in agreement with the previous studies (see Hut 1992, and the references therein).

We also compare how the distributions of periods and semi-major-axis change with eccentricity. The results are shown in Figures 6.2 and 6.3. Figure 6.2 is

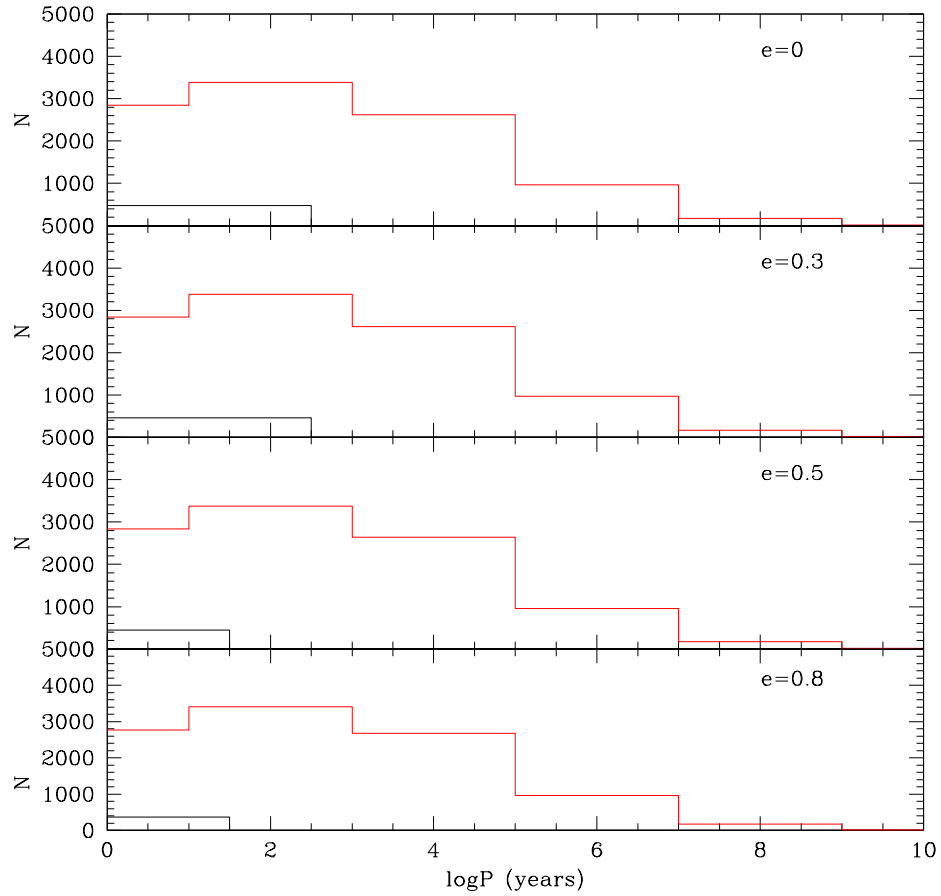


FIGURE 6.3— Histogram of periods at different values of eccentricity. The black line is the histogram for all the simulated populations, the red is the histogram for the binaries found in magnitude range of the observations.

the histogram of semi axis at different values of eccentricity. The red histogram shows the distribution of all the simulated binaries, while in black we plot only those binaries that have their magnitudes in the same range of our observations. Figure 6.3 is the histogram of periods at different values of eccentricity. The red and black histograms are showing the same stars as in Figure 6.2.

We noticed that as the eccentricity increases the number of systems with small semi-axis tend to disappear. On the other hand, for high value of the eccen-

tricity the systems tend to have shorter periods.

Presumably the only reason for any difference in the histograms is that fact that, at higher eccentricity, there can be collisions between the binary components, which tends to remove pairs at low semi-axis (as seen in Fig.6.2).

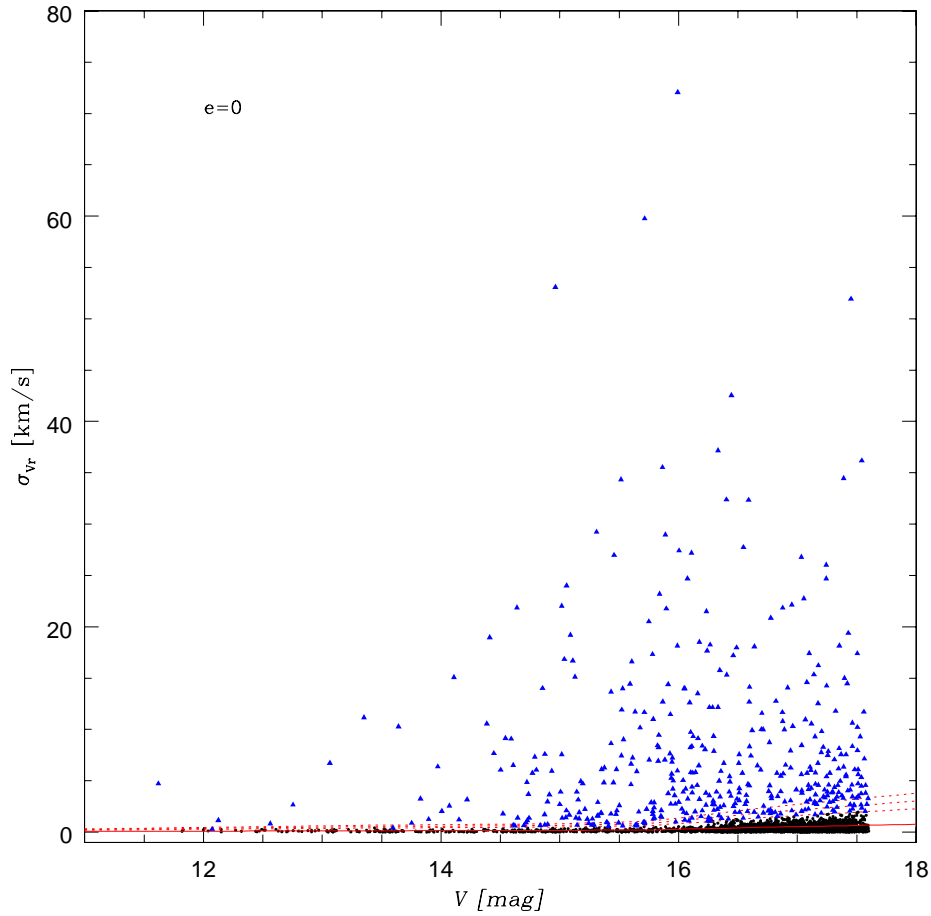


FIGURE 6.4— In this figure we show the scattered plot of radial velocity variation σ_{vr} against the V magnitude for the simulated population with eccentricity 0: the dotted lines indicate the 3, 4, and 5 $\sigma_{\overline{V_r}}$ level, the triangles represent the binary candidates with $\sigma_{vr} > 3\sigma$, where sigma is the standard deviation from the observational errors.

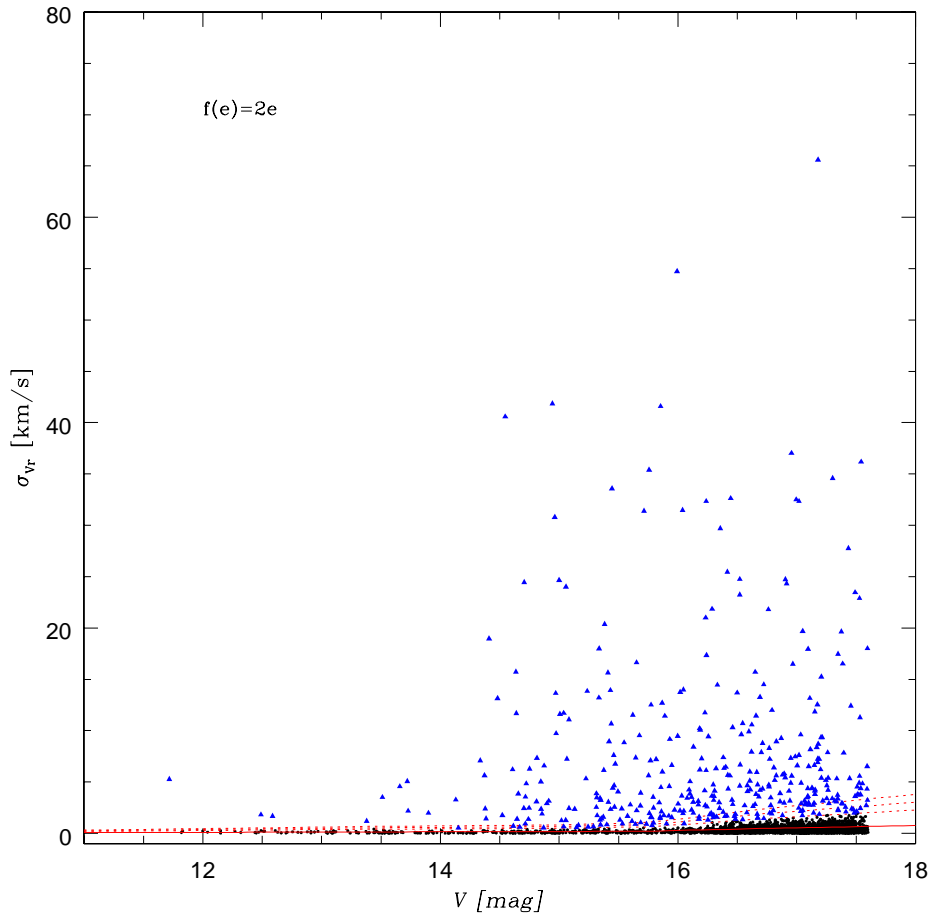


FIGURE 6.5— The same of the previous Figure for the results with a thermal distribution of eccentricities: the dotted lines indicate the 3, 4, and 5 $\langle \sigma_{\overline{v_r}} \rangle$ level, the triangles represent the binary candidates with $\sigma_{vr} > 3\sigma$, where sigma is the standard deviation from the observational errors.

6.2.2 Comparison with the observations

In order to have a direct comparison of the results of the simulations with the observed data we plotted the synthetic dataset in the plot that we used to discover our candidates (Figure 5.1) .

The value of the error σ_{vr} was calculated for the entire population with the same method that we used for the observed stars (see the description in section

5.1).

The comparison is presented in Figure 6.4 for the systems with circular orbits, and in Figure 6.5 for the binaries with the thermal distributions of the eccentricities. In these figures we show the plot of radial velocity variation σ_{vr} against the V magnitude for the simulated population: the dotted lines indicate the 3, 4, and 5 $< \sigma_{\overline{V_r}} >$ level (we used the same threshold of the observed data), the triangles represent the binary candidates with $\sigma_{vr} > 3\sigma$, where sigma is the standard deviation from the observational errors. With the Monte Carlo procedure described above, we simulated more binaries than those show in the figure, but many of these simulated systems are too faint to show up in this diagram. Therefore, the stars plotted in this are not the entire population simulated, but only the binaries found in the same magnitude range of the observations.

As we found above, the number of binaries discovered is larger in the case of circular orbits compared with the elliptical orbits.

Therefore, after we had evolved the sample to 12 Gyr and computed their σ_{vr} , of the binaries which were bright enough to have been observed, 28% would have had a significant σ_{vr} (above 3 sigma) in the first case, and 24% in the second.

It is worth noticing that for the moment we did not take in account the dynamical interactions with other stars and binaries, and the encounters between binary systems. We will consider the dynamic interactions in the next chapter. Then we consider a comparison between the distribution of the observed and simulated candidates, focusing on the distribution of σ_{vr} . The results are shown in Figure 6.6 where the dashed line represents the observed data, the dotted line the simulated sample with eccentricity zero and the solid line represents the binaries with the thermal distribution of the eccentricities.

A Kolmogorov-Smirnov (K-S) test were applied to the cumulative distributions of the σ_{vr} from both the simulated and the real data. A K-S test statistic is useful for rejecting the null hypothesis that the samples are drawn from the same distributions.

This test shows that these populations differ at the 95% confidence level.

On the basis of these results, to evaluate the true binary frequency, we estimated the incompleteness correction using the Monte Carlo simulations described above. We define Discovery Efficiency D_b is the ratio of binaries in the evolved sample, bright enough for observations, with period in some range about the stated value, with σ_{rv} above 3σ , divided by the number of binaries in the evolved sample, bright enough for observations, with period in this range about the stated value.

The results of that are presented in Figure 6.7. This plot represent the Discovery efficiency D_b as a function of the periods (in years) for both the simulations

with circular orbits $e=0$ (black dots) and for thermal distributions $f(e)=2e$ (red triangles). Each point in the plot represents the mean of 500 simulation tries. From this figure we can confirm what we noted above, and conclude that it is generally harder to find binaries with elliptical orbits than those with circular orbits. This is due to the fact that the stars in a system with elliptic orbits spend much of their orbit moving slowly near apoastron. In the next section we discuss the simulations that include dynamical evolution and conclude about the observed binary fraction in M4.

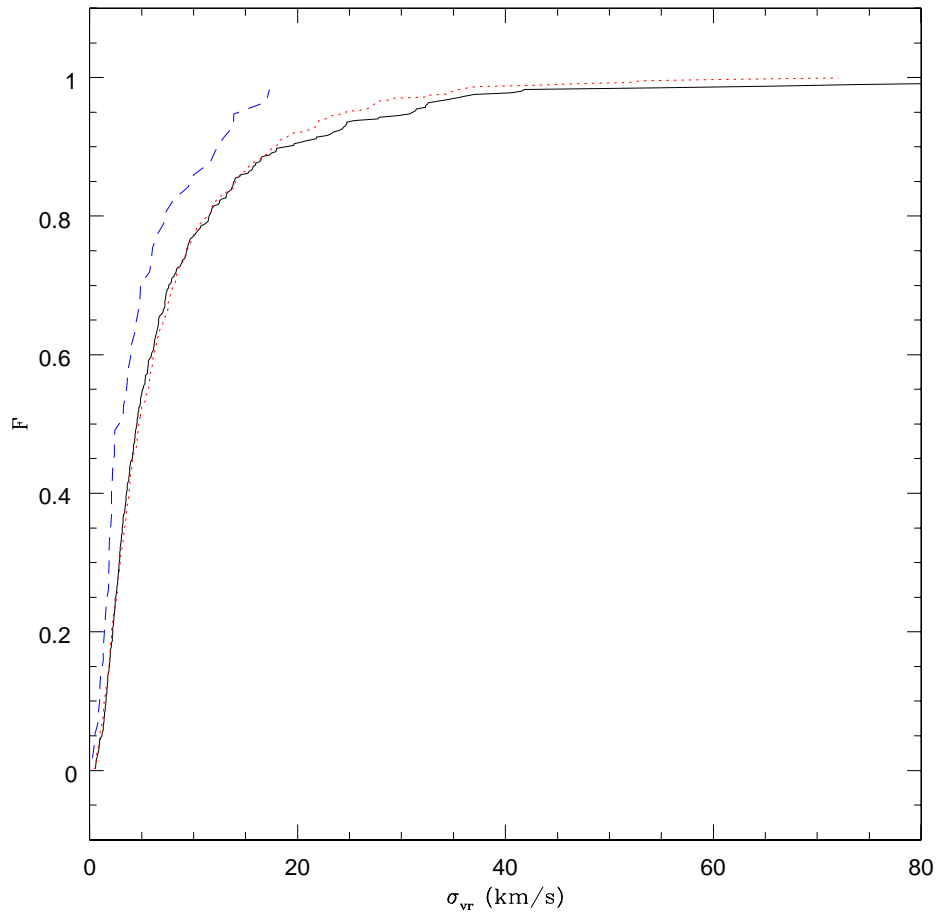


FIGURE 6.6— Cumulative distributions for the observed (dash line), the simulated with $e=0$ (dot line) and the simulated with thermal distribution of the eccentricities (solid line) of the binary candidates (respectively blue, red and black line in the electronic version).

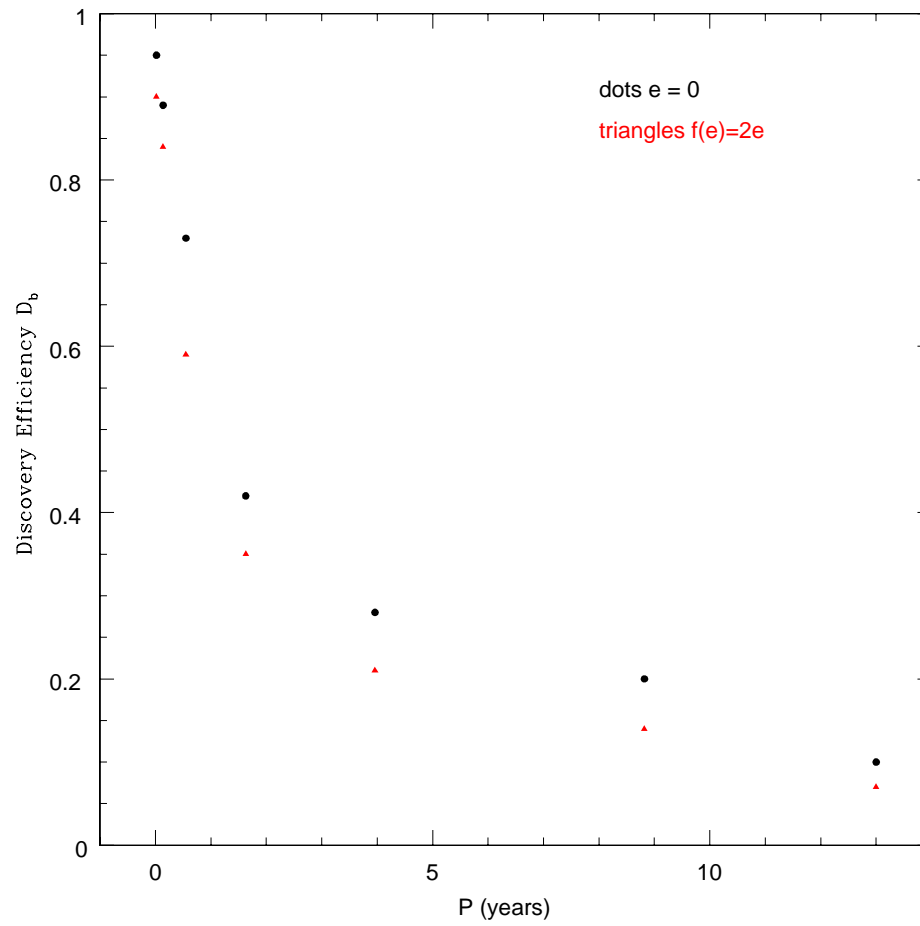


FIGURE 6.7— This plot represent the Discovery efficiency D_b as a function of the periods (in years) for both the simulations with circular orbits $e=0$ (black dots) and for thermal distributions $f(e)=2e$ (red triangles). Each point in the plot represents the mean of 500 simulation tries.

7

Comparison with the dynamical models

In this chapter we will present the comparison of our Monte Carlo simulations, with a model including the dynamical evolution of the cluster and of the binary systems.

The dynamical interactions with other stars and binaries and the encounters between binary systems are important because they are one of the principal processes that can drive and modify the evolution of the binary fraction in a globular cluster.

In fact, during a collision between a single star and a binary system the two objects change their energy. In particular, a fast star moving past a binary with slow internal rotation will lose on average some energy to the binary. Therefore, the star trying to speed up the members of the system, will lead them in a wider orbit with an actually lower velocity. This indicates that a soft system tends to become softer, and indeed this leads to its destrucion.

In opposite, an hard binary can capture a slowly moving field star and form a bound triple system. After some time, one of the star is ejected from the system with a velocity at infinity of the order of the internal binary velocity, and therefore larger than the initial velocity. To give this energy to the star, the binary has to increase its binding energy, and in order to do that the system shrinks and increases its orbital velocity. This suggest that an hard binary tends to become harder.

7.1 The dynamical model

We decided to compare our simulations with the dynamical evolutionary model for M4 recently constructed by Heggie & Giersz 2008, (hereafter HG).

Their model is based on a Monte Carlo simulation including appropriate stellar initial mass functions, a primordial binary population, galactic tidal effects, synthetic stellar and binary evolution, relaxation, and three- and four-body interactions. By adjustment of the initial conditions (total mass, tidal radius, initial mass function, binary fraction), this was brought into satisfactory agreement with the present-day surface brightness and velocity dispersion profiles, and the luminosity function at two radii.

This is the first time such a comprehensive, realistic evolutionary model has been constructed for any cluster.

They found that by 12 Gyr, the binaries exhibit segregation towards the core of the cluster. In addition, they showed that the binaries have evolved dynamically as well as through their internal evolution. In particular most of the soft binaries didn't survive during the dynamical evolution.

The most surprising discovery from this model was that M4 was found to be a post-collapse cluster sustained by binary burning. As a by-product, the model gives detailed predictions for the distribution of the binaries in space and period.

7.2 The dynamical interaction of binary systems

As we already stressed in the previous chapters, the dynamical interactions with other stars and binaries and the encounter between binary systems are important because they are one of the principal processes that can drive and modify the evolution of the binary fraction in a globular cluster.

We have pointed out that binary-binary interactions can halt the collapse of the core in a globular cluster. The other main effect of interactions involving binaries is the effect on the participating stars and binaries.

In a collision between binaries the most probable outcome is the destruction of the softer binaries and hardening on the harder one. As already mentioned in the introduction, soft binaries (with orbital speeds lower than the cluster velocity dispersion) can be disrupted easily by any strong encounter with another passing star or binary. Even hard binaries can be destroyed in resonant binary-binary encounters, which typically eject two single stars and leave only one binary remaining (Mikkola 1983), or produce physical stellar collisions or mergers (Bacon et al. 1996, Fregeau et al. 2004).

And more, also the evaporation could modify the life of a binary system.

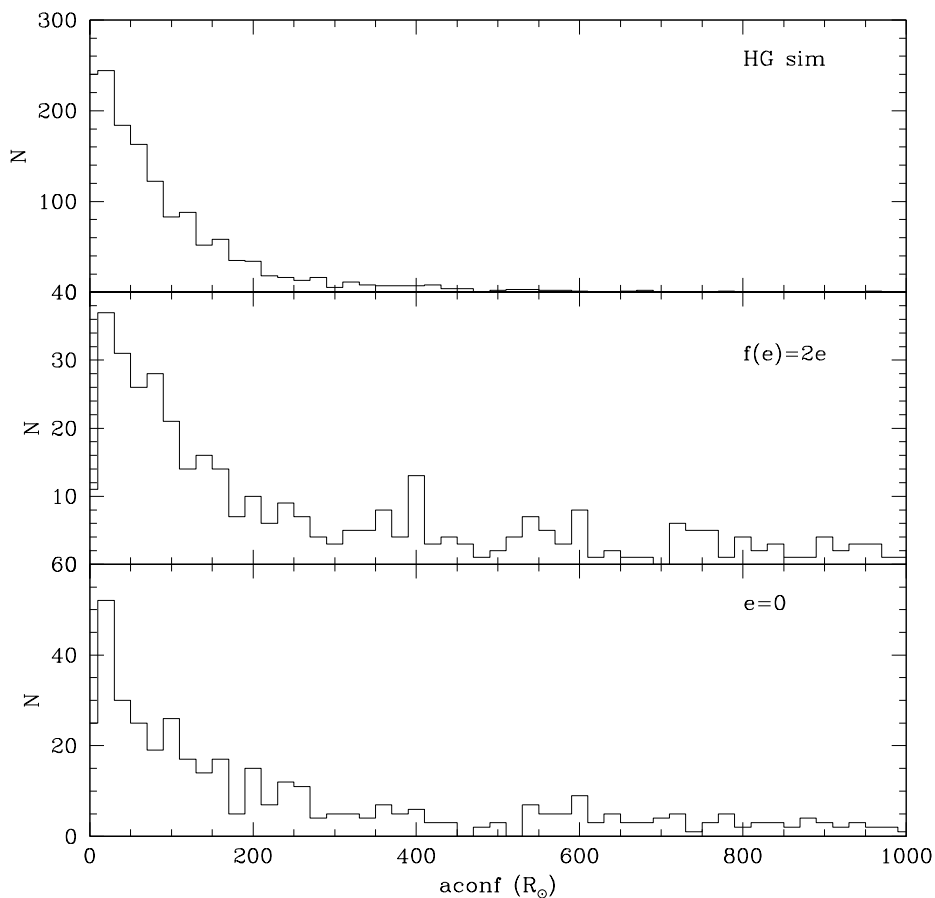


FIGURE 7.1— Comparison of the semi-major axis found in the different simulations that we are dealing with. In the upper panel the result for the Heggie & Giersz, in the middle the result for our Monte Carlo simulation assuming thermal distributions of the eccentricity, and in the bottom panel the result for our Monte Carlo simulation with eccentricity equal to zero. The semi-major axis are in the solar units.

7.3 Comparison with the previous results

In this section we compare the results found in our Monte Carlo simulations, considering both the simulation assuming the eccentricity equal to 0, and assuming the thermal distribution of the eccentricities, with the results found by Heggie & Giersz (2008).

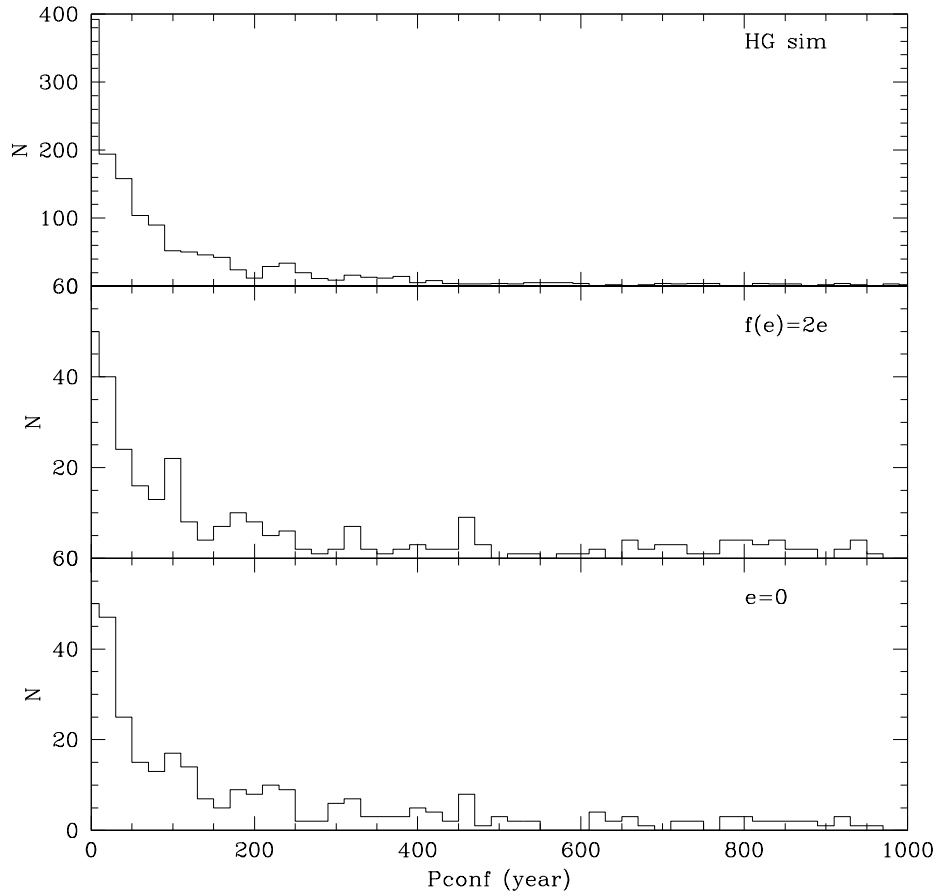


FIGURE 7.2— Comparison of the periods found in the different simulations that we are dealing with. In the upper panel the result for the Heggie & Giersz, in the middle the result for our Monte Carlo simulation assuming thermal distributions of the eccentricity, and in the bottom panel the result for our Monte Carlo simulation with eccentricity equal to zero. The periods are in years.

7.3.1 Periods and semi-axis distribution

One of the main process that drive the evolution of the binary fraction is the process of binary ionization. The binaries which are more subject to this process

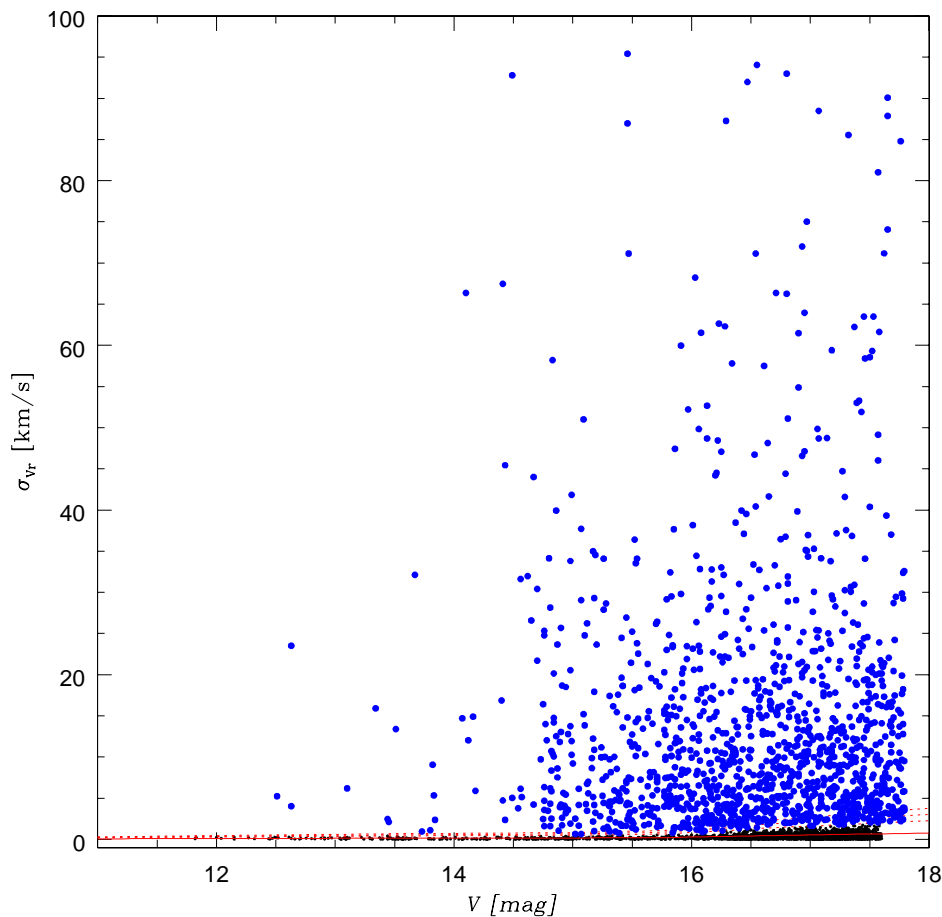


FIGURE 7.3— In this figure we show the plot of radial velocity variation σ_{vr} against the V magnitude for the simulated population of HG: the big dots represent the binary candidates with $\sigma_{vr} > 3\sigma$, where sigma is the standard deviation assuming the observational errors.

are those with smaller binding energy (i.e. longer periods and greater semi-axis). The shape of the periods and semi-axis distribution therefore changes if one takes into account the dynamical evolution of the globular cluster.

In Figure 7.1 and 7.2 we show the comparison of the distribution of the semi-axis and the periods respectively between the simulations that we described in the previous chapter and the dynamical models. In particular, in the upper panel the result for the Heggie & Giersz, in the middle the result for our Monte

Carlo simulation with eccentricity equal to zero, and in the bottom panel the result for our Monte Carlo simulation assuming thermal distributions of the eccentricity. The semi-axis are in the solar units, and the periods in years. It is easy to notice that the wide, long-period binaries have been eliminated by dynamical destruction.

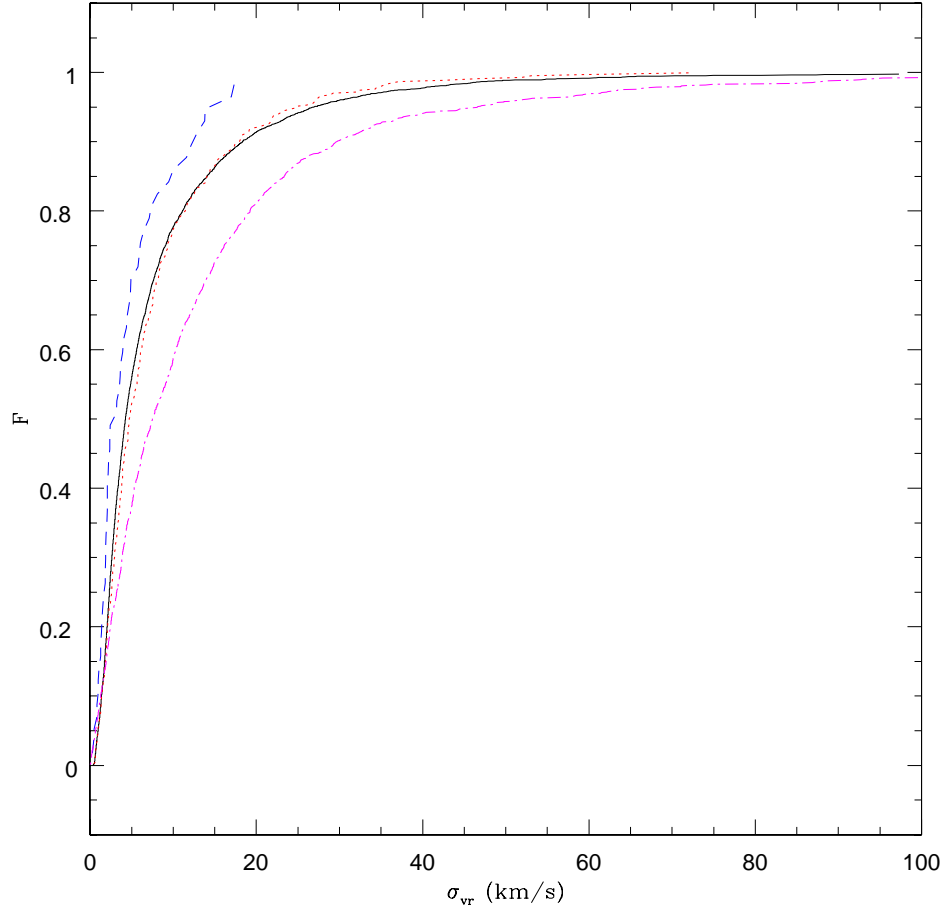


FIGURE 7.4— Cumulative distributions for the observed (dash line), the simulated with $e=0$ (dot line), the simulated with thermal distribution of the eccentricities (solid line) of the binary candidates and the HG simulations (dash-dot line).

7.3.2 Comparison with the observations.

As we have done in the previous chapter, to have a direct comparison of the results of the simulations with the observed data we over-plotted the synthetic dataset in the plot that we used to discover our candidates (Figure 5.1) .

The value of the error σ_{vr} was calculated for the entire population with the same method that we used for the observed stars, (see the description in section 5.1).

The comparison is shown in Figure 7.3 that is the plot of radial velocity variation σ_{vr} against the V magnitude for the simulated population: the blue dots represent the binary candidates with $\sigma_{vr} > 3\sigma$, where sigma is the standard deviation from the observational errors.

In this case, taking into account the dynamics effects, the total binary fraction found is 21%.

At the figure 6.6, where we have considered a comparison between the distribution of the observed and simulated candidates, focusing on the distribution of σ_{vr} , we have add the distribution for the σ_{vr} calculated for the sample extracted with the HG simulations. This is shown in Figure 7.4 where the dash line represents the observed data, the dotted line the simulated sample with eccentricity zero, the solid line represents the binaries with the thermal distribution of the eccentricities, and the dot dash line represent the HG simulations.

We can notice that, the line that represents the HG simulations is on the right with respect to our simulations. The reason is presumably that the wide, long-period binaries have been eliminated by dynamical destruction, which is also confirmed by the results shown in fig. 7.2.

Instead, the fact the line of the observed sample is to the left of the theoretical (model) distributions could be due to two reasons: either the $3\sigma_{vr}$ error level that we consider as our threshold for the detection is not rigorous enough, and therefore the observed distribution still includes objects which are spurious, or there is some instrumental bias against high σ_{vr} in the observational procedure.

7.3.3 The discovery efficiency

Also for these results we calculated the Discovery Efficiency D_b , in this case defined as the ratio of the binaries that we are able to detect over the total population of the binaries simulated. In Figure 7.5 we plotted the discovery efficiency as a function of the period for the three simulations: the stars represent our Monte Carlo simulation with eccentricity equal to zero, the dots represent our Monte Carlo simulation considering the thermal distribution of the eccentricities, and the triangles represent the HG simulations.

There are several methods for using the discovery efficiency to turn a discovery fraction into a binary frequency. One is simply to calculate the average efficiency over a range of periods, and assuming that all binaries discovered are probably within this range of periods and that there are no large variations within the range, dividing the discovery fraction by the discovery efficiency produces an average binary frequency.

In our case, considering the results of HG simulation that take into account the dynamical evolution of the cluster, we estimated the true binary frequency for M4 of about 14%.

This estimate is consistent with the binary fraction for nearby solar-type stars studied by Duquennoy & Mayor 1991.

7.4 The previous studies on the frequency of binaries

Now we want to answer the question: how does our binary fraction compare to the other estimates f_b in M4 and how does it compare to binary fraction measured spectroscopically in other clusters?

In 1995 Sigurdsson & Phinney studied the formation of the hierarchical triple system containing the pulsar PSR 1620-26. He claimed that only one such triple, thought to have formed through an exchange interaction between pre-existing binary milli-second pulsar, is expected for six or seven cluster similar to M4 and having binary fraction of the order of ~ 0.5 . In other words, the very existence of the PSR 1620-26 system argues from a rather large binary fraction. On the contrary, Richer et al. (1996) with the Hubble Space Telescope observations concluded that the approximate value of binary frequency in $1r_c$ among the main sequence stars is about 4%.

Recently, Milone et al. 2008 from HST observations gave a binary fraction in the core of M4 of 10% and 6% outside. But considering the systems with $q \geq 0.5$ they found a value of binaries of 6% inside the core and 4% outside.

We now consider the derived binary fraction measured for other clusters.

Côté & Fischer 1996 using Monte Carlo Simulation extracted for M4 a binary fraction of $15 \pm 15\%$ for systems with periods in the range from 2 days to 3 years and mass ratio between 0.2 and 2.

Hut et al. 1992, using data from (short period) eclipsing binary surveys and considering from Duquennoy & Mayor 1991 a binary fraction in the solar neighborhood of 65%, found a binary fraction in globular clusters between 20% and 35%, i.e. a lower value than the binary frequency in the solar neighborhood.

From the photometric study of stars in M71 conducted by Yan & Mateo 1994, the lower limit for the fraction of primordial binaries found is 1.3% with initial orbital periods in the range 2.5-5 days. From their simulations, they concluded

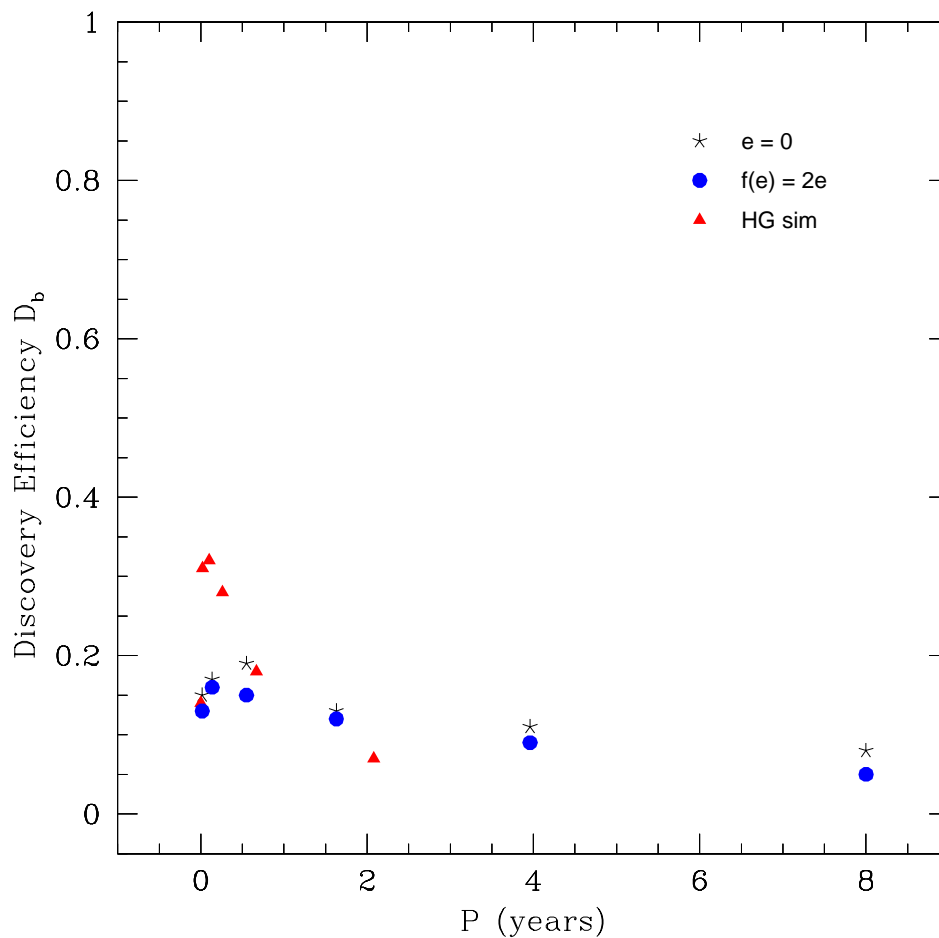


FIGURE 7.5— The discovery efficiency as a function of the period for the three simulations: the stars represent our Monte Carlo simulation with eccentricity equal to zero, the dots represent our Monte Carlo simulation considering the thermal distribution of the eccentricities, and the triangles represent the HG simulations.

that the primordial binary frequency is $f = 22^{+26}_{-12}\%$ for a flat distribution for the periods and $f = 27^{+15}_{-8}\%$ for a sloped distribution.

In 1991 Pryor et al. report preliminary results of a search for binary stars among a sample of 64 giants in two low density cluster NGC5053 and NGC 5466. They found that binary destruction should have been important in both. Estimates of discovery efficiency show that the hypothesis that binary frequency

in NGC5053 and NGC 5466 is the same as a dense cluster can be rejected at the 85%-97% confidence level, depending on how many binaries are included. For M5, Yan & Reid 1996 found a value of primordial binary fraction of $f = 28^{+11}_{-5.8}\%$ with a flat distribution, with the period range 2.5 days and 550 years.

Côté et al. 1996 using Monte Carlo simulations extracted the binary frequency in NGC3201. They found a fraction of binaries $\leq 15\% - 18\%$ under the assumption of thermal distribution of eccentricity, for periods $0.1 \leq P \leq 5 - 10\text{yr}$ and mass ratio $0.1 \leq q \leq 1$. Considering the binaries with circular orbits, the limits found are 6%-10%. With these results it appears that the binary frequency found in NGC3201 is almost equal to that of the field which is equal to 4%-8% in a similar range on period and mass.

Mayor et al 1996, assuming in their simulation for ω Centaury a period distribution found in Duquennoy & Mayor 1991 (the same that we described in the previous chapter 6.1), estimated a global binary fraction of 3%-4%.

Instead for the spectroscopic survey of M22, Côté et 1996, using Monte Carlo simulations, found a binary fraction of 1%-3%.

In summary, our derived binary fraction in M4 is in agreement with that of Côté & Fischer, but has much higher accuracy. It is somewhat lower than what Sigurdsson & Phinney predicted, and is somewhat higher than what was estimated from photometric studies. In other globular clusters derived binary fractions vary considerably, but also the error-bars of these estimates are quite large due to relatively small samples of stars observed. Clearly our study is providing an important improvement in that sense, providing a much more robust binary frequency estimate in a globular cluster.

8

Conclusions

In this section we summarize the results of this thesis. First we describe the conclusions for the observational part and then we present the results coming from the simulations.

8.1 Results of the observations

We have analyzed 5973 individual spectra of 2469 stars in the Galactic globular cluster M4. Each star has been observed at least twice, in a temporal interval of about three years. For 484 stars we have three epochs. All the data were obtained with the same instrument FLAMES+GIRAFFE at VLT, and with the same set-up HR9, centered on 525.8 nm and covering from 514.3-535.6 nm with a resolution of $R=25800$.

This database represents the largest multi-epoch high resolution spectroscopic sample ever collected in a globular cluster.

The observed stars cover a large range in luminosity, from the red giant branch tip to more than 1 magnitude below the TO, and cover most of the cluster extension from the inner core to the outskirts.

We cross-correlated all the stellar spectra with the solar template to derive accurate radial velocities. The average radial velocity of the observed stars is $70.29 \pm 0.07(\pm 0.3)(\pm 0.1) \text{ km s}^{-1}$, where the systematic errors in parenthesis include the effects such as gravitational redshift, convective blue shifts, and the global zero point uncertainty of the radial velocity. No systematic shift in average velocity is observed as a function of the stellar magnitude and color.

The search for variations in radial velocities among the stars with multi-epoch observations yielded 57 binary star candidates. The candidates in the bright sample The candidates in the bright sample ($V \leq 15$) have velocity variations

larger than $\sim 0.3 \text{ km s}^{-1}$ (i.e. 3σ where σ is an estimated of observational errors), while the fainter candidates ($V > 15 \text{ mag}$) have velocity variations larger than $\sim 0.5 \text{ km s}^{-1}$.

There are four binary star candidates out of 97 observed targets inside the core radius, and 53 candidates out of 2372 observed stars outside the core radius.

We have shown that increasing the stellar coverage from two epochs to three epochs, the number of binary candidates increases by 40%. Accounting for this incompleteness affecting stars with only two epochs, we have found that the lower limit for the binary fraction is $f = 3.0 \pm 0.3\%$; the binary fraction in the cluster core is $f = 5.1 \pm 2.3\%$, which decreases to $f = 3.0 \pm 0.4\%$ outside the core. Similarly, we found $f = 4.5 \pm 0.4\%$ and $f = 1.8 \pm 0.6\%$ for the binary fraction inside and outside the half mass radius.

As expected from energy equipartition, the binary fraction is higher in the central parts of the cluster.

8.2 Results of the simulations

In the second part of this thesis, we have presented detailed Monte Carlo simulations to evaluate the completeness of our survey by comparing the results with the observations.

These were then used together with the dynamical evolutionary modeling of Heggie & Giersz (2008) to derive the limits for the binary fraction in M4.

We have examined these models using the same observational constraints (on magnitude, radial distribution and cadence) as in the actual observations of M4 described in the first part of this thesis, in order to test our estimates of the completeness of the observational sample, and to improve our assumptions on the initial abundance and other parameters of the binaries in this cluster.

First, from our Monte Carlo simulation we examined the number of simulated binaries found for different values of the eccentricities. We found an indication that the binaries with elliptical orbits are generally harder to find than those with circular orbits, as published also in previous study.

We then compared the semi-major axis and periods distributions that we found with the Monte Carlo simulations and the results coming from the Heggie & Giersz (HG) simulations. As expected, we found that the wide, long periods binaries have been eliminated by dynamical destruction.

By applying the same criterion used in survey to the simulated data for identifying binary candidates, we calculated the discovery efficiency of our survey, in order to convert the binary discovery fraction to the true frequency.

In our case, considering the results of HG simulation that take into account the dynamical evolution of the cluster, we estimated the true binary frequency for

M4 about 14%.

In the Heggie & Giersz (2008) simulations the current binary fraction is about 1/3 of the original (because of the destruction of soft binaries). Therefore, on the basis on the results that we found in this thesis, i.e. 14%, the primordial binary fraction in M4 could have been about 40%. Value very close to what would be expected for young populations (Kroupa 2008).

From our results, in observational data one would expect to find very few if any variable stars with periods beyond about 1 year.

This prediction of the models will be tested through future observations of orbital parameters of binary star candidates that have been presented in Chapter 5 of the thesis and in Sommariva et al. 2009. The observations are scheduled for FLAMES at the VLT in the first half of 2009.

Finally, we stress again that this work is the best source of information on the actual binary fraction in the globular cluster, which is very important in addressing the question about the dynamical evolution of the globular clusters, including the production of exotic objects.

A

The binary candidates

In this appendix we give the list of the binary system candidates coming from two epochs, three epochs, and in one case with four epoch spectra. For each star, the table gives the radial velocity as measured in the different epochs with the corresponding errors, the coordinates (RA and DEC) in degrees, the Modified Julian Date of the observations, the number of epochs that each star has been observed, the radial distance from the center in arcmin, and the B and V magnitudes from the calibrated photometric catalogue (Momany, private communication).

TABLE A.1— List of the binary system candidates found. The columns are: ID, radial velocity and relative error that comes from the pipeline, the mean of the radial velocity, the weighed error, and the Modified Julian.

ID	$V_{r;i,j}$ [km/s]	$\sigma_{V_{r;i}}\text{-pipe.}$ [km/s]	$\overline{V_{r;i}}$ [km/s]	$\sigma_{\overline{V_{r;i}}}$ [km/s]	MJD
20979	72.37	0.41	70.09	2.23	53933.93
	67.82	0.34			52827.18
26688	85.41	0.28	66.43	11.25	52828.14
	63.03	0.28			53983.10
	50.87	0.28			53947.09
28573	76.79	0.30	66.22	13.86	52841.20
	47.65	0.42			53994.19
31674	61.22	0.18	63.71	2.59	52819.11
	66.20	0.01			53982.97
29065	66.20	0.01	66.72	0.50	52819.11
	67.24	0.01			53984.09
29725	73.13	0.22	81.81	6.47	52819.11
	90.50	0.50			53983.03
33538	72.78	0.20	74.12	1.30	52829.23
	75.46	0.25			53983.03
34848	66.75	0.12	65.53	1.07	52822.21
	64.31	0.07			52982.99
36750	69.10	0.12	71.56	2.43	52822.21
	74.03	0.14			53983.08
32874	67.79	0.02	68.24	0.42	52822.21
	68.70	0.01			53984.09
31015	67.17	0.02	75.29	5.93	52822.21
	79.30	0.01			53983.05
	79.40	0.01			53983.08
35327	71.21	0.28	72.43	1.22	52827.15
	73.65	0.29			53984.98
5195	62.88	0.36	64.10	1.32	52840.14
	65.32	0.31			53995.05
37894	76.21	0.32	78.12	1.91	52840.14
	80.03	0.32			53984.06
5001	67.53	0.44	69.20	1.55	52828.25
	70.87	0.30			53982.01
19378	75.17	0.47	72.44	2.38	52828.25
	69.71	0.27			53947.09
28771	73.42	0.22	65.30	8.13	52828.25

TABLE A.1— List of the binary system candidates found. The columns are: ID, radial velocity and relative error that comes from the pipeline, the mean of the radial velocity, the weighed error, and the Modified Julian.

ID	$V_{r;i,j}$ [km/s]	$\sigma_{V_{r;i}}\text{-pipe.}$ [km/s]	$\overline{V_{r;i}}$ [km/s]	$\sigma_{\overline{V_{r;i}}}$ [km/s]	MJD
30888*	91.20	0.33	78.49	12.13	52848
	65.78	0.46			53994.19
30917	59.07	0.18	66.47	7.13	52840.20
	73.87	0.23			53984.03
36036	82.19	0.06	80.07	2.08	52791.08
	77.96	0.07			53983.08
37488	67.01	0.17	68.43	1.45	52791.08
	69.93	0.17			53984.09
20288	61.82	0.22	65.52	3.70	53982.99
	69.23	0.23			52791.08
33901	58.72	0.17	62.05	3.24	52791.08
	65.38	0.21			53983.08
48830	77.58	0.47	75.41	2.17	53984.06
	73.24	0.45			52840.17
46654	69.32	0.32	71.14	1.81	52840.07
	72.97	0.37			53947.15
36225	76.42	0.29	78.55	2.01	52840.07
	80.69	0.41			53993.99
46544	61.34	0.31	68.04	6.05	52840.07
	74.74	0.20			53947.15
36891	62.00	0.33	59.98	2.00	52840.07
	57.97	0.36			53933.19
32308	38.72	0.24	56.18	16.98	52791.08
	73.65	0.19			53983.03
33234	69.51	0.11	68.64	0.83	52840.20
	67.77	0.16			53983.08
35997	74.88	0.21	76.92	1.86	52841.07
	78.96	0.33			53984.06
33700	64.49	0.49	61.14	7.49	52828.23
	68.48	0.19			53983.10
	50.47	0.36			53947.09

* Binary candidate in common with the photometric binary sample of Milone et al. (2008)

TABLE A.1— List of the binary system candidates found. The columns are: ID, radial velocity and relative error that comes from the pipeline, the mean of the radial velocity, the weighed error, and the Modified Julian.

ID	$V_{r;i,j}$ [km/s]	$\sigma_{V_{r;i,j}}\text{-pipe.}$ [km/s]	$\overline{V_{r;i}}$ [km/s]	$\sigma_{\overline{V_{r;i}}}$ [km/s]	MJD
37047	69.26	0.16	83.26	13.82	52822.21
	97.26	0.14			53983.03
30205	71.34	0.22	66.55	4.00	52841.07
	61.76	0.41			53985.04
29506	74.46	0.26	72.49	1.82	52841.07
	70.52	0.39			53933.99
32568	74.72	0.07	73.86	0.85	52829.20
	73.01	0.07			53982.97
31322	60.57	0.22	62.44	1.87	52829.20
	64.32	0.22			53983.03
46733	69.50	0.35	67.40	2.08	53984.06
	65.31	0.38			52842.08
30901	74.79	0.20	61.91	11.60	52842.08
	49.03	0.31			53994.99
42302	70.38	0.20	72.02	1.61	52840.20
	73.66	0.25			53984.09
29545	70.52	0.02	69.21	1.30	53984.03
	67.90	0.02			52829.18
29951	61.99	0.15	62.97	0.96	52829.18
	63.96	0.18			53983.03
34034	52.95	0.17	62.95	9.99	52829.18
	72.95	0.16			53983.08
37428	67.71	0.19	72.07	4.35	52828.20
	76.43	0.18			53949.07
34880	72.23	0.26	74.63	2.10	52841.07
	77.03	0.44			53994.19
28609	81.53	0.27	74.16	7.36	52841.11
	66.80	0.28			53994.19
19968	63.65	0.50	69.44	4.84	53933.99
	75.23	0.93			52841.11
41610	70.52	0.43	81.73	9.47	52842.15
	92.95	0.35			53948.97

TABLE A.1— List of the binary system candidates found. The columns are: ID, radial velocity and relative error that comes from the pipeline, the mean of the radial velocity, the weighed error, and the Modified Julian.

ID	$V_{r;i,j}$ [km/s]	$\sigma_{V_{r;i}}\text{-pipe.}$ [km/s]	$\overline{V_{r;i}}$ [km/s]	$\sigma_{\overline{V_{r;i}}}$ [km/s]	MJD
29998	72.02	0.14	77.28	3.62	52819.11
	79.26	0.14			53947.06
	80.57	0.18			53983.98
21175	71.67	0.18	65.69	4.73	52819.11
	62.03	0.15			53981.98
	63.37	0.16			53982.97
28498	84.03	0.15	81.89	2.40	53984.09
	78.42	0.15			52829.23
	83.22	0.14			53981.98
36912	69.93	0.11	65.47	3.51	52822.21
	62.64	0.15			53981.98
	63.86	0.22			53984.09
20390	61.05	0.23	62.98	1.40	52842.18
	63.93	0.24			53983.10
	63.93	0.18			53947.09
32898	63.18	0.23	62.62	2.04	53983.10
	60.26	0.23			52828.23
	64.42	0.19			53947.09
34006	64.02	0.00	64.07	0.28	53983.06
	63.82	0.00			52829.20
	64.39	0.00			53984.09
32057	78.73	0.08	74.44	3.92	52829.26
	70.78	0.09			53983.99
	70.82	0.07			53981.98
21652	68.49	0.13	74.80	4.48	52829.26
	77.49	0.14			53947.06
	77.71	0.16			53957.01
	75.07	0.17			53983.98
33529	66.55	0.10	70.40	1.00	52840.20
	64.52	0.08			53947.03
	80.14	0.09			53983.98

TABLE A.2— List of the binary system candidates found. The columns are: ID, the coordinates (RA and DEC), distance from the center in arcminutes, V , B magnitude.

ID	R.A. $_{J2000.0}$ [$^{\circ}$]	Decl. $_{J2000.0}$ [$^{\circ}$]	d[']	V	B
20979	245.8123	-26.5450	4.742	17.378	18.191
26688	245.9139	-26.6006	4.605	16.865	17.788
28573	245.8724	-26.5675	2.881	17.490	18.45
31674	245.9404	-26.5315	2.314	16.532	17.380
29065	245.9413	-26.5607	3.157	12.979	14.266
29725	245.8590	-26.5526	2.655	16.296	17.175
33538	245.9802	-26.5130	4.478	16.426	17.265
34848	245.8927	-26.4988	1.608	14.771	15.895
36750	245.9194	-26.4718	3.405	16.051	17.064
32874	245.9145	-26.5198	0.948	12.717	13.987
31015	245.8970	-26.5379	0.761	12.997	14.211
35327	245.9210	-26.4928	2.308	17.201	18.035
5195	245.8685	-26.3794	8.892	17.261	18.118
37894	245.9490	-26.4502	5.271	17.421	18.242
5001	245.8867	-26.3904	8.112	16.821	17.684
19378	245.8117	-26.6353	8.065	16.992	17.796
28771	245.9437	-26.5648	3.418	16.600	17.513
30888*	245.8761	-26.5393	1.441	17.553	18.528
30917	245.8475	-26.5388	2.824	16.521	17.437
36036	245.8917	-26.4829	2.562	15.488	16.533
37488	245.9620	-26.4586	5.276	16.393	17.238
20288	245.8205	-26.5819	5.372	16.499	17.399
33901	245.8636	-26.5093	2.072	16.493	17.378
48830	246.0294	-26.4270	9.202	17.205	18.001
46654	246.0240	-26.4882	7.125	17.151	17.960
36225	245.8420	-26.4800	4.045	17.630	18.470
46544	246.0017	-26.4915	5.931	17.117	17.957
36891	245.9397	-26.4693	4.036	17.543	18.378
32308	245.9271	-26.5254	1.568	16.470	17.347
33234	245.9176	-26.5161	1.190	15.960	16.944
35997	245.9326	-26.4834	3.127	17.381	18.203
33700	245.9214	-26.5115	1.507	16.775	17.661

* Binary candidate in common with the photometric binary sample of Milone et al. (2008)

TABLE A.3— List of the binary system candidates found. The columns are: ID, the coordinates (RA and DEC), distance from the center in arcminutes, V , B magnitude.

ID	R.A. $_{J2000.0}$ [$^{\circ}$]	Decl. $_{J2000.0}$ [$^{\circ}$]	d[']	V	B
37047	245.8907	-26.4666	3.539	16.360	17.361
30205	245.9273	-26.5468	2.043	17.224	18.083
29506	245.8777	-26.5553	2.104	17.345	18.224
32568	245.8941	-26.5228	0.249	15.115	16.136
31322	245.8841	-26.5348	0.935	16.279	17.099
46733	246.0225	-26.4863	7.085	17.331	18.144
30901	245.9395	-26.5391	2.383	17.271	18.123
42302	246.0015	-26.6027	7.249	16.477	17.366
29545	245.9274	-26.5548	2.378	13.793	14.961
29951	245.9003	-26.5497	1.475	16.180	17.110
34034	245.8745	-26.5079	1.630	16.299	17.262
37428	245.9348	-26.4598	4.400	16.849	17.662
34880	245.9261	-26.4984	2.213	17.327	18.211
28609	245.8587	-26.5670	3.274	17.447	18.304
19968	245.7893	-26.5990	7.316	17.349	18.163
41610	245.9920	-26.6219	7.692	17.020	17.874
29998	245.9307	-26.5492	2.273	16.495	17.395
21175	245.7992	-26.5366	5.340	16.437	17.361
28498	245.8761	-26.5688	2.863	16.443	17.431
36912	245.9136	-26.4690	3.480	16.447	17.321
20390	245.8059	-26.5764	5.812	16.598	17.436
32898	245.9117	-26.5195	0.816	16.698	17.526
34006	245.8713	-26.5082	1.755	11.865	13.366
32057	245.9256	-26.5277	1.496	15.618	16.598
21652	245.7849	-26.5161	6.089	15.973	16.952
33529	245.8953	-26.5131	0.739	16.238	17.24

B

The catalogue

In this appendix we give the list of the stars that we studied for this work. For each star, the table give the radial velocity as measured in the different epochs with the corresponding errors, the coordinates (RA and DEC) in degrees, , and the B , V , U and I magnitudes from the calibrated photometric catalogue (Momany, private communication).

TABLE B.1— Catalogue of stars that we studied. The columns are: ID, the mean of the radial velocity, the weighed error, the coordinates (RA and DEC), and the V , B , U , I *magnitude*.

ID	V_r	σ_{V_r}	R.A.	Decl.	V	B	U	I
5066	69.94	0.31	245.8627	-26.3871	16.458	17.3440	15.1950	17.6170
4692	72.51	0.24	245.8424	-26.4054	16.445	17.3600	15.1330	17.6440
22355	73.20	0.13	245.7943	-26.4825	16.457	17.3880	15.1080	17.6770
35840	74.19	0.18	245.8646	-26.4856	16.526	17.3960	15.2470	17.5470
36663	72.67	0.17	245.8752	-26.4731	16.490	17.3970	15.1870	17.5970
32494	76.92	0.05	245.8602	-26.5236	14.963	16.0500	13.4640	16.4940
32280	73.27	0.17	245.8516	-26.5256	16.490	17.3930	15.1690	17.5580
33480	69.73	0.15	245.8382	-26.5136	16.391	17.3350	15.0400	17.5350
34378	69.92	0.04	245.8924	-26.5040	14.568	15.6580	13.0840	16.2040
36001	62.95	0.05	245.9131	-26.4833	15.070	16.1360	13.6090	16.5970
33683	75.57	0.01	245.8991	-26.5117	13.481	14.6600	11.9110	15.2920
35641	73.60	0.06	245.9223	-26.4884	15.655	16.7030	14.2290	17.1400
35824	68.04	0.10	245.8809	-26.4859	16.187	17.1620	14.8130	17.4760
33788	72.23	0.01	245.9106	-26.5105	12.988	14.2390	11.3760	15.1500
34463	71.05	0.14	245.9136	-26.5030	16.423	17.3270	15.1460	17.4930
35319	69.74	0.06	245.8570	-26.4929	15.595	16.6560	14.1230	17.1130
32739	69.48	0.04	245.9392	-26.5210	14.843	15.9010	13.4180	16.2870
34342	75.25	0.05	245.8861	-26.5045	15.052	16.1170	13.5860	16.5700
5018	53.89	0.05	245.8973	-26.3895	15.218	16.2190	13.9650	16.9470
35690	70.42	0.07	245.9263	-26.4877	15.784	16.8240	14.3610	17.1880
48101	65.77	0.32	246.0622	-26.4491	16.319	17.1500	15.1440	17.2380
48135	68.52	0.26	246.0344	-26.4479	16.434	17.2200	15.3190	17.2490
48182	69.72	0.31	246.0568	-26.4462	16.214	17.0640	15.0290	17.1530
37744	74.22	0.07	245.9769	-26.4532	15.249	16.2650	13.8990	16.6580
32700	70.65	0.01	245.9171	-26.5214	12.521	13.8630	10.8010	14.8810
37271	67.18	0.20	245.9727	-26.4625	16.504	17.3000	15.3680	17.3750
32272	80.97	0.07	245.9184	-26.5257	15.899	16.9440	14.4820	17.2940
35549	74.84	0.09	245.8806	-26.4897	16.090	17.0840	14.6910	17.3790
32158	76.46	0.11	245.9257	-26.5268	16.346	17.2870	15.0070	17.5340
48843	68.13	0.21	246.0163	-26.4266	16.123	16.9770	14.9300	17.1070
34873	74.73	0.18	245.8766	-26.4985	16.458	17.3080	15.2170	17.4530
48868	73.57	0.19	246.0072	-26.4258	15.994	16.9480	14.7230	17.2090
30973	64.07	0.17	245.9437	-26.5383	16.489	17.3430	15.2560	17.4450
47026	76.18	0.19	246.0566	-26.4779	16.243	17.1040	15.0380	17.2180
47939	68.18	0.08	246.0235	-26.4535	14.934	15.9540	13.5830	16.3660
34894	75.32	0.08	245.9250	-26.4982	15.932	16.9560	14.5230	17.3310
35212	79.12	0.11	245.9674	-26.4942	16.227	17.2040	14.8890	17.4900
29599	71.46	0.04	245.9286	-26.5541	14.962	16.0740	13.4510	16.5550
33835	64.36	0.13	245.9748	-26.5100	16.349	17.2730	15.0630	17.4620
35161	69.71	0.03	245.9775	-26.4949	14.119	15.2260	12.6720	15.7860
30492	72.63	0.09	245.9494	-26.5436	16.148	17.1610	14.7630	17.4750

TABLE B.2— Catalogue of stars that we studied. The columns are: ID, the mean of the radial velocity, the weighed error, the coordinates (RA and DEC), and the V , B , U , I *magnitude*.

ID	V_r	σ_{V_r}	R.A.	Decl.	V	B	U	I
44718	70.71	0.17	246.0025	-26.5373	16.406	17.2540	15.1930	17.3370
32465	71.18	0.04	245.9638	-26.5238	14.927	15.9920	13.4900	16.3800
26100	76.30	0.05	245.9683	-26.6133	14.997	16.0730	13.5560	16.5230
33704	71.97	0.05	245.9640	-26.5114	15.348	16.4050	13.9410	16.8360
29998	72.02	0.14	245.9307	-26.5492	16.495	17.3950	15.2040	17.5500
30433	69.88	0.13	245.9420	-26.5443	16.444	17.3650	15.1370	17.5290
29521	75.39	0.12	245.9792	-26.5550	16.386	17.3620	15.0250	17.5890
31145	66.30	0.09	245.9197	-26.5366	16.041	17.0500	14.6380	17.3070
30189	66.13	0.12	245.9777	-26.5470	16.340	17.3450	14.9730	17.6170
30120	75.74	0.07	245.8962	-26.5479	15.667	16.7200	14.2060	17.0810
23844	68.45	0.19	245.8819	-26.6711	16.283	17.2120	14.9500	17.4990
29848	76.95	0.02	245.8921	-26.5510	13.517	14.7510	11.8670	15.4820
29598	72.42	0.02	245.8890	-26.5541	13.676	14.8880	12.0510	15.6490
26825	67.12	0.17	245.8775	-26.5980	16.506	17.3950	15.2060	17.5170
30128	66.85	0.03	245.9565	-26.5478	14.319	15.4480	12.8090	15.9190
27816	68.61	0.08	245.9412	-26.5795	15.962	17.0340	14.4990	17.4340
27693	64.82	0.04	245.9465	-26.5816	14.856	15.9660	13.3510	16.4680
30598	76.80	0.01	245.8965	-26.5423	12.049	13.4900	10.2260	14.7240
28248	69.35	0.14	245.9402	-26.5728	16.457	17.4110	15.0960	17.6100
29075	68.33	0.08	245.9260	-26.5606	15.911	16.9490	14.4720	17.3020
27474	72.37	0.18	245.9203	-26.5853	16.534	17.4380	15.2180	17.5910
29380	73.61	0.08	245.8997	-26.5569	15.661	16.6700	14.2150	16.9460
28847	69.57	0.02	245.9046	-26.5638	13.535	14.7610	11.8750	15.4330
29852	69.15	0.08	245.8712	-26.5510	15.766	16.8550	14.2370	17.3250
19631	74.00	0.45	245.7627	-26.6188	16.411	17.2930	15.1130	17.4580
33311	71.59	0.04	245.8772	-26.5154	14.986	16.0550	13.5160	16.5620
19909	66.88	0.57	245.7547	-26.6023	16.446	17.3180	15.1630	17.4590
26892	63.45	0.15	245.8690	-26.5967	16.449	17.4060	15.0740	17.6540
20383	74.15	0.37	245.7904	-26.5767	16.478	17.3210	15.2340	17.4380
20415	66.15	0.19	245.8074	-26.5746	16.490	17.3670	15.1870	17.5470
28867	63.11	0.11	245.8419	-26.5635	16.322	17.3090	14.9180	17.6560
19919	71.56	0.26	245.7492	-26.6017	16.124	17.1660	14.6830	17.5080
20193	72.37	0.45	245.7957	-26.5867	16.450	17.3530	15.1300	17.5720
20544	65.53	0.24	245.8162	-26.5683	16.491	17.3470	15.2220	17.4810
20711	67.16	0.10	245.7917	-26.5598	15.507	16.5670	14.0320	17.0330
30924	67.84	0.02	245.8962	-26.5388	13.609	14.7920	12.0280	15.4810
31068	71.12	0.06	245.8356	-26.5374	15.244	16.3010	13.7800	16.6870
20073	66.12	0.05	245.7613	-26.5934	13.968	15.1260	12.4170	15.8200
35164	67.55	0.07	245.8743	-26.4949	15.625	16.6380	14.2100	17.0370
31044	63.19	0.09	245.8647	-26.5376	16.229	17.2350	14.8180	17.6040
21175	71.67	0.18	245.7992	-26.5366	16.437	17.3610	15.0980	17.5550

TABLE B.3— Catalogue of stars that we studied. The columns are: ID, the mean of the radial velocity, the weighed error, the coordinates (RA and DEC), and the V , B , U , I *magnitude*.

ID	V_r	σ_{V_r}	R.A.	Decl.	V	B	U	I
31190	77.01	0.04	245.8842	-26.5361	14.779	15.8690	13.2990	16.3800
22001	64.95	0.18	245.7823	-26.5011	16.476	17.3830	15.1550	17.5980
21517	66.35	0.31	245.7743	-26.5219	16.511	17.3830	15.2430	17.5350
21266	73.51	0.23	245.7731	-26.5324	16.485	17.4180	15.1300	17.6450
21161	74.35	0.02	245.7919	-26.5371	13.701	14.9200	12.0790	15.6700
30381	73.95	0.02	245.8336	-26.5448	13.559	14.7410	11.9710	15.4630
22792	68.38	0.07	245.7716	-26.4589	15.298	16.3720	13.7870	16.8710
23427	72.67	0.17	245.7610	-26.4183	15.685	16.7070	14.2550	17.0980
33190	64.18	0.16	245.8672	-26.5165	16.511	17.3900	15.2320	17.5290
23165	71.27	0.29	245.7677	-26.4367	16.456	17.3580	15.1350	17.5990
22753	75.76	0.15	245.7607	-26.4616	16.162	17.1610	14.7380	17.5150
22016	68.57	0.24	245.8125	-26.5005	16.464	17.3360	15.1960	17.5120
34462	60.94	0.08	245.8897	-26.5031	15.283	16.3250	13.8390	16.7720
34855	59.47	0.16	245.8964	-26.4987	16.301	17.2390	14.9730	17.4510
23226	69.95	0.14	245.8155	-26.4326	15.963	16.9880	14.4970	17.4560
39010	66.02	0.24	245.8944	-26.4260	16.466	17.3820	15.1530	17.5710
22215	70.33	0.13	245.8030	-26.4903	15.971	16.9140	14.6210	17.2180
23019	75.48	0.30	245.8151	-26.4463	16.537	17.3890	15.2770	17.5800
23055	64.01	0.15	245.8031	-26.4445	16.265	17.2680	14.8340	17.6640
22446	75.94	0.21	245.8074	-26.4783	16.394	17.3100	15.0730	17.5630
36141	72.17	0.22	245.8975	-26.4813	16.467	17.3430	15.1990	17.4980
21342	64.60	0.17	245.8031	-26.5290	16.177	17.1850	14.7810	17.5820
33447	64.62	0.09	245.8700	-26.5141	15.133	16.1890	13.6740	16.6570
34310	72.82	0.13	245.8440	-26.5048	16.163	17.1680	14.7490	17.5330
22089	71.27	0.02	245.8203	-26.4965	13.137	14.3600	11.5400	15.2800
34580	67.28	0.21	245.8413	-26.5016	16.314	17.1520	15.0890	17.2500
33696	70.47	0.25	245.8344	-26.5115	16.537	17.3710	15.3110	17.4880
21900	66.73	0.24	245.8228	-26.5055	16.498	17.3340	15.2740	17.4740
22280	76.38	0.26	245.8207	-26.4864	16.478	17.3230	15.2430	17.4820
36483	66.58	0.04	245.8391	-26.4759	14.416	15.5380	12.8740	16.1730
37725	69.88	0.16	245.9071	-26.4537	16.453	17.4480	15.0540	17.7440
36912	69.93	0.11	245.9136	-26.4690	16.447	17.3210	15.2020	17.4830
36982	75.56	0.10	245.9212	-26.4677	15.552	16.5820	14.1270	17.0090
35508	72.69	0.03	245.8541	-26.4902	13.801	14.9610	12.2320	15.6640
35704	72.51	0.11	245.8651	-26.4875	15.852	16.8790	14.4180	17.3060
35670	61.31	0.13	245.8697	-26.4880	16.032	17.0290	14.6430	17.4010
33941	72.56	0.07	245.8622	-26.5089	15.051	16.1320	13.5580	16.6370
33886	71.16	0.04	245.8665	-26.5094	14.156	15.3100	12.5810	15.9120
36264	70.09	0.34	245.9789	-26.4795	16.471	17.2330	15.2880	17.2810
46713	73.67	0.30	246.0054	-26.4867	16.440	17.2490	15.3030	17.2950
47511	72.48	0.15	246.0008	-26.4654	15.819	16.8210	14.4930	17.1240

TABLE B.4— Catalogue of stars that we studied. The columns are: ID, the mean of the radial velocity, the weighed error, the coordinates (RA and DEC), and the V , B , U , I *magnitude*.

ID	V_r	σ_{V_r}	R.A.	Decl.	V	B	U	I
48159	66.99	0.08	245.9896	-26.4471	15.007	16.0370	13.6340	16.3770
38443	73.79	0.27	245.9122	-26.4382	16.521	17.3950	15.2720	17.5440
48102	72.75	0.26	246.0103	-26.4490	16.282	17.1020	15.1410	17.1530
38580	77.10	0.07	245.9621	-26.4354	15.113	16.1510	13.7160	16.5750
34005	71.59	0.04	245.8895	-26.5082	14.057	15.1950	12.5210	15.8660
34004	64.45	0.15	245.8953	-26.5082	16.246	17.2390	14.8590	17.5710
48593	69.67	0.34	246.0204	-26.4343	16.319	17.1210	15.1850	17.1760
38399	66.46	0.02	245.8848	-26.4390	13.137	14.3650	11.5100	15.2280
4644	69.86	0.12	245.9422	-26.4072	15.467	16.5140	14.0660	17.0590
35974	72.92	0.19	245.9568	-26.4836	16.252	17.2040	14.9410	17.4180
36443	72.66	0.18	245.9040	-26.4765	16.343	17.2840	15.0060	17.5380
46751	64.98	0.16	246.0166	-26.4856	16.025	17.0120	14.6980	17.2830
34635	68.82	0.09	245.9597	-26.5010	15.182	16.2190	13.7850	16.6430
33657	62.17	0.10	245.9725	-26.5119	15.336	16.3750	13.9350	16.7940
47890	67.21	0.14	245.9913	-26.4549	15.638	16.6460	14.2920	17.0130
46955	71.98	0.14	245.9970	-26.4798	16.000	16.9660	14.7070	17.1840
35601	73.85	0.15	245.8967	-26.4890	16.276	17.2660	14.9110	17.5790
34961	64.62	0.19	245.9195	-26.4973	16.395	17.2890	15.1340	17.4510
43429	76.03	0.18	246.0167	-26.5722	16.027	17.0700	14.6090	17.3940
34502	63.57	0.03	245.9204	-26.5025	13.616	14.7810	12.0940	15.4910
27796	69.60	0.08	245.8933	-26.5798	15.448	16.5590	13.8980	17.0580
34280	70.01	0.05	245.9152	-26.5051	14.631	15.7240	13.1570	16.1830
34167	62.06	0.04	245.9041	-26.5063	13.954	15.0840	12.4390	15.6290
36559	75.27	0.06	245.9159	-26.4746	14.780	15.8540	13.3190	16.3810
29673	59.45	0.08	245.9173	-26.5532	15.326	16.4050	13.8620	16.8140
35765	65.07	0.22	245.9373	-26.4866	16.344	17.2010	15.1410	17.3320
34337	73.20	0.05	245.9390	-26.5045	14.497	15.5850	13.0450	16.1280
29171	67.17	0.03	245.8996	-26.5595	13.732	14.9530	12.0870	15.7180
30566	77.12	0.08	245.9112	-26.5427	15.379	16.4670	13.8750	16.9430
34299	69.01	0.25	245.9535	-26.5049	16.426	17.2820	15.2040	17.3870
25072	74.72	0.34	245.9297	-26.6388	16.472	17.3400	15.2340	17.4740
24332	73.17	0.05	245.9338	-26.6581	14.363	15.4710	12.9260	18.1220
24949	65.23	0.12	245.8966	-26.6417	15.708	16.7500	14.2740	17.1300
25308	73.00	0.26	245.9480	-26.6322	16.361	17.2600	15.0920	17.3750
29680	64.26	0.05	245.9115	-26.5531	14.442	15.5800	12.8830	16.0560
32852	66.05	0.10	245.9227	-26.5200	15.697	16.7570	14.2530	17.1780
32347	64.52	0.01	245.9207	-26.5250	000000	0000000	0000000	0000000
30680	63.43	0.16	245.8909	-26.5415	16.376	17.3420	14.9850	17.6110
31856	65.82	0.05	245.8897	-26.5297	14.485	15.6020	12.9720	16.1340
25169	70.08	0.05	245.8954	-26.6357	14.492	15.5880	13.0040	16.1380
25039	69.30	0.34	245.9117	-26.6397	16.532	17.3990	15.2790	17.5200

TABLE B.5— Catalogue of stars that we studied. The columns are: ID, the mean of the radial velocity, the weighed error, the coordinates (RA and DEC), and the V , B , U , I *magnitude*.

ID	V_r	σ_{V_r}	R.A.	Decl.	V	B	U	I
29583	63.26	0.07	245.8740	-26.5544	15.049	16.1640	13.5160	16.6970
27044	78.57	0.06	245.9350	-26.5936	14.645	15.7830	13.1040	16.3270
24021	69.26	0.05	245.9008	-26.6667	14.142	15.2740	12.6260	17.5020
24895	71.51	0.09	245.9242	-26.6432	15.310	16.3730	13.8760	16.8220
24590	71.54	0.03	245.9166	-26.6508	13.436	14.6740	11.8840	16.8940
26094	62.67	0.14	245.8890	-26.6134	15.600	16.6840	14.1050	17.1180
19397	73.10	0.30	245.8083	-26.6340	16.354	17.2350	15.0660	17.4150
31576	73.86	0.06	245.9120	-26.5325	14.816	15.8880	13.3460	16.3760
26291	65.32	0.07	245.9143	-26.6089	14.755	15.8990	13.1930	16.4690
25922	71.66	0.22	245.9140	-26.6175	16.421	17.3390	15.1010	17.4680
25857	69.30	0.30	245.9006	-26.6193	16.447	17.3080	15.1790	17.4000
19495	74.77	0.33	245.8010	-26.6273	16.490	17.3040	15.2530	17.4170
26213	71.41	0.27	245.8571	-26.6106	16.492	17.3400	15.2380	17.4530
26471	72.00	0.03	245.8812	-26.6051	13.489	14.6990	11.8670	15.3820
32061	75.08	0.17	245.8826	-26.5276	16.396	17.3020	15.0870	17.5200
33736	69.73	0.04	245.8587	-26.5111	14.113	15.2470	12.5580	15.8140
34509	66.34	0.17	245.8575	-26.5025	16.433	17.3770	15.0780	17.6290
33988	71.26	0.22	245.8548	-26.5085	16.473	17.3310	15.2180	17.4900
19899	76.71	0.14	245.7777	-26.6030	15.657	16.7040	14.2150	17.1500
26899	70.81	0.21	245.8955	-26.5966	16.573	17.5470	15.1740	17.7820
19639	72.60	0.26	245.7822	-26.6182	16.203	17.1880	14.8270	17.4530
19849	72.48	0.26	245.7572	-26.6059	16.388	17.2970	15.0730	17.4690
28147	66.45	0.06	245.8677	-26.5744	14.711	15.8330	13.1700	16.4020
32500	75.16	0.23	245.8873	-26.5235	16.492	17.3710	15.2110	17.5650
32782	77.72	0.04	245.8910	-26.5206	13.940	15.1040	12.3820	15.8140
29282	71.34	0.01	245.8554	-26.5581	12.876	14.1720	11.1750	15.1730
28244	78.05	0.12	245.8342	-26.5729	15.889	16.9540	14.4100	17.3550
26800	71.52	0.09	245.8506	-26.5985	15.303	16.3750	13.8140	16.7620
30141	77.55	0.08	245.8392	-26.5477	15.334	16.3830	13.8640	16.7380
29015	75.33	0.06	245.8654	-26.5616	14.593	15.7390	13.0150	16.3340
27001	72.50	0.25	245.8568	-26.5945	16.417	17.3070	15.1160	17.4730
22491	76.29	0.05	245.7913	-26.4759	14.501	15.5980	12.9960	16.1370
29924	73.21	0.25	245.8465	-26.5500	16.515	17.3970	15.2100	17.5090
29272	71.08	0.03	245.8628	-26.5582	13.420	14.6400	11.7550	15.3200
29494	69.89	0.11	245.8654	-26.5554	15.823	16.9100	14.3040	17.3810
30450	68.20	0.02	245.8614	-26.5441	13.340	14.5870	11.6880	15.4440
30055	66.56	0.09	245.8766	-26.5486	15.579	16.6540	14.0830	17.1250
21887	66.54	0.26	245.7837	-26.5061	16.546	17.3960	15.2870	17.5710
30559	77.16	0.18	245.8815	-26.5428	16.380	17.3610	14.9870	17.6710
32281	68.89	0.14	245.8562	-26.5256	16.161	17.1820	14.7350	17.5700
32087	76.22	0.18	245.8699	-26.5275	16.375	17.3580	14.9850	17.6350

TABLE B.6— Catalogue of stars that we studied. The columns are: ID, the mean of the radial velocity, the weighed error, the coordinates (RA and DEC), and the V , B , U , I *magnitude*.

ID	V_r	σ_{V_r}	R.A.	Decl.	V	B	U	I
31878	70.71	0.23	245.8362	-26.5295	16.976	17.8000	15.7420	17.8500
31070	75.63	0.25	245.8429	-26.5374	17.040	17.8620	15.8080	17.9350
31649	68.80	0.16	245.8632	-26.5318	16.617	17.4910	15.3280	17.6290
31730	70.24	0.24	245.8677	-26.5309	16.783	17.6690	15.5250	17.8630
35379	69.07	0.27	245.8614	-26.4921	17.036	17.8560	15.8060	17.9720
31039	76.23	0.17	245.8788	-26.5377	16.660	17.4990	15.4220	17.6160
33623	70.25	0.25	245.9277	-26.5122	16.654	17.4640	15.4620	17.5770
33589	66.62	0.20	245.8690	-26.5125	16.775	17.6140	15.5290	17.7360
34517	73.64	0.17	245.9080	-26.5024	16.664	17.4860	15.4590	17.5740
34832	72.34	0.16	245.9049	-26.4989	16.642	17.4990	15.3860	17.6280
33433	67.27	0.22	245.8760	-26.5143	17.026	17.8460	15.8130	17.9530
38196	68.36	0.26	245.9520	-26.4435	17.015	17.8140	15.8580	17.8900
30889	72.88	0.21	245.9327	-26.5392	16.980	17.8320	15.7290	17.9320
35606	72.88	0.20	245.9191	-26.4890	16.786	17.6320	15.5470	17.7360
35395	67.63	0.17	245.9228	-26.4918	16.704	17.5440	15.4760	17.6720
33700	64.49	0.89	245.9214	-26.5115	16.818	17.6610	15.6010	17.6980
35322	73.90	0.23	245.8801	-26.4928	16.890	17.7250	15.6720	17.8200
37145	70.31	0.25	245.9487	-26.4651	16.935	17.7330	15.7650	17.7960
47676	61.66	0.33	246.0105	-26.4611	16.865	17.6600	15.7360	17.6840
47575	72.80	0.33	246.0253	-26.4633	16.868	17.6520	15.7580	17.6610
37899	74.19	0.33	245.9576	-26.4501	16.911	17.7110	15.7640	17.7790
48337	66.45	0.36	246.0407	-26.4421	16.783	17.5500	15.6960	17.5640
48104	73.71	0.32	246.0450	-26.4489	16.742	17.5150	15.6540	17.5220
48052	73.18	0.31	246.0158	-26.4502	16.860	17.6450	15.7680	17.6250
49169	68.75	0.30	246.0121	-26.4163	16.700	17.4750	15.6170	17.5080
35889	72.09	0.19	245.9694	-26.4849	16.612	17.4460	15.4520	17.5290
48122	67.74	0.23	246.0098	-26.4484	16.525	17.3190	15.4120	17.3750
30371	66.60	0.21	245.9417	-26.5449	16.979	17.8290	15.7420	17.9140
32836	73.41	0.19	245.9167	-26.5201	16.855	17.6870	15.6410	17.7900
46666	69.17	0.29	246.0377	-26.4880	16.872	17.6670	15.7600	17.6710
46958	69.67	0.30	246.0322	-26.4797	16.894	17.6870	15.7830	17.7210
46185	70.21	0.29	246.0152	-26.5006	16.744	17.5500	15.6120	17.5760
46782	70.25	0.34	246.0586	-26.4847	16.856	17.6630	15.7170	17.6940
36581	68.68	0.24	245.9377	-26.4743	16.701	17.5210	15.5200	17.6130
46927	65.31	0.24	245.9893	-26.4804	16.879	17.6770	15.7540	17.6990
34893	63.40	0.20	245.9327	-26.4982	16.657	17.4840	15.4630	17.5760
33477	68.21	0.18	245.9686	-26.5136	16.568	17.3950	15.3860	17.4600
44286	67.72	0.28	246.0377	-26.5491	16.870	17.6970	15.6850	17.7080
43384	73.81	0.27	246.0244	-26.5733	16.853	17.6740	15.6100	17.7000
45476	73.64	0.22	245.9941	-26.5179	16.739	17.5550	15.6020	17.5840
45508	68.26	0.21	246.0347	-26.5172	16.655	17.4680	15.4940	17.5070

TABLE B.7— Catalogue of stars that we studied. The columns are: ID, the mean of the radial velocity, the weighed error, the coordinates (RA and DEC), and the V , B , U , I *magnitude*.

ID	V_r	σ_{V_r}	R.A.	Decl.	V	B	U	I
45366	67.35	0.21	246.0199	-26.5205	16.747	17.5610	15.5880	17.6000
44054	75.06	0.23	246.0705	-26.5552	16.535	17.3420	15.3760	17.3560
44464	71.99	0.22	246.0477	-26.5446	16.532	17.3570	15.3430	17.4010
45581	73.44	0.23	246.0392	-26.5155	16.660	17.4770	15.5210	17.5230
26262	64.21	0.28	245.9537	-26.6096	16.869	17.6970	15.6580	17.7350
25912	74.84	0.24	245.9435	-26.6178	16.807	17.6470	15.5790	17.7130
46018	69.60	0.23	245.9926	-26.5048	16.605	17.4290	15.4320	17.4810
43064	66.91	0.18	245.9905	-26.5821	16.597	17.4690	15.3430	17.5370
31752	73.11	0.20	245.9756	-26.5306	16.823	17.6510	15.6580	17.6980
42060	70.10	0.28	245.9921	-26.6103	16.825	17.6570	15.6220	17.6730
25840	71.83	0.29	245.9399	-26.6197	16.988	17.8310	15.7530	17.8940
43413	65.64	0.25	246.0088	-26.5726	16.866	17.7370	15.6130	17.8110
43805	76.45	0.18	246.0097	-26.5621	16.567	17.4160	15.3490	17.4810
33922	72.62	0.22	245.9492	-26.5091	16.654	17.4670	15.4720	17.5200
44631	67.60	0.25	245.9915	-26.5399	16.770	17.6270	15.5820	17.6960
30558	68.88	0.22	245.8764	-26.5428	16.807	17.6600	15.5630	17.7970
29429	69.62	0.25	245.9772	-26.5562	17.007	17.8530	15.7940	17.9280
28289	70.05	0.23	245.9808	-26.5720	16.872	17.7170	15.6560	17.7550
30095	65.22	0.21	245.9714	-26.5481	16.917	17.7650	15.7160	17.8270
30542	66.91	0.17	245.8701	-26.5429	16.723	17.5820	15.4530	17.6910
29780	65.27	0.23	245.9668	-26.5519	16.742	17.5820	15.5240	17.6250
26636	66.36	0.23	245.9475	-26.6017	16.810	17.6420	15.5960	17.7000
28843	73.08	0.24	245.9639	-26.5639	16.843	17.6810	15.6200	17.7500
28322	74.11	0.26	245.9593	-26.5714	16.943	17.7860	15.7310	17.8290
30855	72.31	0.09	245.9212	-26.5396	16.233	17.2490	14.8260	17.5260
31459	65.44	0.09	245.9199	-26.5335	16.084	17.0250	14.7460	17.2710
27395	74.83	0.23	245.9245	-26.5868	16.983	17.8290	15.7390	17.9210
30513	65.79	0.20	245.9526	-26.5433	16.647	17.4720	15.4410	17.5170
30670	67.31	0.44	245.9498	-26.5416	16.704	17.5420	15.5010	17.6180
30034	69.53	0.23	245.9637	-26.5488	16.866	17.7020	15.6470	17.7780
30788	68.70	0.20	245.8827	-26.5404	16.812	17.6640	15.5580	17.8310
29922	79.37	0.20	245.9416	-26.5501	16.737	17.5820	15.5070	17.6690
29505	70.84	0.26	245.9314	-26.5553	16.845	17.6730	15.6280	17.7390
19468	65.94	0.39	245.7798	-26.6289	16.863	17.6750	15.6620	17.7350
28971	73.17	0.19	245.9540	-26.5622	16.669	17.5300	15.4150	17.6180
27992	68.73	0.18	245.9332	-26.5766	16.781	17.6490	15.5060	17.7520
28345	73.66	0.20	245.8984	-26.5710	16.841	17.7340	15.5180	17.8590
30181	74.57	0.17	245.9282	-26.5471	16.604	17.4830	15.3220	17.6160
28828	80.44	0.17	245.9290	-26.5641	16.659	17.5260	15.3770	17.6420
27173	66.49	0.24	245.9098	-26.5912	16.875	17.7340	15.5940	17.8490
29771	69.27	0.18	245.9277	-26.5521	16.608	17.4540	15.3720	17.5490

TABLE B.8— Catalogue of stars that we studied. The columns are: ID, the mean of the radial velocity, the weighed error, the coordinates (RA and DEC), and the V , B , U , I *magnitude*.

ID	V_r	σ_{V_r}	R.A.	Decl.	V	B	U	I
19377	72.70	0.37	245.7939	-26.6354	16.713	17.5200	15.5090	17.5710
27965	69.92	0.18	245.9210	-26.5770	16.648	17.5060	15.3810	17.6030
28112	75.78	0.23	245.9477	-26.5748	16.791	17.6590	15.5220	17.7450
20176	73.83	0.43	245.7962	-26.5876	16.846	17.6710	15.6170	17.7800
28722	68.29	0.17	245.9037	-26.5656	16.601	17.4960	15.2890	17.6050
19932	70.31	0.51	245.7835	-26.6009	17.038	17.8580	15.8320	17.9380
29003	74.47	0.22	245.8429	-26.5618	16.753	17.5840	15.5130	17.6730
29290	65.16	0.22	245.9057	-26.5580	16.866	17.7380	15.5650	17.8550
26688	85.41	0.28	245.9138	-26.6006	16.907	17.7880	15.6270	17.8520
19645	70.85	0.35	245.7918	-26.6180	16.773	17.5750	15.5680	17.6600
20158	74.12	0.35	245.7636	-26.5890	16.955	17.7710	15.7360	17.8580
19626	66.55	0.51	245.7977	-26.6191	16.881	17.6690	15.6990	17.7110
27329	63.28	0.21	245.8585	-26.5881	16.742	17.5820	15.4980	17.6760
21319	70.96	0.24	245.7785	-26.5301	16.921	17.7530	15.6670	17.8850
22099	67.59	0.25	245.8130	-26.4960	16.950	17.7480	15.7540	17.8940
21932	73.98	0.26	245.8181	-26.5043	16.634	17.4560	15.4350	17.5310
26784	76.57	0.30	245.8665	-26.5988	17.030	17.8660	15.7940	17.9180
26559	73.36	0.21	245.8640	-26.6032	16.783	17.6220	15.5380	17.7190
28222	65.61	0.19	245.8795	-26.5732	16.867	17.7620	15.5050	17.9470
28115	71.39	0.22	245.8527	-26.5748	16.645	17.5200	15.4030	17.6250
27116	65.97	0.22	245.8622	-26.5923	16.739	17.5730	15.4970	17.6680
22551	74.97	0.21	245.8015	-26.4727	16.799	17.6110	15.5780	17.7500
23131	72.68	0.26	245.7954	-26.4392	16.976	17.8110	15.7060	17.9550
32079	59.20	0.18	245.8789	-26.5275	16.632	17.4680	15.4250	17.5570
28925	70.02	0.19	245.8529	-26.5627	16.738	17.5810	15.4790	17.6640
29706	72.71	0.16	245.8565	-26.5529	16.606	17.4650	15.3220	17.5700
29049	73.61	0.23	245.8592	-26.5610	16.799	17.6550	15.5010	17.7740
22521	70.84	0.21	245.7969	-26.4745	16.761	17.5820	15.5450	17.7050
21250	69.28	0.19	245.8084	-26.5332	16.644	17.5030	15.3770	17.6610
22239	68.46	0.24	245.8127	-26.4888	16.859	17.6630	15.6540	17.8130
33341	71.35	0.22	245.9263	-26.5151	16.948	17.7520	15.7420	17.8370
36676	67.49	0.20	245.9490	-26.4728	16.829	17.6410	15.6500	17.7140
32227	72.71	0.25	245.8784	-26.5261	16.641	17.4580	15.4440	17.5570
33111	69.28	0.21	245.8716	-26.5174	17.026	17.8440	15.8170	17.9640
33577	76.83	0.10	245.8945	-26.5127	16.320	17.3320	14.9370	17.6200
34189	73.52	0.19	245.8824	-26.5061	16.914	17.7540	15.6970	17.8590
33449	71.63	0.19	245.9050	-26.5141	17.025	17.8450	15.8400	17.9220
34555	67.06	0.18	245.8848	-26.5019	16.701	17.5190	15.4960	17.6220
33334	73.16	0.04	245.9125	-26.5152	15.008	16.0480	13.5650	16.4860
32985	70.01	0.23	245.8869	-26.5186	16.959	17.8310	15.7250	17.9610
31056	65.84	0.19	245.8733	-26.5376	16.810	17.6620	15.5420	17.7920

TABLE B.9— Catalogue of stars that we studied. The columns are: ID, the mean of the radial velocity, the weighed error, the coordinates (RA and DEC), and the V , B , U , I *magnitude*.

ID	V_r	σ_{V_r}	R.A.	Decl.	V	B	U	I
31512	69.83	0.04	245.8758	-26.5330	15.056	16.1210	13.5860	16.5670
38893	67.20	0.28	245.9532	-26.4285	16.800	17.6060	15.6590	17.6680
32550	70.86	0.25	245.9765	-26.5230	16.674	17.5010	15.4940	17.5560
38604	66.19	0.15	245.9468	-26.4349	16.689	17.4950	15.5340	17.5730
38543	77.37	0.17	245.9374	-26.4361	16.668	17.4800	15.4800	17.5730
5029	68.83	0.16	245.9174	-26.3889	16.489	17.3530	15.2650	17.5990
36049	70.94	0.17	245.9164	-26.4826	16.629	17.4530	15.4200	17.5530
32878	55.07	0.18	245.9186	-26.5197	16.849	17.6730	15.6580	17.7520
38558	66.48	0.17	245.8972	-26.4358	16.813	17.6590	15.5760	17.7770
36463	71.48	0.18	245.9587	-26.4762	16.887	17.7010	15.7530	17.7420
31317	68.99	0.23	245.9447	-26.5348	17.013	17.8270	15.8240	17.8760
33077	77.26	0.18	245.9575	-26.5177	16.914	17.7450	15.7140	17.8100
31271	78.86	0.18	245.9617	-26.5353	16.905	17.7330	15.7160	17.8070
33038	72.91	0.20	245.9794	-26.5181	16.987	17.8150	15.8370	17.8620
32403	73.77	0.19	245.9734	-26.5245	16.755	17.5620	15.6110	17.5820
45314	64.47	0.24	245.9960	-26.5218	16.746	17.5600	15.5910	17.5710
35808	67.96	0.18	245.9368	-26.4860	16.682	17.4960	15.5170	17.5740
35253	66.42	0.20	245.9273	-26.4938	17.035	17.8510	15.8540	17.9250
34646	67.99	0.19	245.9244	-26.5009	16.763	17.5790	15.5860	17.6660
33494	76.63	0.24	245.9304	-26.5135	16.753	17.5150	15.6380	17.6060
30850	67.50	0.18	245.9722	-26.5397	16.917	17.7800	15.7050	17.8500
31303	71.98	0.06	245.9096	-26.5351	15.866	16.8960	14.4330	17.3030
31092	68.66	0.22	245.9701	-26.5371	16.931	17.7620	15.7330	17.8220
47058	66.31	0.26	246.0050	-26.4771	16.885	17.6870	15.7630	17.7110
30161	73.98	0.23	245.9750	-26.5474	16.864	17.7060	15.6530	17.7690
48128	75.36	0.23	246.0127	-26.4481	16.531	17.3150	15.4070	17.3480
43699	65.22	0.21	245.9989	-26.5648	16.894	17.7510	15.6760	17.7890
29095	75.51	0.18	245.9212	-26.5605	16.825	17.6950	15.5490	17.8110
45190	67.14	0.23	246.0033	-26.5249	16.897	17.7170	15.7340	17.7310
29101	70.30	0.24	245.9753	-26.5604	17.036	17.8580	15.8390	17.9090
28711	67.20	0.20	245.9466	-26.5657	16.628	17.4990	15.3550	17.5890
27927	71.15	0.21	245.9357	-26.5776	16.942	17.7920	15.6760	17.8650
41956	69.61	0.21	246.0151	-26.6129	16.636	17.5210	15.3840	17.5400
42720	71.62	0.20	245.9948	-26.5912	16.700	17.5420	15.4900	17.5680
26894	79.64	0.15	245.9139	-26.5967	16.651	17.5570	15.3240	17.6990
26304	69.91	0.17	245.9028	-26.6085	16.698	17.5720	15.4010	17.6730
45028	64.60	0.20	246.0528	-26.5289	16.915	17.7420	15.7350	17.7730
30639	63.93	0.12	245.9182	-26.5420	16.565	17.5010	15.2250	17.6900
30317	68.16	0.15	245.9211	-26.5456	16.655	17.5110	15.4030	17.6130
29831	66.25	0.17	245.9422	-26.5512	16.670	17.5180	15.4410	17.6140
25681	75.60	0.24	245.9387	-26.6238	16.825	17.6790	15.5830	17.7740

TABLE B.10— Catalogue of stars that we studied. The columns are: ID, the mean of the radial velocity, the weighed error, the coordinates (RA and DEC), and the V , B , U , I magnitude.

ID	V_r	σ_{V_r}	R.A.	Decl.	V	B	U	I
26007	68.17	0.21	245.9200	-26.6155	16.776	17.6250	15.5300	17.6950
42959	74.90	0.23	245.9976	-26.5850	16.945	17.7810	15.7280	17.8140
27554	68.58	0.17	245.9250	-26.5837	16.717	17.5710	15.4460	17.6670
42109	77.19	0.22	245.9964	-26.6086	16.821	17.6590	15.6070	17.6710
26217	72.10	0.23	245.9414	-26.6106	16.972	17.8100	15.7460	17.8820
41496	65.67	0.21	246.0453	-26.6251	16.553	17.4160	15.3090	17.4630
26020	68.12	0.19	245.9140	-26.6154	16.818	17.6640	15.5690	17.7420
41723	66.89	0.23	245.9954	-26.6188	16.867	17.7190	15.6480	17.7350
42007	67.13	0.23	245.9907	-26.6117	16.790	17.6470	15.5710	17.6820
27379	69.19	0.18	245.9193	-26.5870	16.843	17.6990	15.5850	17.7870
25493	68.76	0.28	245.8622	-26.6279	16.973	17.8010	15.7540	17.8630
23513	71.52	0.19	245.9164	-26.6841	16.751	17.6350	93.5600	17.8530
25795	75.62	0.21	245.8653	-26.6208	16.976	17.7980	15.7400	17.8690
24639	71.51	0.22	245.9043	-26.6496	16.815	17.6330	15.6350	17.7560
24404	66.36	0.21	245.9040	-26.6563	16.707	17.5250	15.5100	17.6370
24996	70.56	0.22	245.9080	-26.6406	16.946	17.7960	15.7280	17.8670
23896	71.63	0.24	245.9408	-26.6699	16.815	17.6390	15.6810	20.3240
25580	70.48	0.23	245.9576	-26.6260	16.745	17.5840	15.5260	17.6450
19205	66.94	0.39	245.8205	-26.6494	17.032	17.8170	15.8330	17.8960
25978	75.92	0.23	245.8436	-26.6162	17.017	17.8570	15.7590	17.9340
27801	65.72	0.22	245.9103	-26.5797	16.957	17.8070	15.6980	17.9300
25785	67.55	0.28	245.8783	-26.6210	16.760	17.5850	15.5400	17.6530
24735	67.53	0.15	245.8528	-26.6470	16.455	17.2940	15.2170	17.3990
24916	69.18	0.26	245.8639	-26.6429	16.978	17.8030	15.7530	17.8920
27582	70.00	0.18	245.8999	-26.5833	16.903	17.7730	15.6030	17.8990
25478	65.92	0.22	245.8487	-26.6283	16.943	17.7450	15.7560	17.7920
26867	69.90	0.19	245.8850	-26.5973	16.875	17.7560	15.5560	17.8610
31089	72.75	0.19	245.8876	-26.5373	16.856	17.6810	15.6500	17.7990
27913	66.94	0.14	245.8984	-26.5779	16.700	17.6270	15.3320	17.8300
19207	67.61	0.31	245.8070	-26.6491	16.789	17.5870	15.5850	17.6720
21987	65.79	0.23	245.8135	-26.5018	16.940	17.7490	15.7420	17.8620
29688	74.47	0.16	245.9087	-26.5531	16.778	17.6570	15.4940	17.7730
28175	71.85	0.18	245.8620	-26.5740	16.659	17.5090	15.3960	17.6150
31455	66.56	0.20	245.8548	-26.5335	16.928	17.7670	15.6980	17.8840
29472	70.16	0.19	245.9199	-26.5557	16.944	17.7870	15.6840	17.9010
30067	66.52	0.18	245.8608	-26.5485	16.734	17.6000	15.4590	17.7160
28913	67.42	0.15	245.8860	-26.5628	16.681	17.5670	15.3670	17.7270
30861	62.00	0.17	245.8693	-26.5396	16.772	17.6310	15.5120	17.7150
20465	76.94	0.29	245.7335	-26.5724	16.904	17.7390	15.6340	17.8540
30528	71.33	0.20	245.9007	-26.5431	17.009	17.8160	15.8100	17.9010
29836	68.91	0.18	245.8889	-26.5512	16.915	17.7630	15.6740	17.8500

TABLE B.11— Catalogue of stars that we studied. The columns are: ID, the mean of the radial velocity, the weighed error, the coordinates (RA and DEC), and the V , B , U , I magnitude.

ID	V_r	σ_{V_r}	R.A.	Decl.	V	B	U	I
32542	67.97	0.15	245.8566	-26.5230	16.607	17.4660	15.3380	17.5960
31023	71.66	0.19	245.8631	-26.5378	16.761	17.6000	15.5270	17.7140
32151	76.53	0.01	245.8370	-26.5268	13.380	14.5850	11.7490	15.4070
36828	69.47	0.21	245.8949	-26.4704	17.035	17.8550	15.8260	17.9400
22403	72.63	0.17	245.7936	-26.4805	16.723	17.5470	15.5100	17.6630
36492	71.51	0.23	245.8950	-26.4759	17.031	17.8530	15.8310	17.9380
29082	69.45	0.18	245.8900	-26.5606	16.858	17.7260	15.5650	17.8370
22080	65.25	0.19	245.8072	-26.4971	16.821	17.6330	15.6180	17.7680
33522	68.70	0.18	245.8352	-26.5132	16.651	17.4850	15.4160	17.6020
28405	64.68	0.21	245.8645	-26.5701	16.817	17.6590	15.5590	17.7560
32799	75.86	0.18	245.8543	-26.5204	16.820	17.6660	15.5830	17.7990
30546	65.65	0.19	245.8453	-26.5429	16.762	17.6040	15.5080	17.6850
37151	68.31	0.19	245.9365	-26.4650	16.860	17.6990	15.6670	17.7670
33966	66.79	0.20	245.8358	-26.5086	16.964	17.7880	15.7190	17.8800
36710	65.23	0.17	245.9294	-26.4724	16.805	17.6180	15.6290	17.7010
34317	65.49	0.16	245.8599	-26.5047	16.758	17.6070	15.5120	17.7210
37056	73.53	0.19	245.8882	-26.4665	16.696	17.5230	15.4820	17.6270
35201	69.95	0.22	245.9083	-26.4944	17.025	17.8430	15.8380	17.9200
35424	74.93	0.37	245.9092	-26.4914	16.921	17.7450	15.7210	17.8240
37374	71.94	0.22	245.8835	-26.4607	17.038	17.8690	15.8210	17.9820
35714	70.87	0.23	245.9076	-26.4873	17.031	17.8380	15.8430	17.9080
38157	76.30	0.25	245.9360	-26.4445	16.680	17.5160	15.4540	17.6330
38152	71.38	0.27	245.8974	-26.4446	16.658	17.4980	15.4290	17.6410
37860	76.34	0.24	245.8881	-26.4510	16.840	17.6610	15.6220	17.7810
37590	67.48	0.25	245.9269	-26.4563	16.828	17.6350	15.6520	17.7010
38113	66.00	0.31	245.8921	-26.4455	16.865	17.6820	15.6740	17.9580
37098	63.78	0.23	245.8603	-26.4658	16.680	17.5290	15.4080	17.6660
36620	75.41	0.29	245.8782	-26.4737	17.025	17.8390	15.8160	17.9380
38828	72.62	0.36	245.8373	-26.4300	17.040	17.8640	15.8090	17.9710
37972	66.83	0.32	245.9440	-26.4485	16.688	17.4900	15.5360	17.5560
5218	73.02	0.25	245.9139	-26.3778	16.630	17.4870	15.4150	17.7160
39426	76.88	0.23	245.9404	-26.4151	16.623	17.4430	15.4200	17.5720
5494	74.97	0.48	245.9019	-26.3611	16.795	17.6490	15.5600	17.8650
37791	69.95	0.25	245.9040	-26.4524	16.851	17.7270	15.5700	17.8620
38186	68.75	0.25	245.9398	-26.4437	16.987	17.7830	15.8260	17.8620
37897	72.79	0.32	245.9749	-26.4501	17.006	17.7990	15.9000	17.8400
4914	72.42	0.31	245.9760	-26.3954	16.821	17.6200	15.7080	17.7740
5192	69.55	0.40	245.9788	-26.3795	16.966	17.7780	15.8290	17.9340
4675	77.65	0.34	245.9684	-26.4062	16.695	17.5160	15.5610	17.7000
39127	66.91	0.26	245.9634	-26.4230	16.872	17.6670	15.7450	17.7300
5172	73.07	0.33	245.9497	-26.3805	16.638	17.4720	15.4670	17.6750

TABLE B.12— Catalogue of stars that we studied. The columns are: ID, the mean of the radial velocity, the weighed error, the coordinates (RA and DEC), and the V , B , U , I magnitude.

ID	V_r	σ_{V_r}	R.A.	Decl.	V	B	U	I
45675	66.56	0.25	245.9963	-26.5131	16.622	17.4360	15.4740	17.4650
48001	63.28	0.50	246.0635	-26.4518	16.742	17.5320	15.6150	17.5450
33703	69.01	0.22	245.8975	-26.5115	16.575	17.4240	15.3500	17.5760
33817	68.63	0.24	245.9082	-26.5101	16.920	17.7130	15.7420	17.8200
34499	70.90	0.28	245.9625	-26.5026	16.882	17.6990	15.7140	17.7570
20	67.31	0.41	246.0262	-26.4083	16.780	17.5980	15.6820	17.5880
47187	73.63	0.36	246.0116	-26.4738	16.854	17.6420	15.7350	17.6430
38435	69.04	0.27	245.9579	-26.4383	16.898	17.6860	15.7540	17.7590
37693	75.80	0.26	245.9782	-26.4543	16.689	17.4660	15.5800	17.5340
45987	76.87	0.32	246.0490	-26.5055	16.895	17.7050	15.7670	17.7260
37527	62.94	0.32	245.9093	-26.4576	16.990	17.8110	15.7980	17.9030
35943	74.98	0.32	245.9126	-26.4841	16.903	17.7250	15.6870	17.8370
35298	67.92	0.28	245.9107	-26.4932	16.978	17.7990	15.7740	17.8720
47018	74.89	0.53	246.0322	-26.4780	16.911	17.7050	15.8030	17.6980
37542	71.49	0.28	245.9644	-26.4574	16.900	17.7070	15.7520	17.7690
34444	71.30	0.28	245.9016	-26.5032	16.978	17.7760	15.8060	17.8190
42253	70.13	0.28	246.0490	-26.6042	16.542	17.4270	15.2810	17.4780
32443	73.20	0.23	245.9096	-26.5241	16.637	17.4900	15.3930	17.5950
34541	70.39	0.29	245.9522	-26.5021	16.836	17.6340	15.6520	17.6900
45311	70.33	0.28	245.9971	-26.5220	16.639	17.4570	15.4690	17.4980
42872	69.74	0.27	246.0635	-26.5869	16.785	17.6060	15.6010	17.6250
45048	70.36	0.28	246.0308	-26.5283	16.793	17.6130	15.6340	17.6270
36840	67.13	0.33	245.9362	-26.4702	16.903	17.6990	15.7330	17.8000
33338	72.37	0.28	245.9547	-26.5151	17.001	17.8150	15.8150	17.8870
41591	66.49	0.37	246.0305	-26.6227	16.884	17.7560	15.6270	17.7960
32349	60.77	0.21	245.9410	-26.5250	16.683	17.4930	15.4990	17.5610
42338	69.58	0.32	246.0210	-26.6019	16.691	17.5550	15.4440	17.6070
43349	73.52	0.31	245.9915	-26.5740	16.940	17.7930	15.7040	17.8680
34493	69.50	0.27	245.9457	-26.5027	16.914	17.7320	15.7200	17.7950
24956	72.99	0.28	245.9430	-26.6415	16.924	17.7720	15.7080	17.8890
41361	71.25	0.31	245.9997	-26.6290	16.891	17.7540	15.6680	17.7910
33037	62.98	0.27	245.9730	-26.5181	16.686	17.5160	15.5190	17.5460
34094	66.02	0.07	245.9401	-26.5071	15.300	16.3020	13.9180	16.6310
24866	74.23	0.29	245.8632	-26.6439	16.712	17.5470	15.4680	17.6470
23751	70.45	0.32	245.9383	-26.6733	16.904	17.7180	15.7000	17.8920
31095	72.51	0.29	245.9737	-26.5371	17.025	17.8780	15.8080	17.9390
24432	67.64	0.28	245.9185	-26.6554	16.656	17.4880	15.4640	17.5950
25400	72.01	0.36	245.9268	-26.6300	16.987	17.8260	15.7610	17.8850
26218	63.92	0.25	245.9547	-26.6106	16.688	17.5190	15.4890	17.5640
32784	70.63	0.24	245.9612	-26.5205	16.741	17.5620	15.5550	17.6400
33998	68.48	0.13	245.9453	-26.5084	16.382	17.3410	15.0540	17.5550

TABLE B.13— Catalogue of stars that we studied. The columns are: ID, the mean of the radial velocity, the weighed error, the coordinates (RA and DEC), and the V , B , U , I magnitude.

ID	V_r	σ_{V_r}	R.A.	Decl.	V	B	U	I
29764	69.92	0.24	245.9459	-26.5523	16.708	17.5390	15.4880	17.6050
30913	62.62	0.19	245.9345	-26.5389	16.619	17.4950	15.3460	17.6150
29219	74.96	0.21	245.9132	-26.5590	16.630	17.5050	15.3400	17.6130
27614	69.76	0.30	245.9176	-26.5828	16.926	17.7840	15.6500	17.9330
23543	75.17	0.31	245.8681	-26.6807	16.619	17.4320	15.3980	17.6050
30644	66.75	0.04	245.9225	-26.5419	14.651	15.7810	13.1210	16.3640
25661	75.15	0.32	245.8750	-26.6242	16.892	17.7270	15.6780	17.7550
26002	72.97	0.26	245.9185	-26.6156	16.649	17.4990	15.4090	17.5890
25209	69.17	0.37	245.8704	-26.6348	16.989	17.8110	15.7680	18.4020
19378	75.22	0.47	245.8117	-26.6353	16.992	17.7960	15.7950	17.8850
29869	74.18	0.31	245.8950	-26.5508	17.026	17.8720	15.7830	17.9740
25959	66.32	0.31	245.8697	-26.6166	16.692	17.5090	15.4710	17.5820
31667	67.38	0.26	245.8506	-26.5315	16.944	17.7790	15.7020	17.8760
26514	69.10	0.24	245.8513	-26.6042	16.838	17.6540	15.6090	17.7110
30539	62.75	0.29	245.9180	-26.5430	16.860	17.7160	15.6030	17.7960
28629	76.13	0.17	245.8869	-26.5667	16.641	17.5880	15.2600	17.7690
28695	67.89	0.24	245.9291	-26.5660	16.764	17.6140	15.5170	17.7050
29464	70.47	0.22	245.9364	-26.5559	16.799	17.6570	15.5290	17.7570
29665	70.49	0.24	245.9028	-26.5533	16.693	17.6060	15.3480	17.7800
30698	79.30	0.22	245.9120	-26.5413	16.760	17.5990	15.5200	17.7150
26961	69.72	0.24	245.8637	-26.5953	16.912	17.7510	15.6570	17.8450
20853	70.42	0.26	245.8101	-26.5518	16.825	17.6370	15.6130	17.7420
31357	70.18	0.25	245.8718	-26.5344	16.995	17.8260	15.7680	17.9400
34693	72.28	0.28	245.8703	-26.5005	17.026	17.8610	15.7760	17.9710
35245	73.35	0.23	245.8721	-26.4939	16.977	17.7910	15.7820	17.8880
31443	66.83	0.22	245.8635	-26.5336	16.611	17.4700	15.3370	17.5910
30632	71.11	0.28	245.9054	-26.5420	17.004	17.8440	15.7410	17.9810
30203	67.01	0.07	245.8874	-26.5468	15.474	16.5580	13.9580	16.9860
21976	70.51	0.25	245.8114	-26.5024	16.605	17.4410	15.3820	17.5870
36314	69.08	0.27	245.8552	-26.4787	16.931	17.7410	15.7140	17.8460
35909	67.42	0.29	245.8870	-26.4847	16.902	17.7140	15.7010	17.8210
36535	70.29	0.32	245.8867	-26.4751	16.966	17.7960	15.7550	17.9030
32792	66.24	0.30	245.8552	-26.5205	16.932	17.7680	15.7000	17.8570
32298	77.47	0.23	245.8584	-26.5255	17.039	17.8780	15.8140	17.9920
33862	71.15	0.28	245.8908	-26.5097	16.945	17.7480	15.7500	17.8370
34278	61.52	0.29	245.8875	-26.5051	16.817	17.6240	15.6040	17.7170
36409	68.31	0.24	245.9004	-26.4771	16.654	17.4780	15.4570	17.5770
37130	75.24	0.20	245.8415	-26.4653	16.616	17.4590	15.3440	17.6100
37070	64.48	0.27	245.8522	-26.4663	16.768	17.5780	15.5570	17.6730
36895	69.20	0.25	245.8984	-26.4693	16.730	17.5550	15.5160	17.6390
37176	61.43	0.41	245.9081	-26.4646	17.020	17.8420	15.8070	17.9580

TABLE B.14— Catalogue of stars that we studied. The columns are: ID, the mean of the radial velocity, the weighed error, the coordinates (RA and DEC), and the V , B , U , I magnitude.

ID	V_r	σ_{V_r}	R.A.	Decl.	V	B	U	I
35219	67.20	0.27	245.8910	-26.4942	17.039	17.8510	15.8420	17.9640
37706	61.10	0.18	245.8952	-26.4541	16.381	17.3550	15.0060	17.6810
38683	71.72	0.05	245.8715	-26.4332	15.024	16.1140	13.5030	16.6760
33659	67.07	0.02	245.8909	-26.5119	14.050	15.1880	12.5210	15.8220
34349	73.36	0.07	245.8807	-26.5044	15.720	16.7600	14.2790	17.1930
36050	76.07	0.06	245.8772	-26.4826	15.447	16.4900	14.0100	16.8940
38614	68.97	0.16	245.8517	-26.4347	16.488	17.4780	15.0560	17.8400
34102	67.19	0.13	245.8937	-26.5071	16.398	17.3220	15.0850	17.5460
33617	70.02	0.02	245.8625	-26.5123	13.359	14.5710	11.7560	15.3820
35931	73.85	0.10	245.8966	-26.4844	16.149	17.1600	14.7610	17.5210
37457	73.65	0.10	245.9123	-26.4591	16.188	17.2070	14.7790	17.5630
35340	61.73	0.11	245.9017	-26.4926	16.299	17.2940	14.9180	17.5750
37559	68.69	0.11	245.9163	-26.4570	16.233	17.1990	14.8780	17.4500
39385	69.42	0.13	245.9207	-26.4164	16.318	17.2870	14.9560	17.6150
4708	66.97	0.05	245.9203	-26.4046	14.854	15.9410	13.4170	16.5460
34241	70.43	0.13	245.9352	-26.5055	16.247	17.1540	14.9830	17.3530
47903	72.06	0.02	246.0612	-26.4546	13.334	14.5020	11.8330	15.2100
36339	67.61	0.18	245.9730	-26.4783	16.461	17.2790	15.2940	17.3760
36356	69.26	0.02	245.9080	-26.4781	13.572	14.7580	12.0130	15.5210
34179	61.43	0.17	245.9204	-26.5061	16.371	17.2380	15.1480	17.3620
35835	70.80	0.15	245.9562	-26.4857	16.363	17.2300	15.1400	17.3760
49125	64.77	0.12	246.0120	-26.4178	15.985	16.9090	14.7350	17.1650
31306	66.19	0.02	245.9260	-26.5350	13.973	15.1240	12.4360	15.7860
30259	71.71	0.09	245.9476	-26.5462	16.032	17.0530	14.6360	17.4020
30786	66.84	0.07	245.9451	-26.5404	15.631	16.7010	14.1960	17.0820
32057	78.76	0.08	245.9256	-26.5277	15.618	16.5980	14.2480	16.8550
31665	76.95	0.01	245.9300	-26.5316	12.845	14.1220	11.1790	14.9440
35487	66.27	0.02	245.9593	-26.4905	13.445	14.6100	11.9500	15.3250
33774	71.95	0.19	245.9450	-26.5106	16.500	17.3490	15.2690	17.4460
30675	65.22	0.02	245.9023	-26.5415	13.578	14.7740	12.0000	15.5230
33505	72.46	0.14	245.9372	-26.5134	16.460	17.3060	15.2330	17.4280
33041	72.06	0.11	245.9399	-26.5181	16.201	17.1500	14.8660	17.3850
31686	74.72	0.08	245.9704	-26.5313	15.754	16.7890	14.3660	17.0920
30783	67.75	0.07	245.9327	-26.5404	15.712	16.7820	14.2340	17.1360
26713	74.74	0.09	245.8697	-26.6001	16.081	17.1230	14.6270	17.4320
25333	70.38	0.16	245.9728	-26.6317	16.353	17.3160	15.0100	17.5140
30302	57.64	0.08	245.8828	-26.5457	16.108	17.1690	14.6350	17.5220
31838	64.20	0.09	245.9165	-26.5298	16.205	17.2260	14.7610	17.6100
25436	71.12	0.16	245.9622	-26.6292	16.321	17.3290	14.9320	17.6120
29317	64.97	0.04	245.8784	-26.5577	14.656	15.7930	13.1030	16.2830
32986	68.60	0.16	245.8625	-26.5186	16.522	17.3760	15.2640	17.5050

TABLE B.15— Catalogue of stars that we studied. The columns are: ID, the mean of the radial velocity, the weighed error, the coordinates (RA and DEC), and the V , B , U , I magnitude.

ID	V_r	σ_{V_r}	R.A.	Decl.	V	B	U	I
32488	71.77	0.06	245.8507	-26.5236	15.522	16.5850	14.0440	17.0560
33376	72.84	0.08	245.8849	-26.5148	15.963	17.0010	14.5210	17.4180
33805	73.20	0.04	245.8461	-26.5102	14.730	15.8170	13.2350	16.3620
31598	69.32	0.04	245.8792	-26.5323	14.777	15.8520	13.3210	16.3300
20766	71.91	0.00	245.8080	-26.5567	12.099	13.5300	10.3260	14.8860
32933	66.69	0.00	245.8391	-26.5192	11.871	13.2860	10.0840	14.5350
21652	68.52	0.13	245.7849	-26.5161	15.973	16.9520	14.5900	17.2400
21406	67.63	0.14	245.7917	-26.5266	16.444	17.4310	15.0460	17.7440
29027	68.73	0.01	245.8480	-26.5614	13.156	14.4020	11.4830	15.1780
22074	70.95	0.14	245.7866	-26.4973	16.453	17.3210	15.1700	17.5100
36993	73.92	0.21	245.8858	-26.4675	16.542	17.3950	15.2920	17.5300
35390	76.06	0.06	245.8945	-26.4918	15.351	16.3810	13.9280	16.7400
39039	64.13	0.34	245.9025	-26.4253	17.543	18.3810	16.3230	18.4990
5299	71.81	0.54	245.8658	-26.3727	17.276	18.1240	16.0430	18.3490
37422	65.95	0.61	245.8641	-26.4598	17.127	17.9650	15.8740	18.1010
4858	70.95	0.42	245.8314	-26.3977	17.530	18.4120	16.2470	18.6310
23248	68.89	0.26	245.8184	-26.4310	17.569	18.4690	16.2410	18.6990
23105	73.53	0.29	245.8155	-26.4406	17.609	18.4410	16.3610	18.5910
7979	75.72	0.35	245.7943	-26.4082	17.614	18.5360	16.2990	18.6540
22522	68.45	0.24	245.8145	-26.4744	17.582	18.4850	16.2950	18.6590
38851	71.82	0.32	245.8312	-26.4296	17.594	18.4110	16.3510	18.4550
8025	74.71	0.40	245.7677	-26.4060	17.598	18.4750	16.3450	18.5690
23494	66.47	0.41	245.7681	-26.4136	17.600	18.4170	16.3610	18.5460
36305	70.07	0.35	245.8366	-26.4789	17.574	18.4310	16.3290	18.5340
39275	72.86	0.31	245.8814	-26.4193	17.587	18.4150	16.3240	18.5340
4726	77.12	0.31	245.8983	-26.4040	17.506	18.3690	16.2840	18.6070
5255	66.95	0.32	245.8967	-26.3756	17.139	18.0070	15.8950	18.2550
38629	70.27	0.33	245.8330	-26.4343	17.613	18.4710	16.3590	18.5950
5384	66.89	0.34	245.8465	-26.3682	17.118	17.9790	15.8550	18.2790
5154	68.23	0.37	245.8907	-26.3815	17.273	18.1360	16.0220	18.3500
34922	71.49	0.24	245.8907	-26.4978	17.286	18.1070	16.0740	18.1930
5036	70.10	0.52	245.9597	-26.3885	17.491	18.3590	16.3000	18.5290
5185	70.51	0.36	245.9605	-26.3798	17.163	17.9840	16.0170	18.1210
38182	75.66	0.29	245.9605	-26.4438	17.593	18.4230	16.4080	18.5060
5306	66.84	0.41	245.9352	-26.3725	17.221	18.0530	16.0390	18.2590
4921	27.11	0.12	245.9401	-26.3948	17.162	18.0750	15.9760	18.5320
28092	70.12	0.35	245.9437	-26.5750	17.599	18.4750	16.3280	18.5560
48856	66.06	0.48	246.0465	-26.4262	17.529	18.3590	16.3770	18.4090
48495	71.00	0.41	246.0505	-26.4370	17.528	18.3460	16.3760	18.3520
38708	70.08	0.31	245.9262	-26.4328	17.594	18.4500	16.3880	18.5280
37572	72.25	0.30	245.8995	-26.4568	17.605	18.4750	16.3520	18.5860

TABLE B.16— Catalogue of stars that we studied. The columns are: ID, the mean of the radial velocity, the weighed error, the coordinates (RA and DEC), and the V , B , U , I magnitude.

ID	V_r	σ_{V_r}	R.A.	Decl.	V	B	U	I
38634	75.87	0.40	245.9683	-26.4342	17.601	18.4100	16.4450	18.4750
48723	72.01	0.61	246.0141	-26.4302	17.496	18.3260	16.3560	18.3550
45750	67.33	0.36	246.0286	-26.5115	17.481	18.3120	16.2960	18.3260
46834	66.14	0.35	245.9907	-26.4832	16.945	17.7330	15.8160	17.7800
46544	61.36	0.31	246.0017	-26.4915	17.117	17.9570	15.9320	17.9800
37881	72.13	0.32	245.9466	-26.4504	17.561	18.3710	16.3760	18.4550
36424	64.32	0.24	245.8907	-26.4769	17.103	17.9090	15.8980	18.0110
45008	67.62	0.28	246.0016	-26.5294	17.522	18.3560	16.3580	18.3760
43773	75.53	0.36	246.0209	-26.5630	17.483	18.3570	16.2320	18.3820
44873	71.11	0.29	246.0260	-26.5333	17.456	18.2960	16.2660	18.3180
35869	69.45	0.31	245.9503	-26.4853	17.545	18.3760	16.3250	18.4420
44884	71.58	0.53	246.0646	-26.5330	17.554	18.4070	16.3540	18.4880
35985	67.61	0.26	245.9340	-26.4835	17.607	18.4280	16.4120	18.4950
34298	72.93	0.33	245.9797	-26.5049	17.565	18.4030	16.3810	18.4800
33743	77.20	0.26	245.9495	-26.5110	17.633	18.4830	16.4240	18.5650
34422	77.75	0.31	245.9714	-26.5035	17.625	18.4820	16.4330	18.5490
36504	64.14	0.29	245.9684	-26.4756	17.574	18.4090	16.3910	18.4580
34604	71.43	0.12	245.9454	-26.5013	16.352	17.2370	15.0890	17.3970
34350	71.66	0.26	245.9656	-26.5044	17.484	18.3200	16.3010	18.3990
43785	71.03	0.38	246.0151	-26.5626	17.465	18.3310	16.2510	18.3580
26440	69.94	0.36	245.9582	-26.6059	17.567	18.4230	16.3470	18.4460
33229	69.03	0.25	245.9140	-26.5162	17.593	18.3970	16.3970	18.4870
35380	68.87	0.30	245.9489	-26.4921	17.570	18.4080	16.3630	18.4600
33808	70.67	0.21	245.9172	-26.5102	17.579	18.4970	16.2870	18.6930
33885	72.71	0.23	245.9400	-26.5095	17.328	18.2210	16.0930	18.3470
28087	69.95	0.28	245.9552	-26.5751	17.077	17.8930	15.8680	17.9310
23602	71.65	0.30	245.9473	-26.6777	17.270	18.1150	16.0530	18.3320
23631	68.52	0.41	245.9400	-26.6771	17.569	18.2420	16.4090	19.5530
26661	69.27	0.26	245.9770	-26.6013	17.628	18.4700	16.4140	18.5380
24298	76.08	0.43	245.9100	-26.6590	17.500	18.3400	16.2870	18.4820
24995	67.85	0.32	245.9542	-26.6406	17.592	18.5140	16.3240	18.6280
24226	68.05	0.48	245.9764	-26.6610	17.572	18.4720	16.2890	21.0260
26395	70.31	0.32	245.8637	-26.6066	17.549	18.3890	16.2920	18.4750
30313	71.36	0.30	245.9411	-26.5456	17.484	18.3420	16.2270	18.4520
28261	81.87	0.25	245.9217	-26.5725	17.556	18.4500	16.2560	18.5340
24486	70.40	0.26	245.9052	-26.6537	17.288	18.1280	16.0920	18.2000
24573	75.29	0.37	245.9015	-26.6513	17.458	18.3010	16.2750	20.1480
24085	73.70	0.31	245.8887	-26.6651	17.578	18.4360	16.3290	18.5660
29733	74.48	0.33	245.9762	-26.5525	17.572	18.4400	16.3390	18.4970
23599	63.98	0.24	245.9124	-26.6778	17.091	17.9330	15.8370	18.1650
31184	70.28	0.27	245.9755	-26.5362	17.610	18.4740	16.3990	18.5350

TABLE B.17— Catalogue of stars that we studied. The columns are: ID, the mean of the radial velocity, the weighed error, the coordinates (RA and DEC), and the V , B , U , I magnitude.

ID	V_r	σ_{V_r}	R.A.	Decl.	V	B	U	I
28178	77.28	0.37	245.9402	-26.5740	17.573	18.4230	16.2930	18.4980
27641	63.01	0.32	245.8593	-26.5825	17.615	18.4720	16.3520	18.5370
25879	78.35	0.29	245.8440	-26.6188	17.564	18.4300	16.2890	18.4560
28110	69.95	0.24	245.8598	-26.5748	17.163	17.9990	15.9310	18.0790
28504	68.02	0.26	245.9324	-26.5687	17.627	18.5040	16.3310	18.6030
28090	72.49	0.28	245.9126	-26.5750	17.600	18.4580	16.3130	18.5430
27830	68.91	0.30	245.9401	-26.5793	17.576	18.4700	16.2920	18.5400
27837	71.06	0.35	245.9461	-26.5792	17.591	18.4770	16.3130	18.5100
26544	64.81	0.30	245.8887	-26.6036	17.609	18.5000	16.3050	18.6000
29138	68.69	0.30	245.9282	-26.5600	17.635	18.5030	16.3750	18.6030
27256	75.14	0.36	245.9413	-26.5895	17.574	18.4710	16.2740	18.5250
29498	66.72	0.27	245.8669	-26.5553	17.591	18.5000	16.2470	18.6410
33065	70.97	0.22	245.8818	-26.5178	17.575	18.4750	16.3100	18.6460
30491	68.77	0.25	245.8732	-26.5436	17.307	18.1380	16.0610	18.2380
30228	71.47	0.28	245.8773	-26.5465	17.640	18.5140	16.3670	18.6020
19720	73.62	0.36	245.7766	-26.6141	17.575	18.4290	16.3260	18.5220
31406	66.70	0.30	245.8404	-26.5339	17.546	18.3920	16.3100	18.4660
28836	73.46	0.36	245.9122	-26.5640	17.613	18.4800	16.3440	18.5570
34392	75.28	0.23	245.8828	-26.5038	17.589	18.4370	16.3580	18.5410
22594	71.13	0.27	245.7701	-26.4702	17.632	18.4820	16.3560	18.6180
35174	71.47	0.27	245.8889	-26.4948	17.427	18.2570	16.2250	18.3470
28455	65.13	0.31	245.8749	-26.5693	17.561	18.4370	16.2680	18.5300
35644	61.59	0.52	245.8906	-26.4883	17.162	17.9720	15.9700	18.0800
28533	69.86	0.31	245.8939	-26.5681	17.593	18.4810	16.2830	18.5940
29930	71.57	0.28	245.8939	-26.5500	17.599	18.4710	16.3520	18.5610
21123	72.09	0.27	245.8197	-26.5385	17.581	18.4080	16.3590	18.5470
35768	58.83	0.21	245.8828	-26.4866	17.146	17.9560	15.9410	18.0520
23382	70.16	0.42	245.7840	-26.4216	17.624	18.4640	16.3570	18.6100
33043	71.40	0.34	245.8966	-26.5180	17.588	18.4120	16.3990	18.5530
22805	70.21	0.29	245.8207	-26.4583	17.562	18.3920	16.3100	18.5240
34515	63.72	0.26	245.8892	-26.5024	17.634	18.4900	16.4000	18.5710
33393	66.20	0.27	245.8461	-26.5146	17.572	18.4210	16.3280	18.5150
5401	65.27	0.39	245.8400	-26.3671	17.234	18.1090	15.9570	18.2960
4924	76.99	0.38	245.8989	-26.3946	17.347	18.2000	16.1300	18.4220
5126	69.90	0.42	245.8600	-26.3834	17.182	18.0320	15.9440	18.2620
5195	62.87	0.36	245.8685	-26.3794	17.261	18.1180	16.0140	18.3810
34881	67.71	0.23	245.8896	-26.4984	17.249	18.0560	16.0470	18.1350
34574	65.94	0.20	245.8832	-26.5017	17.334	18.2160	16.0700	18.3830
35552	72.98	0.19	245.8512	-26.4897	17.494	18.4230	16.1630	18.5790
8174	66.12	0.33	245.8128	-26.3964	17.449	18.3570	16.1230	18.5220
35649	61.97	0.26	245.8996	-26.4883	17.269	18.0910	16.0870	18.1470

TABLE B.18— Catalogue of stars that we studied. The columns are: ID, the mean of the radial velocity, the weighed error, the coordinates (RA and DEC), and the V , B , U , I magnitude.

ID	V_r	σ_{V_r}	R.A.	Decl.	V	B	U	I
35674	63.06	0.26	245.8430	-26.4879	17.465	18.3110	16.2230	18.3830
34721	65.37	0.26	245.9785	-26.5001	17.541	18.4180	16.3940	18.4510
4768	72.71	0.27	245.9392	-26.4022	17.446	18.3040	16.2320	18.5020
33720	65.62	0.23	245.9371	-26.5113	17.326	18.1440	16.1340	18.1930
4961	72.13	0.29	245.9309	-26.3929	17.304	18.1400	16.0920	18.3480
35374	70.04	0.20	245.8556	-26.4922	17.266	18.0930	16.0330	18.2020
34114	68.53	0.12	245.9412	-26.5070	16.436	17.3300	15.1650	17.4640
5157	73.19	0.40	245.9045	-26.3812	17.334	18.1870	16.1180	18.3760
5108	67.33	0.32	245.8968	-26.3842	17.428	18.2890	16.2020	18.4930
46790	73.80	0.21	246.0031	-26.4845	16.860	17.6580	15.7330	17.6940
32110	62.80	0.25	245.9596	-26.5272	17.374	18.2040	16.1690	18.2630
35352	74.14	0.04	245.9586	-26.4925	15.242	16.2820	13.8520	16.7200
34434	62.47	0.29	245.9470	-26.5033	17.387	18.2260	16.1770	18.2810
34508	75.44	0.25	245.9678	-26.5025	17.340	18.1640	16.1630	18.2350
47441	71.00	0.41	246.0580	-26.4671	17.306	18.1380	16.1360	18.1540
47243	69.58	0.40	246.0374	-26.4723	16.961	17.7520	15.8470	17.7410
35058	66.61	0.34	245.8922	-26.4963	17.433	18.2600	16.2360	18.3540
47119	69.23	0.34	246.0091	-26.4756	17.237	18.0440	16.0980	18.0560
49032	68.52	0.31	246.0325	-26.4210	17.388	18.2100	16.2540	18.2310
46846	68.23	0.14	245.9935	-26.4830	16.272	17.1220	15.0930	17.1780
30334	67.73	0.21	245.9015	-26.5454	17.170	18.0080	15.9370	18.0960
44379	64.06	0.27	246.0266	-26.5471	17.399	18.2480	16.2060	18.2630
47068	73.22	0.25	246.0345	-26.4768	17.067	17.9300	15.8920	17.9970
46175	70.04	0.36	246.0649	-26.5008	17.126	17.9430	15.9740	17.9420
26234	71.12	0.27	245.9756	-26.6103	17.485	18.3310	16.2710	18.3180
31478	66.85	0.28	245.9226	-26.5333	17.420	18.2700	16.1910	18.3590
28616	67.81	0.26	245.8886	-26.5669	17.361	18.2540	16.0210	18.3710
32100	69.70	0.30	245.9406	-26.5273	17.490	18.3290	16.2760	18.3800
46486	71.36	0.26	246.0001	-26.4930	17.237	18.0640	16.0750	18.0800
30117	64.69	0.30	245.9132	-26.5479	17.518	18.4110	16.2320	18.5220
28270	73.02	0.27	245.8838	-26.5723	17.505	18.3860	16.1850	18.5020
26171	66.16	0.28	245.9597	-26.6117	16.994	17.8140	15.8100	17.8360
29941	73.02	0.21	245.8992	-26.5498	17.241	18.1250	15.9800	18.2500
28046	81.03	0.25	245.8934	-26.5756	17.186	18.0750	15.8730	18.1680
26660	73.37	0.35	245.9566	-26.6013	17.463	18.3150	16.2530	18.3450
27538	69.89	0.21	245.9515	-26.5841	16.561	17.4400	15.3000	17.5440
29916	73.92	0.37	245.8622	-26.5501	17.380	18.2390	16.1080	18.3340
26065	69.51	0.25	245.8913	-26.6140	17.082	17.9180	15.8390	17.9970
26659	73.15	0.36	245.9507	-26.6013	17.380	18.2330	16.1480	18.3110
21133	70.75	0.04	245.8183	-26.5381	14.889	15.9470	13.4290	16.3970
27788	72.00	0.28	245.8840	-26.5800	17.364	18.2250	16.0580	18.3640

TABLE B.19— Catalogue of stars that we studied. The columns are: ID, the mean of the radial velocity, the weighed error, the coordinates (RA and DEC), and the V , B , U , I magnitude.

ID	V_r	σ_{V_r}	R.A.	Decl.	V	B	U	I
28011	69.57	0.23	245.8805	-26.5763	17.068	17.9450	15.7680	18.0490
28128	67.64	0.22	245.8589	-26.5746	17.414	18.2900	16.1060	18.4250
30072	63.95	0.20	245.8570	-26.5484	17.225	18.0840	15.9480	18.1990
33785	70.14	0.26	245.8687	-26.5106	17.370	18.2100	16.1320	18.3060
20194	72.36	0.25	245.7706	-26.5867	17.002	17.8320	15.7800	17.9260
19651	52.46	0.16	245.7705	-26.6176	17.336	18.2470	16.0600	18.4860
19409	77.09	0.30	245.8060	-26.6330	17.343	18.1530	16.1260	18.2530
33924	68.51	0.22	245.8537	-26.5091	17.290	18.0990	16.0770	18.1930
32922	69.65	0.23	245.8728	-26.5193	17.149	17.9810	15.9470	18.0820
34111	70.47	0.20	245.8616	-26.5070	17.253	18.0740	16.0230	18.1660
21094	72.19	0.21	245.8127	-26.5403	17.511	18.3490	16.2870	18.4460
20447	66.09	0.24	245.8103	-26.5731	16.906	17.7340	15.6500	17.8870
21218	70.95	0.24	245.7692	-26.5345	17.297	18.1320	16.0480	18.2660
35233	75.68	0.20	245.8711	-26.4940	17.259	18.0900	16.0340	18.1850
21454	71.94	0.24	245.7725	-26.5247	17.299	18.1330	16.0620	18.2690
21171	65.93	0.23	245.7758	-26.5366	17.166	18.0050	15.9050	18.1510
20272	64.57	0.24	245.7393	-26.5828	16.925	17.7430	15.6880	17.8360
35386	73.70	0.22	245.8483	-26.4919	17.273	18.1070	16.0440	18.1670
20586	71.72	0.23	245.7870	-26.5661	17.283	18.0970	16.0670	18.1650
20892	69.52	0.22	245.7918	-26.5499	17.143	17.9750	15.8900	18.1100
22243	65.42	0.20	245.7257	-26.4886	16.756	17.6100	15.4720	17.7740
22008	72.84	0.27	245.7181	-26.5008	17.265	18.1180	15.9970	18.2320
21738	69.21	0.24	245.7542	-26.5126	17.163	18.0110	15.8930	18.1380
21397	74.16	0.36	245.7334	-26.5269	17.513	18.3870	16.1870	18.5140
21579	73.37	0.29	245.7240	-26.5190	17.469	18.3620	16.1510	18.5120
22132	70.50	0.27	245.7700	-26.4940	17.464	18.3170	16.1760	18.4280
21374	73.04	0.31	245.7478	-26.5278	17.346	18.2040	16.0440	18.3490
21497	74.27	0.26	245.7685	-26.5230	17.255	18.0860	16.0120	18.1440
36263	74.56	0.23	245.9011	-26.4796	17.286	18.1100	16.0850	18.1790
37433	64.72	0.24	245.8554	-26.4597	17.430	18.2610	16.1960	18.3840
22839	71.60	0.25	245.7373	-26.4562	17.330	18.1480	16.1000	18.2830
22777	61.06	0.23	245.7381	-26.4599	17.181	17.9830	15.9640	18.1150
22763	63.20	0.32	245.7275	-26.4606	17.305	18.1540	16.0460	18.2890
22417	70.81	0.28	245.7375	-26.4797	17.175	18.0140	15.9040	18.1220
36154	70.23	0.17	245.9277	-26.4811	16.574	17.4410	15.3190	17.5880
36751	67.20	0.24	245.9688	-26.4718	16.587	17.4000	15.3990	17.4210
35621	70.28	0.10	245.9555	-26.4887	16.141	17.1360	14.7780	17.4700
39244	74.51	0.16	245.8772	-26.4201	16.548	17.4770	15.1860	17.7380
39048	69.41	0.19	245.8920	-26.4250	16.565	17.4210	15.3030	17.5590
37852	63.37	0.15	245.8467	-26.4511	16.553	17.4560	15.2180	17.6380
36801	67.33	0.18	245.9325	-26.4708	16.545	17.3690	15.3420	17.4810

TABLE B.20— Catalogue of stars that we studied. The columns are: ID, the mean of the radial velocity, the weighed error, the coordinates (RA and DEC), and the V , B , U , I magnitude.

ID	V_r	σ_{V_r}	R.A.	Decl.	V	B	U	I
39387	67.49	0.22	245.8437	-26.4163	16.578	17.4160	15.3220	17.5750
8171	75.35	0.17	245.8036	-26.3971	16.545	17.5540	15.1440	17.8970
36380	67.04	0.02	245.9062	-26.4776	14.120	15.2400	12.6130	15.8280
38752	72.41	0.18	245.8500	-26.4318	16.571	17.4710	15.2410	17.7120
35315	71.69	0.22	245.9067	-26.4930	16.550	17.3880	15.3160	17.4890
38878	71.68	0.20	245.9607	-26.4289	16.544	17.3390	15.4000	17.4020
33928	71.06	0.20	245.9738	-26.5090	16.582	17.4060	15.3960	17.4810
34369	69.57	0.19	245.9193	-26.5041	16.498	17.3110	15.3270	17.3600
39258	65.95	0.20	245.9353	-26.4198	16.589	17.4340	15.3530	17.5700
34843	66.64	0.16	245.9254	-26.4988	16.549	17.3970	15.3290	17.5040
35923	62.30	0.16	245.8807	-26.4845	16.498	17.3570	15.2390	17.5090
35955	69.91	0.17	245.8862	-26.4840	16.511	17.3650	15.2620	17.4960
32092	63.28	0.21	245.9422	-26.5274	16.584	17.4160	15.3760	17.4960
31003	69.38	0.17	245.9423	-26.5380	16.590	17.4360	15.3570	17.5240
31334	76.61	0.15	245.9149	-26.5347	16.542	17.3980	15.2830	17.5220
30345	64.83	0.02	245.9499	-26.5452	13.835	14.9950	12.3090	15.6430
47867	64.15	0.25	246.0013	-26.4556	16.471	17.2670	15.3480	17.3160
31785	68.01	0.14	245.9295	-26.5303	16.406	17.3350	15.0780	17.5410
29460	75.84	0.18	245.9555	-26.5560	16.547	17.4350	15.2600	17.5710
33001	76.15	0.11	245.9470	-26.5185	16.116	17.0950	14.7610	17.3400
28917	74.05	0.21	245.9479	-26.5628	16.568	17.4290	15.3050	17.5490
29878	64.85	0.15	245.8667	-26.5507	16.592	17.5280	15.2320	17.6900
42352	67.08	0.27	245.9893	-26.6015	16.457	17.3110	15.2580	17.3220
28591	77.10	0.21	245.9273	-26.5672	16.577	17.4430	15.3050	17.5610
26832	75.54	0.21	245.8405	-26.5979	16.553	17.4530	15.2180	17.6050
30650	71.10	0.10	245.9347	-26.5418	16.294	17.2950	14.8850	17.6050
24154	70.96	0.20	245.9366	-26.6633	16.363	17.2240	15.1200	17.3790
24581	70.36	0.20	245.9243	-26.6510	16.479	17.3210	15.2690	17.4370
31565	67.94	0.08	245.9255	-26.5326	15.820	16.8670	14.3650	17.2600
30719	68.50	0.02	245.9030	-26.5411	13.971	15.1280	12.4270	15.7910
31063	61.06	0.10	245.9207	-26.5374	16.191	17.2070	14.7810	17.5700
24919	70.62	0.22	245.8338	-26.6429	16.562	17.3680	15.3420	17.4530
28308	62.91	0.20	245.8472	-26.5715	16.575	17.4470	15.2790	17.5650
28355	74.96	0.16	245.8609	-26.5708	16.564	17.4400	15.2600	17.5860
24775	67.83	0.20	245.8545	-26.6460	16.577	17.3980	15.3580	17.4890
28192	68.41	0.17	245.8524	-26.5738	16.566	17.4420	15.2810	17.5580
29776	66.42	0.17	245.9192	-26.5520	16.563	17.4290	15.3020	17.5420
29363	67.55	0.17	245.9220	-26.5571	16.573	17.4680	15.2850	17.5910
31392	68.38	0.20	245.8576	-26.5340	16.577	17.4350	15.2890	17.5440
33900	69.67	0.02	245.8458	-26.5093	13.505	14.6890	11.9270	15.4780
30215	71.34	0.18	245.8442	-26.5466	16.579	17.4490	15.2910	17.5710

TABLE B.21— Catalogue of stars that we studied. The columns are: ID, the mean of the radial velocity, the weighed error, the coordinates (RA and DEC), and the V , B , U , I magnitude.

ID	V_r	σ_{V_r}	R.A.	Decl.	V	B	U	I
34413	71.12	0.16	245.8386	-26.5036	16.590	17.4180	15.3620	17.5330
28808	69.51	0.13	245.8467	-26.5643	16.432	17.3760	15.0870	17.5680
20049	68.73	0.23	245.7706	-26.5947	16.599	17.4440	15.3500	17.5370
33195	62.88	0.01	245.8642	-26.5165	13.121	14.3940	11.4480	15.2980
21460	68.56	0.19	245.8120	-26.5246	16.585	17.4170	15.3550	17.5570
34020	76.51	0.13	245.8865	-26.5080	16.517	17.3980	15.2460	17.5460
21172	73.06	0.19	245.8078	-26.5366	16.608	17.4260	15.3210	17.5470
19770	75.86	0.21	245.7557	-26.6114	16.558	17.4330	15.3020	17.5880
22299	69.44	0.17	245.7857	-26.4856	16.562	17.4200	15.2810	17.6240
22592	75.43	0.22	245.8079	-26.4703	16.588	17.4100	15.3610	17.5540
21965	68.42	0.19	245.8159	-26.5029	16.592	17.4230	15.3680	17.5800
22082	72.83	0.18	245.8232	-26.4971	18.207	19.0790	16.9110	19.3670
36993	75.40	0.17	245.8858	-26.4675	16.542	17.3950	15.2920	17.5300
37256	70.20	0.16	245.8753	-26.4630	16.578	17.4370	15.3130	17.5610
34674	74.98	0.56	245.8376	-26.5006	16.589	17.4170	15.3570	17.5240
33529	66.56	0.10	245.8953	-26.5131	16.238	17.2460	14.8370	17.5800
38016	66.74	0.16	245.8968	-26.4476	16.558	17.4480	15.2640	17.6230
23072	64.52	0.19	245.8136	-26.4433	16.590	17.4440	15.3150	17.6400
35267	70.63	0.14	245.8937	-26.4936	16.438	17.3240	15.1650	17.5010
22994	68.31	0.18	245.8104	-26.4474	16.584	17.4240	15.3300	17.6020
35653	73.72	0.32	245.9417	-26.4882	17.426	18.2500	16.2550	18.3160
34707	68.09	0.40	245.8929	-26.5003	17.322	18.1220	16.1290	18.1880
35657	66.67	0.24	245.9466	-26.4881	17.396	18.2240	16.2080	18.3080
39279	68.42	0.30	245.8778	-26.4191	17.465	18.3080	16.2290	18.4440
36731	74.44	0.22	245.9475	-26.4721	17.305	18.1330	16.1170	18.1950
39183	71.77	0.24	245.8684	-26.4214	17.344	18.1760	16.1130	18.2920
33962	77.63	0.20	245.9217	-26.5087	17.063	17.8700	15.8800	17.9330
37833	66.14	0.29	245.8899	-26.4516	17.215	18.0460	16.0210	18.1260
37343	73.54	0.26	245.9119	-26.4612	17.444	18.2800	16.2370	18.3720
38550	65.82	0.22	245.8620	-26.4360	17.202	18.0270	15.9610	18.1370
38705	60.61	0.34	245.8437	-26.4328	17.239	18.0730	15.9840	18.2160
37323	69.87	0.23	245.9401	-26.4615	17.151	17.9760	15.9560	18.0670
35039	68.75	0.20	245.9167	-26.4965	17.473	18.3290	16.2500	18.4020
33841	64.33	0.23	245.9605	-26.5098	17.328	18.1440	16.1460	18.2150
34698	74.41	0.21	245.9215	-26.5004	17.416	18.2470	16.2300	18.3210
32930	72.93	0.21	245.9298	-26.5193	17.299	18.1120	16.1070	18.1800
33090	66.07	0.21	245.9332	-26.5176	17.401	18.2180	16.2070	18.2990
35457	76.44	0.25	245.9302	-26.4909	17.481	18.3470	16.2470	18.4140
36486	73.42	0.25	245.9634	-26.4759	17.443	18.2610	16.2700	18.3330
32131	67.14	0.21	245.9385	-26.5270	17.191	18.0210	15.9790	18.0990
33520	69.89	0.26	245.9705	-26.5132	17.512	18.3540	16.3230	18.3950

TABLE B.22— Catalogue of stars that we studied. The columns are: ID, the mean of the radial velocity, the weighed error, the coordinates (RA and DEC), and the V , B , U , I magnitude.

ID	V_r	σ_{V_r}	R.A.	Decl.	V	B	U	I
33520	69.89	0.26	245.9705	-26.5132	17.512	18.3540	16.3230	18.3950
38123	74.68	0.22	245.9632	-26.4452	17.441	18.2680	16.2840	18.2780
38311	72.00	0.22	245.9565	-26.4411	17.300	18.1170	16.1570	18.1870
32672	67.88	0.25	245.9650	-26.5218	17.494	18.3460	16.2950	18.3860
39269	73.90	0.26	245.9425	-26.4195	17.180	17.9960	16.0090	18.0420
45310	72.67	0.27	245.9897	-26.5220	17.296	18.1180	16.1370	18.1300
35076	70.31	0.25	245.9383	-26.4959	17.331	18.1440	16.1540	18.2210
45496	70.20	0.21	246.0112	-26.5174	16.985	17.8090	15.8240	17.8290
29484	66.92	0.26	245.9605	-26.5556	17.271	18.1460	16.0090	18.1940
27996	75.43	0.24	245.9632	-26.5766	17.349	18.1830	16.1410	18.2160
46402	70.50	0.25	246.0030	-26.4952	17.248	18.0860	16.0870	18.0940
46026	65.75	0.27	246.0124	-26.5045	17.183	18.0220	16.0140	18.0320
29860	73.37	0.19	245.9462	-26.5509	17.180	18.0200	15.9620	18.0860
29415	69.46	0.26	245.9715	-26.5564	17.482	18.3520	16.2510	18.4120
29654	68.89	0.25	245.9560	-26.5534	17.336	18.1790	16.0980	18.2400
36125	61.72	0.31	245.9710	-26.4816	17.449	18.2770	16.2810	18.3120
31216	69.68	0.18	245.8995	-26.5359	17.524	18.4190	16.2420	18.6800
28313	72.58	0.27	245.9195	-26.5715	17.537	18.4250	16.2530	18.4880
27750	71.61	0.26	245.9633	-26.5807	17.325	18.1680	16.1140	18.1530
28521	69.80	0.20	245.9568	-26.5684	17.272	18.1280	16.0230	18.1920
44987	74.23	0.34	246.0240	-26.5298	17.185	18.0150	16.0090	18.0200
45045	67.65	0.29	246.0387	-26.5284	17.389	18.2430	16.1850	18.2750
45218	77.19	0.31	246.0246	-26.5243	17.163	17.9880	15.9990	17.9920
26185	71.36	0.22	245.9277	-26.6114	17.372	18.2330	16.1270	18.2860
42581	66.23	0.23	246.0106	-26.5951	17.375	18.2660	16.1150	18.2900
26401	68.57	0.26	245.9258	-26.6066	17.391	18.2450	16.1330	18.2910
32630	62.06	0.20	245.9095	-26.5221	17.354	18.1780	16.1440	18.3040
42960	70.00	0.25	246.0010	-26.5850	17.293	18.1540	16.0330	18.1960
29107	69.99	0.22	245.9434	-26.5603	17.245	18.1090	16.0120	18.1670
44002	63.10	0.26	246.0073	-26.5567	17.287	18.1540	16.0370	18.1700
31765	70.44	0.22	245.9044	-26.5305	17.452	18.2580	16.2360	18.3900
26326	71.68	0.25	245.9094	-26.6081	17.276	18.1350	15.9990	18.2190
25140	70.84	0.37	245.9800	-26.6366	17.525	18.3790	16.2920	18.5040
43512	65.85	0.26	246.0520	-26.5696	17.069	17.8940	15.8880	17.9140
30890	74.60	0.22	245.9136	-26.5392	17.511	18.3180	16.2780	18.4090
27279	61.95	0.23	245.9250	-26.5890	17.437	18.3010	16.1670	18.3610
27235	73.12	0.20	245.9433	-26.5898	17.324	18.1900	16.0670	18.2790
42055	64.22	0.28	246.0146	-26.6104	17.343	18.2190	16.0980	18.2430
25870	74.44	0.28	245.9497	-26.6190	17.513	18.3760	16.2920	18.4630
30820	65.25	0.19	245.8877	-26.5401	17.204	18.0180	15.9490	18.1500
30849	70.11	0.21	245.9073	-26.5398	17.267	18.1480	16.0310	18.2650

TABLE B.23— Catalogue of stars that we studied. The columns are: ID, the mean of the radial velocity, the weighed error, the coordinates (RA and DEC), and the V , B , U , I magnitude.

ID	V_r	σ_{V_r}	R.A.	Decl.	V	B	U	I
27279	61.95	0.23	245.9250	-26.5890	17.437	18.3010	16.1670	18.3610
27235	73.12	0.20	245.9433	-26.5898	17.324	18.1900	16.0670	18.2790
42055	64.22	0.28	246.0146	-26.6104	17.343	18.2190	16.0980	18.2430
25870	74.44	0.28	245.9497	-26.6190	17.513	18.3760	16.2920	18.4630
30820	65.25	0.19	245.8877	-26.5401	17.204	18.0180	15.9490	18.1500
30849	70.11	0.21	245.9073	-26.5398	17.267	18.1480	16.0310	18.2650
25725	73.34	0.30	245.9477	-26.6226	17.357	18.2130	16.1170	18.2450
29996	68.98	0.23	245.8937	-26.5492	17.508	18.3620	16.2530	18.4400
29266	78.11	0.22	245.9122	-26.5583	17.266	18.1040	16.0090	18.1560
26081	62.85	0.22	245.8850	-26.6138	17.246	18.0810	15.9850	18.4700
29727	64.49	0.20	245.9023	-26.5526	17.277	18.1400	16.0040	18.2280
31053	71.94	0.23	245.8812	-26.5376	17.157	17.9990	15.9420	18.1000
30761	79.41	0.19	245.8782	-26.5408	17.229	18.0380	16.0160	18.1560
30701	76.91	0.28	245.8725	-26.5413	17.405	18.2570	16.1570	18.3310
28778	68.32	0.26	245.8842	-26.5648	17.314	18.1930	16.0210	18.2920
32734	64.29	0.20	245.8644	-26.5211	17.420	18.2540	16.1590	18.3890
32533	61.15	0.23	245.8688	-26.5231	17.402	18.2470	16.1480	18.3610
23942	37.63	0.15	245.8561	-26.6685	17.458	18.3780	16.1710	18.7090
26908	72.18	0.24	245.8665	-26.5964	17.438	18.2870	16.1730	18.3490
27931	70.80	0.22	245.8662	-26.5776	17.540	18.3970	16.2510	18.4650
33324	64.94	0.24	245.8554	-26.5152	17.354	18.1890	16.1250	18.2580
32607	70.65	0.20	245.8734	-26.5224	17.374	18.2050	16.1450	18.2890
34346	65.18	0.31	245.8482	-26.5044	17.400	18.2380	16.1670	18.3040
32819	71.45	0.20	245.8422	-26.5202	17.259	18.0950	16.0320	18.1690
31177	75.24	0.25	245.8472	-26.5363	17.538	18.3920	16.2740	18.4820
32566	67.21	0.21	245.8835	-26.5228	17.520	18.4080	16.2340	18.6540
33083	69.93	0.22	245.8502	-26.5176	17.378	18.2210	16.1260	18.3130
29809	74.30	0.22	245.8463	-26.5515	17.482	18.3380	16.2260	18.4200
36630	73.35	0.25	245.8602	-26.4735	17.373	18.2230	16.1070	18.3380
22217	65.71	0.25	245.8125	-26.4901	17.515	18.3490	16.3030	18.4740
35658	61.75	0.22	245.8670	-26.4881	17.508	18.3460	16.2880	18.4090
36790	72.99	0.26	245.8542	-26.4711	17.386	18.2140	16.1640	18.3200
34598	70.67	0.24	245.8761	-26.5014	17.414	18.2420	16.1940	18.3520
34780	70.18	0.22	245.8660	-26.4995	17.525	18.3670	16.2760	18.4470
35733	75.32	0.23	245.8447	-26.4870	17.219	18.0460	15.9780	18.1500
34513	68.01	0.21	245.8330	-26.5024	17.366	18.1730	16.1850	18.2320
22499	64.43	0.19	245.8188	-26.4753	17.548	18.3900	16.3220	18.5080
37933	64.77	0.35	245.8550	-26.4493	17.507	18.3640	16.2310	18.4750
22317	73.28	0.27	245.7915	-26.4848	17.199	18.0130	15.9780	18.1570
22158	73.07	0.23	245.7722	-26.4927	17.202	18.0290	15.9420	18.1700
22276	71.03	0.22	245.8115	-26.4865	17.050	17.8640	15.8460	17.9730

TABLE B.24— Catalogue of stars that we studied. The columns are: ID, the mean of the radial velocity, the weighed error, the coordinates (RA and DEC), and the V , B , U , I magnitude.

ID	V_r	σ_{V_r}	R.A.	Decl.	V	B	U	I
37269	66.70	0.24	245.8326	-26.4626	17.329	18.1740	16.0860	18.2840
21355	69.89	0.31	245.7216	-26.5285	17.452	18.3310	16.1240	18.4640
21955	70.83	0.25	245.8217	-26.5032	17.265	18.0530	16.0810	18.1510
36773	73.08	0.22	245.8726	-26.4714	17.078	17.9060	15.8490	18.0180
37814	67.71	0.20	245.9117	-26.4520	17.085	17.9150	15.8430	18.0340
37980	68.13	0.23	245.9329	-26.4484	17.449	18.2830	16.2540	18.3850
38201	65.06	0.27	245.8554	-26.4435	17.514	18.3710	16.2600	18.4970
36151	74.60	0.27	245.9078	-26.4811	17.462	18.2930	16.2620	18.3700
22797	71.05	0.23	245.7923	-26.4586	17.339	18.1490	16.1230	18.2620
36321	76.66	0.22	245.9109	-26.4786	17.505	18.3430	16.2940	18.4370
36685	74.39	0.20	245.9034	-26.4728	17.308	18.1760	16.0420	18.3390
36871	66.63	0.24	245.9114	-26.4696	17.280	18.0980	16.0870	18.1840
22600	72.27	0.25	245.8063	-26.4700	17.398	18.2050	16.1840	18.3180
35375	64.66	0.20	245.8697	-26.4922	17.182	18.0240	15.9660	18.1120
37008	69.45	0.29	245.9639	-26.4673	17.444	18.2740	16.2720	18.3330
35492	66.06	0.38	245.9493	-26.4904	17.483	18.3040	16.2890	18.3820
37061	69.80	0.29	245.9527	-26.4664	17.351	18.1810	16.1600	18.2640
37414	68.01	0.28	245.9167	-26.4600	17.300	18.1240	16.1050	18.2390
36724	65.98	0.22	245.9539	-26.4721	17.188	18.0150	16.0200	18.0860
36524	70.24	0.22	245.9523	-26.4753	17.394	18.2260	16.2130	18.2860
35891	62.43	0.20	245.9380	-26.4849	17.355	18.1720	16.1900	18.2460
36428	65.43	0.23	245.9333	-26.4768	17.192	18.0170	16.0060	18.0890
23285	68.60	0.29	245.8180	-26.4282	17.348	18.1840	16.0980	18.3060
23425	70.89	0.32	245.8197	-26.4185	17.428	18.2520	16.1560	18.4070
35525	68.46	0.30	245.9161	-26.4900	17.198	18.0190	15.9890	18.1170
38897	78.61	0.23	245.9424	-26.4285	17.321	18.1380	16.1390	18.1840
4838	67.75	0.21	245.9251	-26.3984	17.191	18.0480	15.9920	18.2570
4632	67.93	0.25	245.9357	-26.4077	17.129	17.9790	15.9470	18.1550
38503	68.66	0.31	245.9559	-26.4368	17.538	18.3510	16.3780	18.3940
34864	75.22	0.23	245.8607	-26.4986	17.386	18.2340	16.1410	18.3370
39131	71.85	0.21	245.9140	-26.4229	17.226	18.0540	16.1020	18.7250
38798	68.50	0.25	245.9218	-26.4306	17.148	17.9660	15.9760	18.0380
37797	65.00	0.22	245.9441	-26.4523	17.352	18.1660	16.1910	18.2570
33836	73.32	0.22	245.9531	-26.5100	17.258	18.0930	16.0620	18.1320
33434	67.19	0.20	245.9636	-26.5143	17.285	18.1130	16.0950	18.1570
39220	72.93	0.22	245.9648	-26.4206	17.072	17.8720	15.9520	17.9290
34639	68.44	0.19	245.9036	-26.5010	17.156	18.0050	15.9300	18.1250
39146	64.30	0.26	245.9532	-26.4226	17.536	18.3680	16.3590	18.4420
38546	74.40	0.29	245.9597	-26.4360	17.311	18.1100	16.1710	18.1740
46925	69.35	0.30	246.0669	-26.4805	17.091	17.8980	15.9380	17.9170
47408	71.12	0.31	246.0410	-26.4681	17.155	17.9510	16.0380	17.9640

TABLE B.25— Catalogue of stars that we studied. The columns are: ID, the mean of the radial velocity, the weighed error, the coordinates (RA and DEC), and the V , B , U , I magnitude.

ID	V_r	σ_{V_r}	R.A.	Decl.	V	B	U	I
46373	76.17	0.32	245.9970	-26.4960	17.369	18.2000	16.2080	18.2120
48637	70.56	0.31	246.0396	-26.4329	17.400	18.2390	16.2610	18.2650
46428	73.59	0.38	245.9940	-26.4945	17.133	17.9610	15.9860	17.9640
46079	74.55	0.30	246.0145	-26.5031	17.209	18.0360	16.0590	18.0300
29929	69.33	0.22	245.9795	-26.5500	17.174	18.0230	15.9650	18.1090
33739	70.68	0.21	245.9465	-26.5111	17.275	18.1000	16.0770	18.1780
32923	78.08	0.23	245.9660	-26.5193	17.278	18.1020	16.1100	18.1520
31001	70.15	0.21	245.9095	-26.5380	17.294	18.1110	16.0790	18.2170
32025	71.91	0.23	245.9755	-26.5279	17.466	18.3140	16.2900	18.3550
43649	69.55	0.29	246.0037	-26.5661	17.448	18.3160	16.2040	18.3590
44341	71.59	0.25	246.0087	-26.5480	17.090	17.9260	15.8970	17.9600
43600	78.57	0.26	245.9919	-26.5675	17.203	18.0490	15.9620	18.1090
46017	63.10	0.45	246.0478	-26.5049	17.395	18.2250	16.2280	18.2720
46935	66.71	0.30	246.0743	-26.4803	17.044	17.8430	15.8920	17.8550
44227	71.44	0.22	245.9985	-26.5507	17.275	18.1390	16.0560	18.1630
27102	77.29	0.24	245.9211	-26.5927	17.514	18.3900	16.2260	18.4960
28137	68.30	0.20	245.9349	-26.5744	17.177	18.0430	15.8940	18.1090
26442	71.36	0.27	245.9685	-26.6058	17.296	18.1310	16.0970	18.1450
42600	65.45	0.26	246.0370	-26.5946	17.252	18.1160	16.0220	18.1430
43590	74.86	0.25	246.0702	-26.5678	17.296	18.1380	16.1220	18.1340
43221	64.06	0.33	246.0670	-26.5777	17.378	18.2120	16.1880	18.2160
29348	75.64	0.26	245.9770	-26.5572	17.291	18.1360	16.0670	18.2170
29796	71.74	0.24	245.8953	-26.5517	17.515	18.3730	16.2330	18.4770
33252	67.42	0.22	245.9131	-26.5160	17.382	18.2350	16.1630	18.3910
28888	74.86	0.20	245.9179	-26.5632	17.238	18.0880	15.9680	18.1810
29162	59.58	0.21	245.8606	-26.5596	17.330	18.1820	16.0390	18.2750
26048	72.65	0.20	245.9367	-26.6145	17.359	18.2120	16.1140	18.2620
30379	71.68	0.21	245.8786	-26.5448	17.526	18.3960	16.2290	18.5160
32424	73.70	0.20	245.9257	-26.5243	17.481	18.3170	16.2780	18.3310
28744	63.35	0.24	245.9594	-26.5653	17.467	18.3520	16.2200	18.4060
26032	72.76	0.29	245.9711	-26.6151	17.436	18.1580	16.1480	18.1770
29111	75.58	0.18	245.9025	-26.5603	17.178	18.0490	15.8810	18.1790
31084	73.19	0.21	245.8937	-26.5373	17.246	18.0780	16.0380	18.2070
31187	65.31	0.24	245.9003	-26.5361	17.230	18.0700	15.9880	18.1910
34126	70.60	0.23	245.9276	-26.5068	17.301	18.1150	16.1200	18.1730
20934	71.76	0.31	245.8150	-26.5476	17.385	18.2070	16.1670	18.2900
29652	71.08	0.21	245.8540	-26.5534	17.506	18.3650	16.2280	18.4640
27343	71.24	0.19	245.8573	-26.5878	17.157	18.0030	15.9080	18.0870
29572	72.80	0.20	245.8450	-26.5545	17.266	18.0900	16.0250	18.1680
30045	74.44	0.17	245.8616	-26.5487	17.179	18.0420	15.9260	18.1390
33395	66.74	0.21	245.8436	-26.5146	17.334	18.1820	16.0990	18.2740

TABLE B.26— Catalogue of stars that we studied. The columns are: ID, the mean of the radial velocity, the weighed error, the coordinates (RA and DEC), and the V , B , U , I magnitude.

ID	V_r	σ_{V_r}	R.A.	Decl.	V	B	U	I
29899	69.22	0.18	245.8312	-26.5503	17.200	18.0090	15.9720	18.0800
31274	66.89	0.21	245.8335	-26.5353	17.499	18.3620	16.2580	18.4520
26708	64.94	0.24	245.8839	-26.6003	17.452	18.3010	16.1830	18.4100
27634	72.25	0.22	245.8732	-26.5825	17.151	17.9970	15.8700	18.1010
26124	79.37	0.24	245.8960	-26.6126	17.191	18.0250	15.9500	18.1050
27290	70.64	0.22	245.8455	-26.5888	17.532	18.3890	16.2630	18.4370
21469	67.73	0.25	245.8023	-26.5240	17.402	18.2380	16.1740	18.3580
21582	74.87	0.20	245.8224	-26.5188	17.402	18.2220	16.1910	18.3240
31632	52.72	0.25	245.8450	-26.5320	17.195	18.0700	15.8620	18.1600
20521	71.67	0.21	245.7959	-26.5696	16.905	17.7250	15.6710	17.8220
20647	71.81	0.21	245.8101	-26.5628	17.365	18.2000	16.1210	18.3080
19131	69.02	0.31	245.8117	-26.6562	17.348	18.1620	16.1370	18.2510
20361	74.46	0.18	245.7996	-26.5779	16.608	17.4420	15.3560	17.5870
33543	71.81	0.19	245.8585	-26.5130	17.414	18.2320	16.1950	18.3360
33171	72.81	0.20	245.8621	-26.5168	17.161	17.9920	15.9450	18.0810
19667	79.29	0.33	245.7870	-26.6169	17.524	18.3800	16.2810	18.4370
20190	71.11	0.18	245.7773	-26.5868	16.716	17.5460	15.4920	17.6440
26428	69.06	0.28	245.8926	-26.6061	17.342	18.2130	16.0750	18.2710
36069	68.27	0.24	245.8424	-26.4823	17.495	18.3410	16.2490	18.4170
37448	72.70	0.20	245.8605	-26.4592	17.191	18.0150	16.0020	18.4300
20035	69.23	0.29	245.7394	-26.5956	17.533	18.3890	16.2640	18.4910
36897	71.63	0.24	245.8525	-26.4692	17.110	17.9240	15.9070	17.9950
35700	73.72	0.25	245.8486	-26.4875	17.285	18.1350	16.0310	18.2010
21069	65.18	0.20	245.7858	-26.5413	17.180	18.0160	15.9510	18.1150
20169	68.70	0.20	245.7725	-26.5884	16.703	17.5130	15.4920	17.6010
34692	65.82	0.20	245.8338	-26.5004	17.431	18.2630	16.2270	18.2980
22310	72.18	0.20	245.7629	-26.4851	16.983	17.8460	15.6810	18.0280
22714	67.20	0.25	245.7922	-26.4639	17.463	18.2720	16.2310	18.3960
22140	67.29	0.28	245.7944	-26.4935	17.536	18.3610	16.3060	18.4590
36791	65.13	0.18	245.8823	-26.4710	16.805	17.6270	15.5960	17.7450
34112	67.88	0.23	245.8914	-26.5070	17.216	18.0120	16.0110	17.9300
37266	67.24	0.19	245.8380	-26.4628	17.204	18.0320	15.9920	18.1290
34609	65.01	0.25	245.8807	-26.5013	17.408	18.2400	16.2010	18.3030
34908	76.24	0.21	245.8724	-26.4980	17.244	18.0680	16.0360	18.1450
37951	66.92	0.22	245.9009	-26.4490	17.123	17.9810	15.8830	18.1110
36464	71.37	0.24	245.9061	-26.4762	17.378	18.2120	16.1750	18.2860
23268	72.50	0.28	245.7642	-26.4294	17.531	18.3660	16.2920	18.4850
23190	68.85	0.24	245.7922	-26.4352	17.229	18.0860	15.9100	18.2500
23059	67.54	0.24	245.7688	-26.4442	17.359	18.1690	16.1160	18.3180
37351	70.71	0.25	245.8860	-26.4610	17.488	18.3440	16.2620	18.4320
22819	65.47	0.23	245.8115	-26.4573	17.362	18.1790	16.1350	18.3030

TABLE B.27— Catalogue of stars that we studied. The columns are: ID, the mean of the radial velocity, the weighed error, the coordinates (RA and DEC), and the V , B , U , I magnitude.

ID	V_r	σ_{V_r}	R.A.	Decl.	V	B	U	I
37616	70.46	0.23	245.8926	-26.4559	17.435	18.2670	16.1890	18.3840
22487	69.89	0.26	245.7821	-26.4763	17.396	18.2390	16.1300	18.3920
39368	74.88	0.32	245.8495	-26.4169	17.178	17.9900	15.9500	18.1350
37566	61.52	0.21	245.8755	-26.4570	17.209	18.0430	15.9750	18.1690
4818	73.06	0.49	245.8321	-26.3996	17.368	18.2470	16.1060	18.4130
36833	70.01	0.23	245.8345	-26.4703	17.188	18.0120	15.9350	18.1180
32710	73.94	0.20	245.8733	-26.5213	17.525	18.3450	16.2850	18.4370
35746	65.71	0.19	245.8770	-26.4869	17.208	18.0330	15.9780	18.1320
32755	70.31	0.18	245.8781	-26.5208	17.211	18.0450	15.9900	18.1220
33588	70.59	0.19	245.8782	-26.5125	17.319	18.1980	16.0640	18.3340
32983	73.08	0.19	245.8878	-26.5186	17.179	18.0090	15.9650	18.1160
23299	73.06	0.27	245.8104	-26.4268	17.114	17.9300	15.8690	18.0620
30722	72.23	0.20	245.8566	-26.5411	17.302	18.1380	16.0560	18.2340
22559	65.00	0.25	245.8200	-26.4722	17.247	18.0590	16.0180	18.1910
39374	70.67	0.31	245.8862	-26.4168	17.263	18.0880	15.9270	18.1690
34591	75.11	0.19	245.8379	-26.5014	17.148	17.9540	15.9470	18.0440
34182	67.61	0.19	245.8451	-26.5061	17.188	18.0130	15.9780	18.0980
33059	76.52	0.19	245.8461	-26.5179	17.282	18.1250	16.0240	18.2310
33721	73.23	0.18	245.8552	-26.5112	17.349	18.2060	16.1020	18.3070
33796	68.44	0.20	245.8609	-26.5104	17.424	18.2460	16.2180	18.3350
32484	65.70	0.18	245.8658	-26.5236	17.188	18.0190	15.9640	18.1370
21509	70.12	0.21	245.8116	-26.5225	17.398	18.2510	16.1700	18.3540
5019	73.03	0.26	245.8606	-26.3894	17.171	18.0050	15.9470	18.2400
35872	61.58	0.18	245.9089	-26.4852	17.240	18.0580	16.0490	18.1350
38162	75.66	0.21	245.8825	-26.4444	17.268	18.0810	16.0530	18.2130
37277	72.90	0.20	245.8853	-26.4624	17.240	18.1040	15.9600	18.2530
38526	66.41	0.23	245.8788	-26.4364	17.278	18.1050	16.0610	18.1960
34793	78.58	0.18	245.8932	-26.4994	17.048	17.8940	15.8280	17.9960
29322	76.02	0.19	245.9230	-26.5577	17.150	18.0060	15.8780	18.1270
29163	70.49	0.23	245.9307	-26.5596	17.312	18.1760	16.0390	18.2670
36135	76.00	0.20	245.8816	-26.4815	17.216	18.0750	15.9960	18.1570
36552	70.00	0.19	245.8822	-26.4749	17.422	18.3210	16.1360	18.4630
36679	69.32	0.28	245.8791	-26.4728	17.232	18.0460	16.0290	18.1400
28854	69.61	0.25	245.9335	-26.5638	17.357	18.2100	16.0950	18.3060
36622	71.54	0.29	245.9216	-26.4737	17.411	18.2310	16.2260	18.3140
28770	69.83	0.26	245.9504	-26.5648	17.198	18.0330	15.9790	18.0890
32275	67.61	0.22	245.9591	-26.5257	17.138	17.9690	15.9420	18.0150
30587	69.78	0.25	245.9100	-26.5424	17.433	18.2970	16.1660	18.3950
34847	66.43	0.21	245.9165	-26.4988	17.163	18.0420	15.9230	18.1400
34259	18.11	0.11	245.9305	-26.5053	17.077	17.9650	15.8360	18.1640
47588	72.47	0.40	246.0399	-26.4630	17.218	18.0310	16.0840	18.0520

TABLE B.28— Catalogue of stars that we studied. The columns are: ID, the mean of the radial velocity, the weighed error, the coordinates (RA and DEC), and the V , B , U , I magnitude.

ID	V_r	σ_{V_r}	R.A.	Decl.	V	B	U	I
27187	79.30	0.20	245.8922	-26.5908	17.059	17.9220	15.7790	17.9980
28719	73.88	0.22	245.9106	-26.5656	17.145	18.0340	15.8370	18.1180
36018	66.25	0.24	245.9226	-26.4830	17.543	18.4020	16.2860	18.5060
36866	72.36	0.20	245.9457	-26.4697	17.226	18.0510	16.0460	18.1230
28890	67.88	0.25	245.9705	-26.5631	17.486	18.3560	16.2460	18.4000
29814	66.63	0.23	245.9747	-26.5514	17.321	18.1660	16.0930	18.2510
36197	68.77	0.25	245.9281	-26.4805	17.378	18.2450	16.1620	18.3570
28098	67.65	0.23	245.9213	-26.5749	17.248	18.0980	15.9940	18.1820
30271	69.39	0.20	245.8794	-26.5460	17.366	18.2730	16.0870	18.3820
27452	69.19	0.26	245.8879	-26.5857	17.532	18.4000	16.2430	18.5240
30040	67.76	0.19	245.8735	-26.5488	17.158	18.0210	15.9020	18.1320
28980	77.97	0.19	245.8982	-26.5621	17.199	18.0670	15.9220	18.1490
26489	73.15	0.25	245.9099	-26.6048	17.396	18.2550	16.1410	18.3050
28580	74.40	0.21	245.8898	-26.5674	17.236	18.0990	15.9570	18.2110
29751	69.45	0.24	245.9088	-26.5523	17.479	18.3180	16.2250	18.4020
30655	73.05	0.28	245.8843	-26.5418	17.405	18.2580	16.1500	18.2990
28040	71.29	0.21	245.8830	-26.5758	17.190	18.0620	15.8850	18.1710
29019	74.96	0.22	245.8790	-26.5616	17.224	18.1540	15.9100	18.2170
24231	72.48	0.34	245.9262	-26.6609	17.507	18.3700	16.2790	18.4940
31213	63.15	0.22	245.9719	-26.5359	17.296	18.1180	16.0940	18.1630
23728	77.52	0.25	245.9307	-26.6739	17.177	17.9980	15.9580	18.1970
23886	66.94	0.31	245.9560	-26.6702	17.271	18.1170	16.0260	18.3320
23549	73.04	0.28	245.9354	-26.6801	17.276	18.1260	16.0480	18.4030
30283	63.07	0.25	245.8539	-26.5459	17.468	18.3140	16.2150	18.3770
28989	77.38	0.20	245.8506	-26.5619	17.099	17.9120	15.8730	18.0950
29414	68.57	0.24	245.8549	-26.5564	17.450	18.2990	16.1870	18.3850
25248	71.13	0.28	245.8425	-26.6338	17.363	18.1910	16.1460	18.2490
24918	68.68	0.27	245.8849	-26.6429	17.337	18.1760	16.0810	18.2530
24579	76.62	0.30	245.9125	-26.6511	17.490	18.3640	16.2630	18.4470
25253	66.43	0.24	245.9035	-26.6337	17.446	18.2910	16.2180	18.3630
24473	61.55	0.29	245.9025	-26.6541	17.448	18.2750	16.2350	19.4540
24307	68.67	0.25	245.8879	-26.6586	17.186	17.9640	15.9290	19.5390
24194	73.33	0.25	245.8635	-26.6619	17.176	18.0030	15.9400	18.1170
24464	72.72	0.25	245.9164	-26.6545	17.074	17.8940	15.8710	17.9790
25658	63.91	0.26	245.8359	-26.6243	17.482	18.3100	16.2770	18.3590
26830	64.38	0.27	245.8682	-26.5980	17.143	17.9910	15.8740	18.1060
24764	67.75	0.29	245.8567	-26.6462	17.459	18.2990	16.2350	18.4050
25939	77.01	0.26	245.8710	-26.6171	17.469	18.3170	16.2250	18.3720
25665	70.70	0.23	245.8794	-26.6241	17.328	18.1730	16.0990	18.2340
25887	71.41	0.29	245.8779	-26.6186	17.404	18.2570	16.1370	18.2880
25881	72.42	0.26	245.8567	-26.6187	17.479	18.3370	16.2410	18.3790

TABLE B.29— Catalogue of stars that we studied. The columns are: ID, the mean of the radial velocity, the weighed error, the coordinates (RA and DEC), and the V , B , U , I magnitude.

ID	V_r	σ_{V_r}	R.A.	Decl.	V	B	U	I
24890	65.89	0.23	245.8790	-26.6433	17.124	17.9740	15.8710	18.0460
27009	79.20	0.23	245.8341	-26.5943	17.157	18.0090	15.8980	18.0770
21640	79.31	0.25	245.8192	-26.5166	17.458	18.2860	16.2440	18.4060
19070	66.45	0.45	245.8103	-26.6611	17.371	18.1850	16.1480	18.3200
35757	69.39	0.18	245.8410	-26.4867	17.123	17.9630	15.8680	18.0480
29265	76.65	0.20	245.8446	-26.5583	17.508	18.3710	16.2320	18.4490
19894	68.14	0.36	245.7485	-26.6031	17.362	18.2000	16.1160	18.2640
20166	73.41	0.39	245.7543	-26.5886	17.536	18.3880	16.2910	18.4610
19991	74.17	0.29	245.7521	-26.5981	17.335	18.1630	16.1020	18.2410
26196	70.26	0.21	245.8526	-26.6112	17.239	18.0870	15.9520	18.1410
26170	73.00	0.26	245.8767	-26.6118	17.144	17.9740	15.9210	18.0500
26986	65.30	0.23	245.8675	-26.5948	17.141	17.9790	15.8880	18.0560
26811	68.60	0.34	245.8425	-26.5982	17.436	18.2930	16.1640	18.3400
27146	74.42	0.21	245.8578	-26.5918	17.424	18.2620	16.1880	18.3140
22479	71.00	0.21	245.7970	-26.4767	17.347	18.1710	16.1100	18.2770
21380	70.87	0.23	245.8093	-26.5276	17.519	18.3510	16.2990	18.4930
29547	77.55	0.13	245.8518	-26.5548	16.546	17.4180	15.2620	17.5480
22447	72.21	0.22	245.8097	-26.4782	17.241	18.0510	16.0250	18.1560
28803	70.54	0.20	245.8459	-26.5645	17.167	18.0130	15.9320	18.0980
21289	70.21	0.26	245.8009	-26.5313	17.479	18.3270	16.2330	18.4590
27831	71.53	0.29	245.8603	-26.5793	17.376	18.2220	16.1200	18.3340
23353	72.98	0.28	245.7925	-26.4238	17.235	18.0890	15.9030	18.2460
21475	74.61	0.24	245.8079	-26.5236	17.403	18.2530	16.1660	18.3580
23212	73.50	0.26	245.7635	-26.4336	17.202	18.0110	16.0040	18.1030
22965	77.24	0.30	245.7912	-26.4493	17.505	18.3360	16.2520	18.4540
30968	77.05	0.22	245.8695	-26.5383	17.293	18.1200	16.0530	18.2140
30940	67.31	0.25	245.8856	-26.5386	17.470	18.3180	16.2250	18.4200
22722	67.83	0.26	245.7840	-26.4634	17.380	18.2190	16.1050	18.3560
33889	67.06	0.19	245.9310	-26.5094	17.095	17.9120	15.9110	17.9740
38421	64.55	0.30	245.8869	-26.4386	17.100	17.9220	15.8890	18.0500
35312	72.27	0.21	245.8788	-26.4930	17.075	17.8920	15.8860	17.9710
34453	70.98	0.20	245.8767	-26.5031	17.095	17.9330	15.8590	18.0510
34138	75.09	0.21	245.8746	-26.5067	17.050	17.8740	15.8200	17.9990
31925	77.43	0.23	245.8686	-26.5290	17.077	17.9110	15.8400	18.0170
33470	70.55	0.20	245.8744	-26.5138	17.081	17.9090	15.8620	18.0040
34092	66.75	0.22	245.9095	-26.5072	17.083	17.8890	15.9160	17.9900
32589	68.81	0.20	245.8596	-26.5225	17.077	17.9050	15.8490	18.0070
37756	67.90	0.20	245.8859	-26.4530	16.766	17.6080	15.5420	17.7090
33343	66.92	0.19	245.9158	-26.5151	17.090	17.9000	15.9010	17.9550
36246	68.35	0.18	245.9255	-26.4798	17.048	17.8520	15.8620	17.9330
48314	64.33	0.18	246.0123	-26.4426	17.010	17.8090	15.8950	17.8240

TABLE B.30— Catalogue of stars that we studied. The columns are: ID, the mean of the radial velocity, the weighed error, the coordinates (RA and DEC), and the V , B , U , I magnitude.

ID	V_r	σ_{V_r}	R.A.	Decl.	V	B	U	I
38236	69.41	0.20	245.9371	-26.4427	17.082	17.8960	15.8990	17.9950
39313	71.08	0.24	245.9646	-26.4183	17.098	17.8750	15.9900	18.1700
38538	66.36	0.22	245.9358	-26.4361	17.123	17.9290	15.9660	17.9990
39281	76.53	0.23	245.9480	-26.4190	17.131	17.9400	15.9780	18.0050
5092	60.88	0.18	245.9717	-26.3851	17.013	17.8970	15.8220	18.1470
5204	66.82	0.30	245.9554	-26.3787	17.077	17.9130	15.9120	18.0730
47685	71.94	0.21	246.0203	-26.4608	16.572	17.3520	15.4660	17.3610
31831	73.82	0.18	245.9499	-26.5299	16.824	17.6580	15.6430	17.7080
35362	74.96	0.21	245.9296	-26.4924	17.071	17.9060	15.8640	17.9590
45790	74.25	0.20	245.9978	-26.5105	16.989	17.8110	15.8400	17.8120
33831	70.23	0.14	245.9372	-26.5100	16.694	17.5160	15.5020	17.5920
47226	70.25	0.28	245.9972	-26.4727	17.039	17.8640	15.8640	17.8920
48870	68.16	0.29	245.9992	-26.4258	17.023	17.8260	15.9190	17.8600
38941	73.85	0.24	245.9574	-26.4274	17.103	17.9300	15.9600	17.9490
48916	66.68	0.22	245.9940	-26.4242	16.961	17.7490	15.8610	17.7940
37118	64.83	0.21	245.9532	-26.4655	17.120	17.9580	15.8970	18.0420
33095	67.59	0.21	245.9341	-26.5175	17.089	17.9190	15.8850	18.0130
45650	69.77	0.30	246.0575	-26.5139	17.008	17.8200	15.8520	17.8170
31682	77.72	0.23	245.9590	-26.5313	17.080	17.8920	15.8970	17.9440
46482	69.88	0.25	246.0416	-26.4932	16.978	17.7820	15.8620	17.7610
46879	69.64	0.29	246.0500	-26.4819	16.988	17.7970	15.8440	17.8110
45302	74.78	0.33	246.0288	-26.5221	17.011	17.8090	15.8660	17.8210
38072	69.85	0.21	245.9355	-26.4464	17.124	17.9340	15.9560	18.0400
45786	72.94	0.30	246.0432	-26.5106	17.037	17.8570	15.8880	17.8660
44254	61.99	0.21	246.0023	-26.5498	17.005	17.8530	15.7870	17.9100
44333	69.48	0.24	246.0122	-26.5481	17.001	17.8500	15.8050	17.8770
45027	66.94	0.21	246.0239	-26.5289	16.999	17.8240	15.8250	17.8380
33932	63.53	0.03	245.9447	-26.5090	14.801	15.8860	13.3300	16.3380
33686	76.04	0.23	245.9427	-26.5116	17.066	17.8940	15.8740	17.9680
44813	72.68	0.22	246.0202	-26.5348	17.024	17.8420	15.8500	17.8630
44585	66.12	0.25	246.0752	-26.5410	16.623	17.4230	15.4770	17.4300
31707	78.30	0.46	245.9326	-26.5311	17.098	17.9790	15.8310	18.0770
44973	75.26	0.24	246.0383	-26.5301	17.031	17.8620	15.8420	17.8860
28926	75.59	0.24	245.9570	-26.5627	17.091	17.9210	15.8780	17.9780
28065	71.15	0.24	245.9535	-26.5754	17.085	17.9130	15.8540	17.9600
34595	72.95	0.21	245.9699	-26.5014	17.042	17.8590	15.8880	17.9280
28264	66.31	0.20	245.9775	-26.5724	17.063	17.8930	15.8270	17.9160
42168	70.72	0.29	246.0082	-26.6069	17.051	17.9190	15.7850	17.9520
29202	71.34	0.24	245.9782	-26.5592	17.112	17.9650	15.8750	18.0480
43456	76.71	0.20	246.0082	-26.5716	16.957	17.8140	15.7020	17.8710
34404	70.33	0.19	245.9550	-26.5037	17.062	17.8800	15.8860	17.9130

TABLE B.31— Catalogue of stars that we studied. The columns are: ID, the mean of the radial velocity, the weighed error, the coordinates (RA and DEC), and the V , B , U , I magnitude.

ID	V_r	σ_{V_r}	R.A.	Decl.	V	B	U	I
42793	68.11	0.25	246.0090	-26.5892	17.018	17.8660	15.7900	17.9100
27612	68.31	0.28	245.9737	-26.5828	17.055	17.8850	15.8470	17.9440
30656	61.23	0.20	245.9387	-26.5417	17.088	17.9270	15.8680	17.9930
30881	70.54	0.19	245.9307	-26.5394	17.103	17.9350	15.8690	17.9830
30601	69.19	0.20	245.9648	-26.5423	17.082	17.9180	15.8760	17.9620
31171	77.69	0.17	245.9264	-26.5363	17.114	17.9280	15.9050	17.9970
32303	63.06	0.20	245.9153	-26.5255	17.099	17.9190	15.8990	18.0360
26962	75.72	0.24	245.9499	-26.5952	17.109	17.9650	15.8690	18.0190
26363	70.34	0.27	245.9664	-26.6074	17.093	17.9170	15.9090	17.9350
31522	73.76	0.22	245.9101	-26.5329	17.044	17.8470	15.8550	17.9320
29774	66.20	0.20	245.9068	-26.5520	17.057	17.9230	15.7840	18.0290
29793	74.58	0.24	245.9546	-26.5518	17.053	17.8850	15.8490	17.9430
26878	68.65	0.25	245.9189	-26.5970	17.102	17.9580	15.8130	18.0120
28606	67.49	0.22	245.8916	-26.5671	17.119	17.9730	15.8220	18.0890
28144	72.81	0.25	245.8751	-26.5744	17.119	17.9760	15.8320	18.0880
30125	68.42	0.18	245.9455	-26.5478	16.863	17.6980	15.6390	17.7830
26463	73.07	0.22	245.9055	-26.6053	17.063	17.9270	15.7940	18.0080
30126	72.10	0.21	245.9760	-26.5478	17.115	17.9450	15.8990	18.0030
19236	66.74	0.49	245.7961	-26.6468	17.062	17.8720	15.8420	17.9750
27598	68.49	0.28	245.8674	-26.5831	17.101	17.9350	15.8460	18.0210
27666	65.63	0.19	245.9271	-26.5820	17.104	17.9500	15.8640	18.0400
24571	70.76	0.30	245.8346	-26.6514	17.065	17.8970	15.8150	18.0040
28307	69.54	0.19	245.9150	-26.5716	17.049	17.9080	15.7800	17.9990
20390	61.06	0.23	245.8059	-26.5764	16.598	17.4360	15.3550	17.5790
19021	73.70	0.35	245.8210	-26.6651	17.107	17.9060	15.9040	18.0030
20285	65.60	0.20	245.7789	-26.5821	16.723	17.5430	15.5060	17.6300
20658	72.17	0.28	245.7965	-26.5623	17.071	17.8960	15.8350	18.0250
21681	69.53	0.17	245.7798	-26.5147	16.661	17.5320	15.3750	17.6750
20319	66.84	0.31	245.7623	-26.5802	16.980	17.8010	15.7470	17.9040
21721	65.49	0.25	245.7870	-26.5132	17.035	17.8690	15.7870	18.0270
20933	71.39	0.31	245.7498	-26.5476	17.179	17.9330	15.8440	18.0840
26725	71.40	0.22	245.9027	-26.5998	17.139	18.0000	15.8450	18.1140
26652	73.96	0.24	245.8651	-26.6014	17.121	17.9600	15.8780	18.0330
20321	69.99	0.20	245.7714	-26.5801	16.558	17.3970	15.3100	17.5190
30324	66.44	0.21	245.9097	-26.5455	17.106	17.9510	15.8670	18.0470
22005	76.19	0.18	245.7666	-26.5010	16.725	17.6200	15.3900	17.8200
21727	74.96	0.31	245.7705	-26.5130	17.074	17.9080	15.8280	18.0430
30549	67.70	0.02	245.8881	-26.5429	13.664	14.8620	12.0510	15.5210
29096	70.83	0.17	245.8497	-26.5605	16.724	17.5850	15.4500	17.6880
21268	72.43	0.19	245.7931	-26.5323	16.848	17.6800	15.5910	17.8120
21490	71.13	0.30	245.7202	-26.5231	16.874	17.7530	15.5530	17.8890

TABLE B.32— Catalogue of stars that we studied. The columns are: ID, the mean of the radial velocity, the weighed error, the coordinates (RA and DEC), and the V , B , U , I *magnitude*.

ID	V_r	σ_{V_r}	R.A.	Decl.	V	B	U	I
21490	71.13	0.30	245.7202	-26.5231	16.874	17.7530	15.5530	17.8890
20444	68.73	0.18	245.8148	-26.5733	16.769	17.6040	15.5260	17.7400
20741	71.96	0.21	245.7623	-26.5578	16.774	17.5380	15.4360	17.6870
20355	71.35	0.23	245.7889	-26.5780	16.715	17.5150	15.4940	17.6150
36027	68.68	0.15	245.9120	-26.4830	16.572	17.4170	15.3380	17.5520
31997	65.30	0.21	245.8585	-26.5283	17.080	17.9230	15.8280	18.0440
32097	69.81	0.22	245.8436	-26.5273	17.110	17.9280	15.8800	18.0220
29663	71.45	0.17	245.8531	-26.5533	16.801	17.6370	15.5560	17.7210
29671	73.34	0.19	245.8716	-26.5532	16.976	17.8350	15.6730	17.9550
35432	70.35	0.17	245.9132	-26.4913	16.637	17.4650	15.4260	17.5650
29307	68.97	0.22	245.8734	-26.5578	17.074	17.9300	15.7910	18.0490
29754	70.48	0.23	245.8840	-26.5523	17.054	17.9120	15.7880	18.0220
30140	72.27	0.20	245.8835	-26.5477	17.050	17.9060	15.7660	18.0210

Bibliography

- Albrow, M. D., Gilliland, R. L., Brown, T. M., Edmonds, P. D., Guhathakurta, P. Sarajedini, A., 2001, ApJ, 559, 1060
- Anderson, J., 1997, PhD thesis, 8
- Anderson, J., Cool, A., M., King, I., R., 2003, ApJ, 597, 137
- Anderson, J., Bedin, L.R., Piotto, G., Yadav, R.S., Bellini, A., 2006, A&A, 454, 1929
- Bacon, D., Sigurdsson, S., Davies, M., B., 1996, MNRAS, 281, 830
- Bailyn, C. D., 1995, A&A, 33, 133
- Baranne, A., Queloz, M., Mayor, M., Adrianyk, G., et al. 1996, A&A, 119, 373
- Barden, S. C., Armandroff, T. E., Pryor, C. P., 1996, ASPC, 90, 89
- Bellazzini M, Fusi Pecci, F., Montegriffo, P., Messineo, M., Monaco, L., Rood, R. T., 2002, ApJ, 123, 2541
- Blecha, A., Cayatte, V., North, P., Royer, F., & Simond, G., 2000, presented at the Society of Photo-Optical Instrumentation Engineers, SPIE Conference, Vol. 4008, Optical and IR Telescope Instrumentation and Detectors, Eds. M. Iye & A. F. Moorwood, 467
- Bond, I., A., Abe, F., Eguchi, S., Furuta, Y., Hearnshaw, J., B. et al., 2005, ApJ, 620, 103
- Clark, L., L., Sandquist, E., L., Bolte, M., 2004, 128, 3019
- Cohn, H., 1980, ApJ, 242, 765
- Cool, A., M., Bolton, A., S., 2002, ASPC, 263, 163
- Cote, P., Welch, D. L., Fischer, P., Da Costa, G. S., Tamblyn, P., Seitzer, P., Irwin, M. J., 1994, ApJ, 90, 83

- Cote, P. & Fisher, P. 1996, ApJ, 112, 565
- Cote, P., Pryor, C., McClure, R. D., Fletcher, J. M., Hesser, J. E., 1996 ApJ, 112, 574
- de Marchi, G., Paresce, F., 1995, A&A, 304, 211
- Dieball, A., Knigge, C., Zurek, D., R., Shara, M., M., Long, K, S, 2005, ApJ, 625, 156
- Djorgovski, S., & Meylan, G., 1993, AAS, 50, 325
- Dubath, P., Meylan, G., Mayor, M., Magain, P., 1990, A&A, 239, 142
- Duquenooy, A., Mayor, M., 1991, 248, 485
- Elson, R., A., W., Gilmore, G., F., Santiago, B., X., Casertano, S., 1995, AJ, 110, 682
- Ferdman, R., D., Richer, H., B., Brewer, J., Fahlman, G., G., Gibson, B., K., et al., 2004, AJ, 127, 380
- Ferraro, F., R., D'Amico, N., Possenti, A., Mignani, R., P., Paltrinieri, B., 2001, ApJ, 561, 337
- Fregeau, J., M., Cheung, P., Portegies Zwart, S., F., Rasio, F., A., 2004, MNRAS, 532, 1
- Gebhardt, K., Pryor, C., Williams, T., B., Hesser, J., E., 1994, AJ, 107, 2067
- Gierez, M. & Heggie, D.C. 2007, astro-ph e-prints, arXiv:0801.3968v1
- Griffin, R. F., 1967, ApJ, 148, 465
- Gunn, J. E., & Griffin, R. F., 1979, ApJ, 84, 752
- Hansen, B. M. S., Richer, H.B., Fahlman, G. G, et al. 2004, ApJS, 155, 551
- Harris, W. E. 1996, ApJ, 112, 1487
- Heggie, D. C., 1975, MNRAS, 173, 729
- Heggie, D., C., Aarseth, S., J., 1992, MNRAS, 257, 513
- Heggie, D. C., & Giersz, M., 2008, IAUS, 246, 121
- Heggie, D. C., & Giersz, M., 2008, MNRAS, 389, 1858
- Hekker, S., Snellen, I. A. G., Aerts, C., et al. 2008, A&A, 480, 215
- Hurley, J., R., Tout, C., A., Pols, O., R., 2002, MNRAS, 392, 897
- Hut P., 1983, ApJ, 272, 2
- Hut, P., Murphy, B., W., Verbunt, F., 1991, A&A, 241, 137
- Hut, P., et al. 1992, PASP, 104, 981

- Hut, P., McMillan, S., & Romani, R. W., 1992, *ApJ*, 389, 527
- Hut, P., & Makino, J., 1999, *Science*, 283, 501
- Kaluzny, J., Thompson, I. B., Rucinski, S. M., Krzeminski, W., 2008, *ApJ*, 136, 400
- Kroupa, P., Gilmore, G., Tout, C., A., 1991, *MNRAS*, 251, 293
- Kroupa, P., 2008, *arXiv*, 0803.1833
- Kurucz, R. L., Furenlid, I., & Poncet J.L, 1984, *Solar Flux atlas from 296 to 1300 nm*, National solar Observatory Atlas, Sunspot, New Mexico: National Solar Observatory
- Lyne, A., G., Biggs, J., D., Brinklow, A., McKenna, J., Ashworth, M, 1988, *Nature*, 332, 45
- Madsen, S., Dravins, D., Lindegren, L., 2002, *A&A*, 381, 446
- Marino, A., F., Villanova, S., Piotto, G., Milone, A., P., Momany, Y., Bedin, L., R., Medling, A., M., 2008, *arXiv0808*, 1624
- Margon, B., Downes, R., A., Gunn, J., E., 1981, *ApJ*, 247, 89
- Mateo, M., 1993, *ASCP*, 53, 74
- Meylan, G., Heggie, D., C., 1997, *A&A*, 8, 1
- Milone, A. P., Piotto, G., Bedin, L. R., Sarajedini, A., 2008, *Mem. S.A.It.*, 79, 623
- Mikkola, S., 1983, *MNRAS*, 205, 733
- Moehler, S., Heber, U., Napiwotzki, R., Koester, D., Renzini, A., 2000, *A&A*, 354, 75
- Moehler, S., Koester, D., Zoccali, M., Ferraro, F., R., Heber, U. et al., 2004, *A&A*, 420, 515
- Moni Bidin, C., Moehler, S., Piotto, G., Recio-Blanco, A., Momany, Y., Méndez, R. A., 2006, *A&A*, 451, 499
- Odenkirchen, M., Grebel, E. K., Dehnen, W., Rix, H. W., Cudworth, K. M., 2002, *ApJ*, 124, 1497
- Pasquini, L., Avila, G., Allaert, E., et al. 2000, in *Presented at the Society of Photo-Optical Instrumentation Engineers SPIE Conference*, Vol. 4008, *Proc. SPIE Vol. 4008*, p. 129-140, *Optical and IR Telescope Instrumentation and Detectors*, Masanori Iye; Alan F. Moorwood; Eds., ed. M Iye & A.F. Moorwood, 129-140
- Paresce, F., de Marchi, G., 1994, *ApJ*, 427, 33

- Peterson, R. C., Rees, R.F., & Cudworth, K.M., 1995, *ApJ*, 443, 124
- Portegies Zwart, S. F., Baumgardt, H., Hut, P., Makino, J., McMillan, S. L. W., 2004, *Nature*, 428, 724
- Pryor, C. P., Latham, D. W., Hazen, M. L., 1988, *ApJ*, 96, 123
- Pryor, C., McClure, R. D., Hesser, J. E., Fletcher, J. M., 1989, *ddse.work*, 175
- Pryor, C., Schommer, R., A., Olszewski, E., W., 1991, *ASCP*, 13, 439
- Rasio, F., A., McMillan, S., Hut, P., 1995, *ApJ*, 438, 33
- Rasio, F., A., Pfahl, E., D., Rappaport, S., 2000, *ApJ*, 532, 47
- Richer, H. B., Fahlman, G.G., Brewer, J., et al. 2004, *AJ*, 127, 2771
- Royer, F., Blecha, A., North, P., et al. 2002, Presented at the Society Astronomical Data Analysis II. Edited by Starck, Jean-Luc; Murtagh, Fionn D. Proceedings of the SPIE, Volume 4847, 184-194 (2002), ed. J-L. Starck & F. D. Murthag, 184-194
- Shara, M., M., Bergeron, L., E., Gilliland, R., L., Saha, A., Petro, L., 1996, *ApJ*, 471, 804
- Sigurdsson, S., Phinney, E., S., 1995, *ApJ*, 99, 609
- Sollima, A., Beccari, G., Ferraro, F. R., Fusi Pecci, F., Sarajedini, A., 2007, *MNRAS*, 380, 781
- Tonry, J., & Davis, M., 1979, *ApJ*, 84, 151
- Trager, S., C., King, I., R., Djorgovski, S., 1993, *AJ*, 109, 218
- Trager, S. C., Djorgovski, S., & King, I. R., 1993, in: "Structure and Dynamics of Globular Clusters", eds. S.G. Djorgovski and G. Meylan, *ASPC*, Vol. 50, 347
- Trager, S. C., King, Ivan R., Djorgovski, S., 1995, *ApJ*, 109, 218
- Yan, L., Mateo, M., 1994, *ApJ*, 108, 1810
- Yan, L., Cohen, J. G., 1996, *ApJ*, 112, 1489
- Yan, L., Reid, I., N., 1996, *MNRAS*, 279, 715